

From the: *Institute for Cardiovascular Physiology and Pathophysiology,*
Ludwig-Maximilians University of Munich



Dissertation
zum Erwerb des Doctor of Philosophy (Ph.D.) an der
Medizinischen Fakultät der
Ludwig-Maximilians-Universität zu München

***Environmental signals rather than layered ontogeny
imprint the function of type 2 conventional
dendritic cells in young and adult mice***

vorgelegt von:

Nikolaos Papaioannou

aus:

Athens, Greece

Jahr:
2021

Mit Genehmigung der Medizinischen Fakultät der
Ludwig-Maximilians-Universität zu München

First supervisor: *Prof. Dr. Barbara Schraml-Schotta*

Second supervisor: *Prof. Dr. Christian Schulz*

Third supervisor: *Prof. Dr. med. Markus Sperandio*

Dean: **Prof. Dr. med. dent. Reinhard Hickel**

Datum der Verteidigung:

05/07/2021

Affidavit



Affidavit

Papaioannou, Nikolaos

Surname, first name

Street

Zip code, town

Country

I hereby declare, that the submitted thesis entitled
“Environmental signals rather than layered ontogeny imprint the function of type 2
conventional dendritic cells in young and adult mice”

is my own work. I have only used the sources indicated and have not made unauthorised use of
services of a third party. Where the work of others has been quoted or reproduced, the source is
always given.

I further declare that the submitted thesis or parts thereof have not been presented as part of an
examination degree to any other university.

Athens, Greece, 14/01/2021

Place, date

Nikolaos Papaioannou

Signature doctoral candidate

Confirmation of congruency



Dean's Office
Medical Faculty



Confirmation of congruency between printed and electronic version of the doctoral thesis

Papaioannou, Nikolaos

Surname, first name

Street

Zip code, town

Country

I hereby declare that the electronic version of the submitted thesis, entitled
“Environmental signals rather than layered ontogeny imprint the function of type 2
conventional dendritic cells in young and adult mice”

is congruent with the printed version both in content and format.

Athens, Greece, 14/01/2021

Place, date

Nikolaos Papaioannou

Signature doctoral candidate

Table of content

Affidavit.....	3
Confirmation of congruency.....	4
Table of content	5
List of abbreviations	6
List of publications	8
1. Introductory summary	9
1.1 Dendritic cells as orchestrators of immune responses	9
1.2 Ontogenetic pathways of cells contributing to the mononuclear phagocyte system during development	10
1.3 Conventional dendritic cells exist as subsets with distinct developmental requirements, surface phenotype and unique functions in immunity.....	14
1.4 Mouse models that enable studying the developmental pathways and functional properties of conventional dendritic cells.....	17
1.5 The immune system in early life exhibits quantitative and qualitative differences compared to adults	19
1.6 Contribution to publication: "Clec9a-Mediated Ablation of Conventional Dendritic Cells Suggests a Lymphoid Path to Generating Dendritic Cells In Vivo."	26
1.7 Contribution to publication: "Environmental signals rather than layered ontogeny imprint the function of type 2 conventional dendritic cells in young and adult mice."	27
2. Paper I.....	29
3. Paper II.....	56
References	92
Acknowledgements	102
Curriculum vitae.....	103

List of abbreviations

<i>Bmp2</i>	Bone morphogenic protein 2
CD	Cluster of differentiation
cDC	Conventional dendritic cell
CDP	Common dendritic cell progenitor
CLEC9A	C-type lectin domain family 9 member A
CLP	Common lymphoid progenitor
cMoP	Common monocyte progenitor
CTV	Cell trace violet
DCIR2	Dendritic cell immunoreceptor 2
DNGR-1	Dendritic cell natural killer lectin group receptor 1
EMP	Erythro-myeloid progenitor
DT	Diphtheria toxin
EX	Embryonic day X
FC	Fold change
FLT3L	Fms tyrosine kinase 3 ligand
GF	Germ free
HSCs	Hematopoietic stem cells
icre	Improved cre protein
i.p.	Intraperitoneally
IFN	Interferon
Il7r	Interleukin 7 receptor
ILCs	Innate lymphoid cells
lin	Lineage
MDP	Macrophage dendritic cell progenitor
MFI	Mean fluorescence intensity
MHCII	Major histocompatibility complex II
OVA	Ovalbumin
OVA₃₂₃₋₃₃₉	OVA peptide 323-339
padj	Adjusted p value
PC	Principal component
PCA	Principal component analysis
pDCs	Plasmacytoid dendritic cells

pre-cDC	Pre-conventional dendritic cell
PRR	Pattern recognition receptor
RAG	Recombination activating gene
RNAseq	Bulk mRNA sequencing
scRNA-Seq	Single cell RNA sequencing
SPF	Specific pathogen free
Tfh	T follicular helper
Th17	T helper 17
Th2	T helper type 2
TLR	Toll-like receptor
Treg	Regulatory T cell
UMAP	Uniform manifold approximation and projection
YFP	Yellow fluorescent protein

List of publications

List of publications utilized for the current cumulative thesis

- 1) **Papaioannou NE**, et al. Environmental signals rather than layered ontogeny imprint the function of type 2 conventional dendritic cells in young and adult mice. *Nat Commun.* 2021;12,464. doi: 10.1038/s41467-020-20659-2
- 2) Salvermoser J, van Blijswijk J, **Papaioannou NE**, et al. Clec9a-Mediated Ablation of Conventional Dendritic Cells Suggests a Lymphoid Path to Generating Dendritic Cells In Vivo. *Front Immunol.* 2018 Apr 16;9:699. doi: 10.3389/fimmu.2018.00699

Complete list of publications

- 1) **Papaioannou NE**, et al. Environmental signals rather than layered ontogeny imprint the function of type 2 conventional dendritic cells in young and adult mice. *Nat Commun.* 2021;12,464. doi: 10.1038/s41467-020-20659-2
- 2) Salei N, Rambichler S, Salvermoser J, **Papaioannou NE**, et al. The Kidney Contains Ontogenetically Distinct Dendritic Cell and Macrophage Subtypes throughout Development That Differ in Their Inflammatory Properties. *J Am Soc Nephrol.* 2020 Feb;31(2):257-278. doi: 10.1681/ASN.2019040419
- 3) **Papaioannou NE**, et al. Understanding the Functional Properties of Neonatal Dendritic Cells: A Doorway to Enhance Vaccine Effectiveness? *Front Immunol.* 2019 Jan 10;9:3123. doi: 10.3389/fimmu.2018.03123
- 4) Salvermoser J, van Blijswijk J, **Papaioannou NE**, et al. Clec9a-Mediated Ablation of Conventional Dendritic Cells Suggests a Lymphoid Path to Generating Dendritic Cells In Vivo. *Front Immunol.* 2018 Apr 16;9:699. doi: 10.3389/fimmu.2018.00699
- 5) Samara P, Karachaliou CE, Ioannou K, **Papaioannou NE**, et al. Prothymosin Alpha: An Alarmin and More... *Curr Med Chem.* 2017;24(17):1747-1760. doi:10.2174/0929867324666170518110033
- 6) **Papaioannou NE**, et al. Harnessing the immune system to improve cancer therapy. *Ann Transl Med.* 2016 Jul;4(14):261. doi: 10.21037/atm.2016.04.01
- 7) **Papaioannou NE**, et al. A flow cytometric approach for studying alterations in the cytoplasmic concentration of calcium ions in immune cells following stimulation with thymic peptides. *Cell Immunol.* 2016 Apr;302:32-40. doi: 10.1016/j.cellimm.2016.01.004

Pubmed link: <https://www.ncbi.nlm.nih.gov/pubmed/?term=Papaioannou+N+E>

1. Introductory summary

1.1 Dendritic cells as orchestrators of immune responses

Dendritic cells (DCs) were initially identified in the adult mouse spleen by Steinmann and Cohn, where they were described as stellate cells with high motility ¹. Since then, they have been recognized as immune sentinels with a multifaceted participation in the elicitation and regulation of immune responses ². Due to this fact, it is not seldom for DCs to be seen as a connective link between the innate and the adaptive arm of immunity. Featuring as innate immune cells, DCs constantly sample their microenvironment by engulfing antigenic molecules derived from self or non-self. They possess an array of surface and intracellular receptors that enables them to sense the context within these antigens are met, and whether they are connected to invading pathogens, damaged cells or constitute innocuous antigens. Subsequently, they process these antigens and present them to T cells, thereby activating them in an antigen specific way. However, the simple initiation of effector immune responses against foreign and potentially pathogenic antigens does not guarantee their effectiveness. In order to ensure sufficient protection it is of outmost importance that effector responses will be tailored according to the pathogen met ³. For example, immune responses against intracellular pathogens, like viruses, and extracellular ones, like helminths, while are both designed to fight off pathogenic organisms differ substantially in their elicitation. Therefore, DCs can integrate information regarding the source and the context that foreign antigens are met and polarize the effector responses accordingly through the production of cytokines and provision of specific costimulatory signals to T cells ⁴. This has earned them the title of orchestrators of immune responses. On the other hand, establishing and maintaining tolerance against self and innocuous antigens is equally important and therefore DCs have been described to play a pivotal role in induction of central (in the thymus) and peripheral tolerance ⁴⁻⁶.

1.2 Ontogenetic pathways of cells contributing to the mononuclear phagocyte system during development

DCs are part of the mononuclear phagocyte system together with monocytes and tissue resident macrophages ⁷. According to the current paradigm all members of the mononuclear phagocyte system have well defined ontogenetic relationships and distinct progenitors (**Figure 1**). Among the members of the mononuclear phagocyte system tissue resident macrophages have been documented to arise the earliest during embryogenesis. More specifically, together with the first wave of nucleated blood cells they originate from extra-embryonic yolk sac progenitors already at embryonic day 7.25 (E7.25) ⁸⁻¹⁰. This wave of primitive hematopoiesis has been described to emerge from the so-called early erythro-myeloid progenitors (EMPs). Notably, a second wave of yolk sac derived progenitors emerges at E8.25. These late EMPs belong to the so-called transient definitive hematopoiesis and they can give rise to non-nucleated red blood cells and a bigger variety of myeloid lineages except for macrophages ¹¹. Interestingly, late EMPs can migrate as precursors to the fetal liver, thereby sustaining hematopoiesis until the next wave arises or seed embryonic tissues producing terminally differentiated cells. Among the late EMP progeny are also macrophages that colonize most embryonic tissues except the brain, due to the natural obstacle presented by the blood-brain barrier ^{9,10}. Interestingly, whether the second wave of tissue resident macrophages emerges through an intermediate state of fetal monocytes is still debated ^{8,10,12}. Similar to other immune cells arising from yolk sac progenitors, e.g. mast cells ¹³, embryonically derived macrophages persist in their tissues of residence for extended periods after birth. Their replacement kinetics by cells deriving from the definitive wave of hematopoiesis have been described to vary depending on the organ they reside in ^{9,14}. At E10.5, definitive hematopoietic stem cells (HSCs) emerge from the aorto-gonado-mesonephros region and migrate to the fetal liver where they expand and differentiate after E12.5 into all lineages of hematopoietic cells in a c-Myb dependent process. Shortly after birth hematopoiesis shifts to the bone marrow ^{9,11}. Therefore, it is evident that hematopoiesis commences early on during the development of a newly formed organism and during embryogenesis takes place in spatially and temporally overlapping waves. Each hematopoietic wave is characterized by different potential to produce distinct immune cell lineages that either transiently exist in the embryo or even persist after birth.

Apart from tissue resident macrophages, also DCs and monocytes have been reported to exist in embryonic tissues ^{12,15}. Fetal monocytes were shown to develop from fetal liver resident progenitors in contrast to their adult counterparts that derive from bone marrow HSCs ¹². Notably, the developmental pathways of DCs in early life remain still poorly studied and thus our knowledge regarding their development is solely based on studies performed in adults. Therefore, an important aim of the present study was to delineate whether DC-poiesis in early life emerges from a distinct hematopoietic source compared to their adult counterparts.

Adult bone marrow contains a fraction of myeloid progenitor cells capable of generating monocytes and DCs, that has therefore been termed macrophage and DC progenitor (MDP) ¹⁶. MDPs further give rise to so-called common monocyte progenitors (cMoPs) ¹⁷ and common DC progenitors (CDPs) ¹⁸⁻²². cMoPs are the immediate upstream progenitors of monocytes. It is worth mentioning that monocytes under both steady state and inflammatory conditions can egress to peripheral tissues and differentiate to monocyte-derived cells with features resembling that of DCs or macrophages ^{23,24}. On the other hand, CDPs were initially thought to exclusively generate plasmacytoid DCs (pDCs) and conventional DCs (cDCs). pDCs are critical for defending against viruses due to their ability to respond to viral antigens and secrete copious amounts of type I interferons (IFN) ^{25,26}. They were described to terminate their differentiation in the bone marrow in a manner dependent upon the transcription factor E2-2 ^{25,26}. Interestingly, recent studies have challenged the myeloid origin of pDCs suggesting that they originate primarily from lymphopoiesis ^{27,28}. cDCs excel in the activation of adaptive immune responses by presenting antigens to T cells. In mice, cDC-restricted progenitors are distinguished within the CDP fraction by the expression of the C-type lectin receptor DNGR-1 (encoded by the *Clec9a* gene) ²¹. This cDC-committed CDP fraction further differentiates to pre-conventional dendritic cells (pre-cDCs), which continue to express DNGR-1, exit the bone marrow and migrate to lymphoid and non-lymphoid tissues to complete their differentiation into cDC subsets, namely cDC1 and cDC2. Initially it has been thought that pre-cDC differentiation to either cDC subset was solely driven in response to environmental cues ²⁹. However, according to recent studies, pre-cDCs were found to be a heterogeneous mosaic of subpopulations, some of which are pre-committed to a specific cDC subtype even before egressing from the bone marrow ^{30,31}. While this debate is not fully resolved it

could have very interesting implications in explaining the noted variation in the qualitative representation of cDC subsets in different tissues and in the same tissue during different developmental timepoints, especially given the distinct functions of each cDC subset in immune responses. For the development of both pDCs and cDCs the growth factor-receptor axis between fms tyrosine kinase 3 ligand (FLT3L) and its receptor FLT3/CD135 has been found to be vital. Mice deficient for FLT3L have markedly reduced numbers of cDCs and pDCs in lymphoid organs such as thymus, spleen and lymph nodes ^{32,33}. In these mice, the cellularity of the spleen is also decreased due to reduced numbers of B and T cells together with NK cell deficiency ³². FLT3 is expressed on DC progenitors and thus cultures of total murine bone marrow cells with recombinant or in house produced FLT3L have been used to generate the *in vitro* equivalents of pDCs and cDCs ³⁴. Additionally, *in vivo* administration of recombinant FLT3L has been used as a means to induce expansion of cDCs and pDCs ³⁵⁻³⁷. Collectively, while in recent years many studies have contributed in delineating the distinct ontogenetic pathways throughout development of the members of the mononuclear phagocyte system, the developmental pathways of DCs during embryogenesis and early neonatal life have yet to be studied adequately.

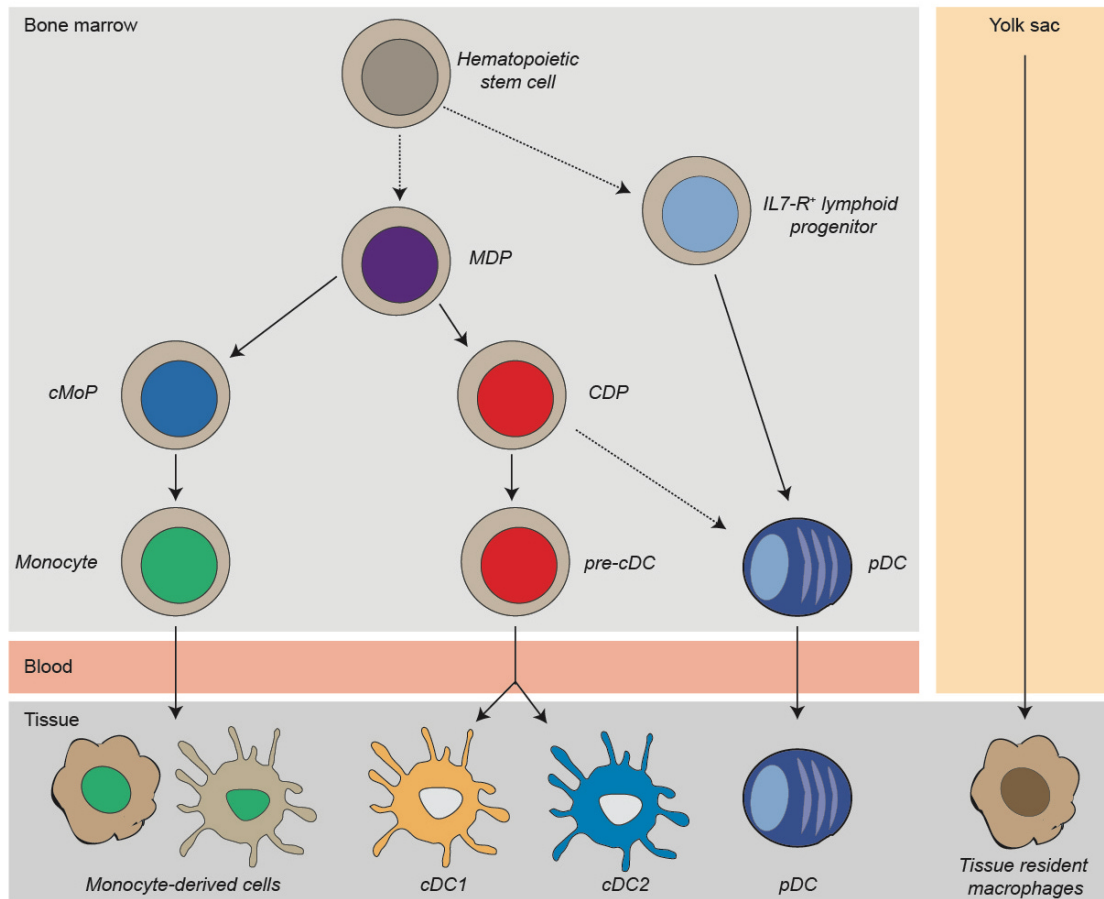


Figure 1 Developmental scheme of mononuclear phagocytes. In adults the macrophage and dendritic cell progenitor (MDP) gives rise to the common monocyte progenitors (cMoP) and the common dendritic cell progenitor (CDP). cMoPs differentiate already in the bone marrow to monocytes that egress in the blood stream and can seed peripheral tissues. There either under steady state or inflammatory conditions they can give rise to monocyte-derived cells resembling macrophages or dendritic cells. CDPs give rise to pre-conventional dendritic cells (pre-cDC) that seed peripheral tissues and give rise to both conventional dendritic cell subsets. CDPs were also thought to generate pDCs, however recent publications suggest that a lymphoid progenitor is the main source of pDCs. All mononuclear phagocytes in adults originate from bone marrow hematopoietic stem cells (HSCs) with the exception of some tissue resident macrophages that emerge during embryogenesis and are not replaced by HSC-derived cells. Dotted arrows emerging from HSCs delineate intermediate progenitor steps not depicted in this image.

1.3 Conventional dendritic cells exist as subsets with distinct developmental requirements, surface phenotype and unique functions in immunity

In the adult state, cDC1 and cDC2 comprise developmentally and functionally distinct subsets that exhibit remarkable division of labor when it comes to their role in immune responses ^{2,7,38} (**Figure 2**). Both cDC subsets are characterized by a high expression of CD11c and MHC-II but can be distinguished by their differential dependence on transcription factors and expression of other surface markers. Core cDC1 and cDC2 transcriptional programs have been described ^{39,40}, however, these cells can adapt their transcriptomic signature according to signals met in their microenvironment ^{22,41,42}.

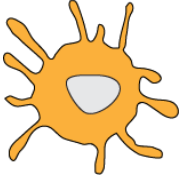

cDC subset	 cDC1	 cDC2
Transcription factors	IRF8, ID2, BATF3	IRF4, ZEB2, KLF4, RELB
Distinguishing phenotypic markers	XCR-1, CD24, CD8 α , CLEC9A/DNGR-1, CD205, CD103	CD11b, CD172a, CLEC4A4, CD4
Characteristic functions	<ul style="list-style-type: none"> • Cross-presentation • Defense against intracellular pathogens • Induction of Th1, Treg Responses 	<ul style="list-style-type: none"> • Proficient in activating CD4⁺ T cells • Defense against extracellular pathogens • Induction of Th2, Th17, Tfh responses

Figure 2 Transcription factors, phenotypic markers and functional properties typically associated with each conventional dendritic cell subset.

cDC1 rely on the transcription factors ID2, IRF8 and BATF3 for their development ^{40,43,44}. Studies have described a severe and systematic depletion of cDC1 when IRF8 or BATF3 are absent, thus identifying their continuous and high expression as prerequisites for maintaining the developmental and functional program of this subset ^{43,44}. cDC1 can be reliably identified across tissues by the expression of XCR-1, DNGR-1/CLEC9A, CD24 and CD205 ^{7,42}. In addition, CD8 α is a characteristic molecule for

cDC1 in lymphoid tissues while the integrin CD103 is used as a non-lymphoid tissue cDC1 marker, despite its expression also on an intestinal cDC2 subset⁴². Functionally, cDC1 have a dominant role of inducing Th1 polarized responses against intracellular pathogens like viruses, bacteria (e.g. *Listeria monocytogenes*) and others^{2,44-46}. They are remarkable activators of CD8⁺ T cells due to their ability of cross-presenting extra-cellular antigens on MHC-I molecules^{2,44-46}. Additionally, they possess a strong capacity to produce copious amounts of the cytokine IL-12 that enhances Th1 responses both directly, by acting on T cells themselves, and indirectly, by promoting production of a Th1-favorable cytokine milieu from other cells^{2,44-46}.

Notably, in the spleen cDC1 share many phenotypic markers with a unique DC population, termed BATF3-independent non-canonical CD8 α ⁺ DCs⁴⁷⁻⁴⁹. More specifically both DC populations stain positive for CD24 and CD8 α , however non-canonical CD8 α ⁺ DCs lack expression of XCR-1 and CD205 while they stain positive for markers typically associated with cDC2 like CD172a and CX3CR-1^{47,49}. Developmentally, non-canonical CD8 α ⁺ DCs are similar to pDCs as they depend on E2-2 and exhibit somatic rearrangements in the genes of the immunoglobulin heavy chain⁴⁹. Their transcriptomic profile resembles more that of cDC2⁴⁹ and therefore, these cells were recently suggested as a transitional cell type with pDC and cDC2 characteristics⁵⁰. Functionally, they have lower ability to produce type I IFNs than pDCs and IL-12 compared cDC1 while seem unable to cross-present cell associated antigens^{47,49}. While the full spectrum of their functional properties has yet to be described, transcriptomic analysis has shown that non-canonical CD8 α ⁺ DCs possess a unique array of pattern recognition and endocytic receptors suggesting a unique place within the DC immunosurveillance network⁵¹. As non-canonical CD8 α ⁺ DCs were only recently described, their example clearly illustrates the need for using multiple phenotypic markers in order to properly dissect the heterogeneity of the DCs in organ like the spleen.

Regarding the developmental requirements of cDC2, studies have identified a major role for the transcription factors IRF4, ZEB2, KLF4 and RELB. Additionally, other signaling pathways involving NOTCH2 and retinoic acid have also been described to have an influence in a tissue dependent manner^{40,42}. Characteristic cDC2 surface markers include CD11b, CD172a, CD4 and CLEC4A4^{7,42}. cDC2 are generally believed to be more efficient in inducing CD4⁺ T cell activation and polarization towards Tfh, Th2 or Th17 effector responses that are crucial for T cell-dependent antibody

responses, defense against multicellular pathogens like helminths or extracellular bacteria and fungi, respectively ⁵²⁻⁵⁶. Another recent study identified a new and unexpected functional property of cDC2 in mice. More specifically, Fujita et al. described splenic cDC2 as an important source of FLT3L ⁵⁷. The membrane bound FLT3L of splenic cDC2 was cleaved and shed by the A disintegrin and metalloproteinase (ADAM) 10 contributing vitally to the systemic levels of this vital DC growth factor. This cell autonomous circuit was vital for the development and maintenance of a NOTCH2-dependent subset of cDC2 as when disrupted the researchers observed an immediate depletion of this subset and an accumulation of cDC2-committed pre-cDCs in the spleen ⁵⁷.

Additionally, cDC2 have been found to exhibit marked diversity and heterogeneity depending on their tissue of residence. In support of the above, while IRF4 is considered a hallmark transcription factor for cDC2 its deletion does not lead to a complete halt in cDC2 development in all organs ^{54,55}. However, IRF4 deficiency negatively affects the ability of cDC2 to migrate from peripheral tissues to their draining lymph nodes ⁵⁸ and also diminishes their ability to induce Th17 responses ^{54,55}. Notably, in some cases even within the same organ cDC2 exhibit a remarkable heterogeneity. For example in spleen, they can be subdivided to ESAM^{high} and ESAM^{low} subpopulations that diversify in terms of functional properties, surface markers and defining transcription factors ⁵⁹⁻⁶¹. ESAM^{high} cDC2 require NOTCH2 signaling for their development while their transcriptional program is maintained by RUNX3 ^{59,61,62}. Functionally, *in vivo* they have been found to excel in induction of Tfh responses and germinal center formation ⁶⁰. ESAM^{low} cDC2 were described to excel at presenting low dose antigen to T cells *in vitro* ⁶⁰. Additionally, compared to their ESAM^{high} counterparts, they were shown to be better producers of pro-inflammatory cytokines after *in vitro* stimulation with Toll-like receptor (TLR) agonists ⁵⁹. A recent publication suggested a different segregation of splenic cDC2, delineated by the expression of the transcription factor T-bet, into T-bet expressing cDC2A and T-bet non-expressing cDC2B ⁶³. While cDC2A resembled ESAM^{high} and cDC2B ESAM^{low} cells further investigations are warranted to elucidate whether ESAM and T-bet expression perfectly correlate and reflect the same subsets of cells. Finally, the versatility and heterogeneity of cDC2 was shown to be even greater upon an ongoing inflammation. This was supported by Bosteels et al. showing that upon infection in the lung a new population of inflammatory cDC2 emerges with

functional characteristics that are not typically attributed to cDC2. This population exhibited functional properties of cDC1 like the high production of IL-12 and cross-presentation of extracellular antigens to CD8⁺ T cells as well as expressed surface markers typical of macrophages, while retaining the proficiency in CD4⁺ T cell activation ⁶⁴. Collectively, cDC2 exhibit marked heterogeneity that is often translated in functional specialization of their subsets as seen in the case of ESAM^{high/low} populations in the spleen. Additionally, as shown by recent publications, cDC2 have high potency in adapting and diversifying their ability to induce effective immune responses under both steady state and inflammatory conditions thus, making them a key target in strategies aiming to boost protective immunity.

1.4 Mouse models that enable studying the developmental pathways and functional properties of conventional dendritic cells

Deciphering the developmental and functional properties of cDCs in various tissues has been accelerated by the emergence of various mouse models that introduce generalized or more targeted genetic modifications in a constitutive or inducible manner ². One approach is the induction of controlled cell death in the cell type of interest driven by the expression of the diphtheria toxin (DT) A-chain or the simian/human DT receptor downstream of a cell specific promoter. The expression of DTA is sufficient to induce cell death as it disrupts protein translation while in the case of DTR expression exogenous administration of DT is required for inducing cell death. Widely used examples are the *Itgax-DTR* ⁶⁵ which targets all CD11c-expressing and the *Zbtb46-DTR* ⁶⁶ that allowed for a more targeted approach to cDCs, albeit with concomitant undesired targeting of endothelial cells as was later described ⁶⁷. To specifically target cDC subsets mouse models like *Xcr1-DTRvenus* (cDC1) ⁶⁸ or *Clec4a4-DTR* (cDC2) ⁶⁹ have been used. Another approach is the deletion of cDC lineage defining transcription or growth factors. Widely used mouse models are the *Irf8*^{-/-} and *Batf3*^{-/-} strains aiming at two well-defined cDC1 transcription factors. *Batf3* total knockout mice are selectively deficient in cDC1 in almost all lymphoid and non-lymphoid tissues ⁴⁴ as the particular transcription factor interacts with IRF8 in order to positively regulate the maintenance of cDC1 identity ⁷⁰. On the same logic, *Irf8* total knockout mice exhibit a marked impairment in cDC1 development ⁴³ however, also other lineages are affected

like B cells and monocytes. Additionally, as mentioned above, *Flt3l^{-/-}* mice exhibit defects in the development of several lymphoid lineages apart from an almost complete absence of DCs ^{32,71}.

In order to increase the specificity of the genetic interventions and thereby reduce the unwanted side effects on other lineages, the *Cre-loxP* system ⁷² was adopted for conditional deletion of genes. The principle of this system is that the gene, exon or sequence of interest is flanked by two loxP sites and therefore designated as floxed. The recombination between the two loxP sites is mediated by a recombinase encoded by the *Cre* gene of the P1 bacteriophage and leads to the deletion of the intervening DNA and the subsequent inactivation of the floxed gene. Using this strategy, it was possible, for example, to study the depletion of *Irf8* specifically in CD11c-expressing cells using the *Itgax-cre* strain ⁷³ but also decipher many aspects of the cDC2 developmental biology like the NOTCH2 dependence of ESAM^{high} splenic cDC2 (*Notch2^{ff} Itgax-cre* ^{59,62}) or the functional defects driven by the deletion of *Irf4* and *Klf4* in CD11c-expressing cells (*Irf4^{ff} Itgax-cre* ^{54,55,58} and *Klf4^{ff} Itgax-cre* ⁵⁶ respectively). However, also other lineages can be affected from the aforementioned models as CD11c expression is not solely restricted to DCs ⁷⁴. Taking advantage of the DNNGR-1/CLEC9A expression in cDC committed progenitors ²¹, the *Clec9a-cre* strain was created in which the improved Cre (icre) sequence was used to replace the two first exons of the endogenous *Clec9a* sequence ²¹. By crossing mice expressing CRE-recombinase under the *Clec9a* promoter to Rosa^{lox-stop-lox}-Yellow fluorescent protein (YFP) or Rosa^{lox-stop-lox}-Tomato mice, a fate mapping model enabling for the faithful tracing of the cDC lineage has been generated ^{21,75,76}. In these mice, a construct encoding for a fluorescent reporter is knocked in the murine Rosa locus, selected due to its constitutive and robust transcription. However, the expression of the reporter is halted by the presence of a floxed STOP signal. Consequently, in any CLEC9A-expressing cell the Cre-recombinase will excise the lox-stop-lox construct thus allowing for the expression of the fluorescent reporter and the irreversible marking of the CLEC9A⁺ cell and its progeny with a fluorescent signal. This is important as it instantly describes the power and the limitations of this model. On the one hand the *Clec9a* promoter is not active in other myeloid or lymphoid cells, contributing to the specificity of the model, however, it is also active in cDC1 and pDCs therefore any labeling in these cells cannot be interpreted as sign of their developmental origin ^{21,75,76}. Only in cDC2, in which *Clec9a* expression is lost after the terminal differentiation from their precursors, the presence

of fluorescent labeling is a true indication of their ontogeny (**Figure 3**). Consequently, using this model cDC2 can be reliably identified without relying solely in expression of surface markers that can overlap with monocytes/macrophages at steady state or that are induced in a plastic way under inflammatory conditions ^{24,42,64}.

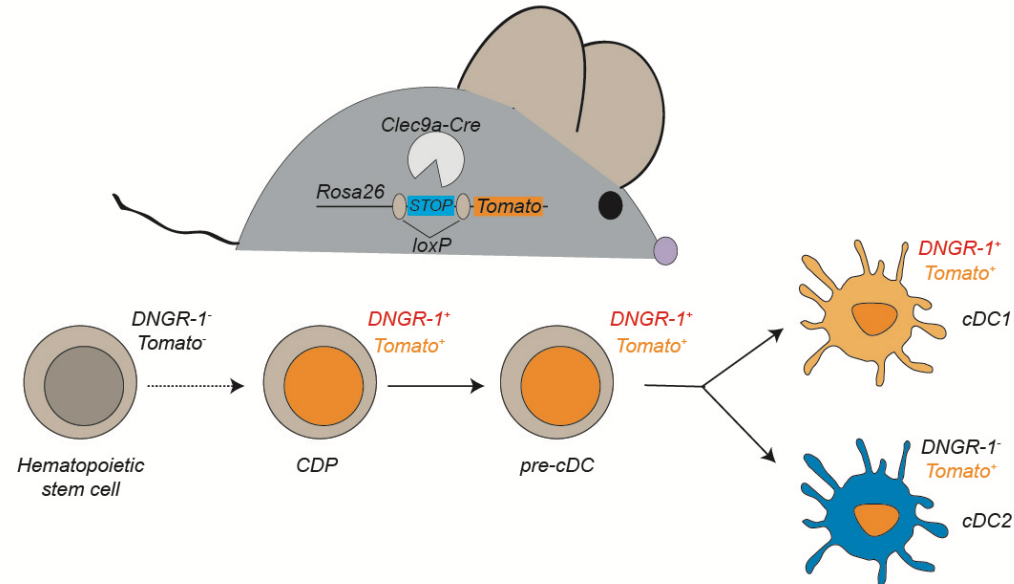


Figure 3 Schematic illustrating the principle of lineage tracing using *Clec9a-cre* fate mapping models. The Cre recombinase under the control of the *Clec9a* promoter will excise the STOP sequence lining between the two loxP sites enabling the transcription of a fluorescent reporter (in this case Tomato). Therefore, any cell expressing DNDR-1/CLEC9A and its progeny will be labeled irreversibly with the particular reporter. Since cDC2 do not express DNDR-1/CLEC9A in their differentiated state any labeling would result from their DNDR-1/CLEC9A-expressing cDC committed progenitors. The same is not true for cDC1 for their active expression of DNDR-1/CLEC9A prevents interpreting their labeling status as an indication of their ontogeny.

1.5 The immune system in early life exhibits quantitative and qualitative differences compared to adults

The neonatal period in mammals is inherently unique as the newly born organism transits from an insulated and sterile embryonic environment to the external world. It may not be an overstatement that newborns are exposed to a plethora of antigenic stimuli that are encountered for the first time. Mounting an immune response against all these new antigens would be detrimental for the survival of the new organism ⁷⁷ taking also into consideration that many of these antigens are harmless or part of its expanding microflora. Therefore, it is crucial that the organism successfully establishes tolerance to innocuous environmental antigens and commensal microorganisms ⁷⁸⁻⁸⁰, as failing to do so can result in detrimental and lifelong impacts for the individual. On the other hand, such tolerance establishment should be balanced with

properly orchestrated host defense to pathogens as the contrary could have immediate life-threatening implications for the survival of the organism. Thus, it is well-perceived why the neonatal period is characterized as a critical window in the life of an organism.

Many studies have highlighted that several components of the neonatal immune system seem to be tailored towards a reduced pro-inflammatory capacity and as such they have been thought to be immature compared to their adult counterparts⁸¹⁻⁸³. This implies that they are intrinsically predisposed to induce immune responses of low efficiency and magnitude. However, from another perspective the lower responsiveness of the neonatal immunity to any newly encountered antigen, be it pathogenic or not, is an actively and tightly regulated procedure with deep roots in promoting the survivability of the organism⁷⁷. Deploying any strategy of host defense involves a cost in both the energy allocated to that purpose and the collateral damage caused by the immune response. Neonates are able to afford neither the energetic nor the immune cost for mounting a full response against any potential pathogenic organism encountered as they mainly allocate their energy reserves for growth. Additionally, the resulting immunopathology would compromise the development of many organs like the lungs and kidneys that is still ongoing after birth^{77,84}. Therefore, it is an emerging concept that a strategy of disease tolerance is selected over disease resistance that may serve the energetic demands of the neonatal life and confer protection from the resulting immunopathology. Interestingly, this approach functions as a double-edged sword because on many occasions increases the neonatal susceptibility to certain life-threatening infections^{79,85} but also proves beneficial when facing pathogens that cause severe manifestation of immunopathology in adults, like SARS-CoV-2⁸⁶. Admittedly, experimental and clinical data converge on the idea that nearly all the components of the neonatal immune system exhibit quantitative and qualitative differences compared to adult hosts. These differences will be the subject of the following paragraphs and can manifest as an altered repertoire of immune cells and in the form of functional differences of each individual neonatal population to its adult counterpart.

Given the fact that neonates are particularly susceptible to pathogens with an intracellular life cycle like viruses and certain bacteria, many studies have focused on neonatal CD8⁺ T cells. Smith et al. showed recently that CD8⁺ T cells emerging during the neonatal period in mice differ in the type and kinetics of their response to infection compared to their counterparts emerging later during development⁸⁷. Interestingly, this

study identified that the functional differences between neonatally and adult derived CD8⁺ T cells were majorly impacted by their developmental origin. More specifically, neonatally derived CD8⁺ T cells, deriving from neonatal HSCs, exhibited a memory-like surface phenotype and were characterized by the authors as early responders to infectious challenge reminiscent of innate immune cells. On the other hand, CD8⁺ T cells derived from adult hematopoietic progenitors had slower kinetics in their response after the first encounter with the antigen but, differentiated more effectively to long lived memory cells that would confer long lasting protection. This study essentially showed that the function of neonatal CD8⁺ T cells was intrinsically pre-programmed and reflected in both their transcriptomic and epigenetic landscapes. In humans, contradictory results have been reported. Similar to what was observed in mice, one study reported that a distinct epigenetic and transcriptomic profile accounted for the lesser cytotoxic effector functions of neonatal CD8⁺ T cells ⁸⁸. On the contrary, some others have shown that CD8⁺ T cells from young children can exhibit adult-like effector functions against specific viruses, as measured by perforin and IFN- γ production ⁸⁹.

Continuing on the T cell field, neonatal murine CD4⁺ T cells were described to produce copious amounts of IL-4 and IL-13 rapidly upon activation in contrast to their adult counterparts ⁹⁰. Chromatin landscape analysis showed that in naïve neonatal CD4⁺ T cells a key regulatory region of the Th2 locus exists in a hypomethylated state rendering the entire locus more accessible for transcription and thus sustaining rapid IL-4 production after activation ⁹⁰. Thus, neonatal CD4⁺ T cell immunity has initially been thought to be entirely biased towards the Th2 polarization. However, seminar studies in mice have shown that upon neonatal antigen exposure *in vivo*, both Th1 and Th2 primary responses develop but, re-challenge with any neonatally encountered antigen would result solely to Th2 responses ⁹¹. Mechanistically, it was discovered that upon primary challenge antigen specific Th1 CD4⁺ T cells upregulate surface expression of the IL-13R α 1, forming a heterodimer with IL-4R α (also called IL-4R α /IL-13R α 1 heteroreceptor (HR)). Upon the secondary challenge, the IL-4 produced by antigen specific Th2 cells would signal through the HR and induce apoptosis specifically to Th1 cells. Notably, IL-13R α 1 upregulation could only be prevented if IL-12p70 was found in adequate amounts during the primary antigen encounter, however it was shown to be insufficiently produced by neonatal DCs, as it will be discussed below ⁹¹. In human fetuses naïve T cells were described to share many transcriptional similarities with regulatory T cells (Tregs) such as expression of the transcription factor Helios and

additionally to have an increased propensity for Treg differentiation after antigen encounter and activation ⁹². Moreover, cytokines, such as TGF- β , are found in higher levels in fetal secondary lymphoid organs further corroborating the Treg polarization of naïve fetal T cells ⁹³.

Humoral responses in neonates from both humans and mice differ significantly to those in adults. More specifically, neonatal T cell dependent humoral responses are characterized by a delayed onset, lower magnitude and affinity while additionally the conferred protection wanes with time ⁸⁴. These phenomena could represent a failure of T cells to provide sufficient help but also go in hand with age dependent differences in the B cell compartment. For example, in the neonatal murine spleen the majority of the B cell compartment is comprised by B1 cells that tend to secrete low affinity antibodies primarily of the IgM isotype. Additionally, any B2 cells existing at that developmental timepoint have a rather immature phenotype ⁸⁴. Notably, mounting of efficient antibody responses is a stepwise process that requires the formation of some architectural structures, namely lymphoid follicles, follicular dendritic cell networks and germinal centers. However, these structures are absent at birth in mice and only fully develop after the first week of life together with the overall splenic architecture ⁸⁴. Additionally, efficient humoral responses followed by the establishment of protective memory cells are heavily impacted by T cell help provided by follicular helper T cells (Tfh). However, a recent study showed that in neonatal mice after immunization with standard alum containing regimens, any differentiating Tfh cell seemed to be transcriptionally lodged at a premature stage with lower expression of key signature markers, like CXCR5, that could ultimately impact their ability to migrate to B cell areas and contribute to the efficient induction of antibody responses ⁹⁴. Finally, a population of B regulatory cells has been described to be expanded in the murine neonatal spleen with profound role in dampening inflammatory responses and efficient T cell priming through an IL-10 mediated manner ⁹⁵.

As far as myeloid immune cells are concerned, early life neutrophils are characterized by a reduced transepithelial extravasation. This impacts negatively their ability to localize in inflamed tissues and is connected to decreased surface expression of the CD11b/CD18 complex and of the P-selectin glycoprotein ligand-1 ^{96,97}. Added to their reduced trafficking, neonatal human neutrophils exhibit impairments in phagocytosis and formation of extracellular traps, two vital functions for their immune protective role

⁹⁸. Data suggest that neonatal monocytes exhibit a reduced expression of the adhesion complexes L-selectin and membrane attack complex-1 and thus, similarly to neutrophils show a defect in their ability to adhere to inflamed endothelium and be recruited in sites of infection. Additionally, fetal and neonatal monocytes seem to hyporespond after stimulation of pattern recognition receptors like TLRs due to reduced activation of the intracellular signaling cascade ^{12,99-101}. In murine neonates, both neutrophils and monocytes have an increased frequency among splenic leukocytes and exhibit functions reminiscent of myeloid suppressor cells as they were shown to directly suppress T cell activation and proliferation *in vitro* ¹⁰².

Similarly to the other immune system cells mentioned above, early life DCs have been documented to differ from their adult counterparts in terms of both their function and quantitative distribution ⁸³. As such it has been considered that DCs in early life are under-developed and immature, however the underlying reasons of these differences have not been investigated in detail. For example, until the point that the present study was conducted no data existed on whether neonatal DCs are intrinsically preprogrammed to function differently due to an altered developmental pathway in early life, as mentioned above for CD8⁺ T cells, or their function was instructed by different microenvironmental cues during development. In both human and murine neonates, the DC compartment is smaller than that of adults ^{15,103,104}. Indicatively, in the murine spleen the numbers of cDCs are much lower than in adults and additionally their frequency among the splenic leukocytes is around ten-fold lower than the respective one in the adult spleen ¹⁵. While similar scarcity of neonatal cDCs is noted in other lymphoid and non-lymphoid tissues in humans and mice ^{15,103,104} the subset distribution differs between these species. In mice, the neonatal cDC compartment is dominated by cDC1 and inversely cDC2 are the main cDC subtype in adult tissues ^{15,103,105}. In contrast, in most human tissues the relative frequency of cDC1 and cDC2 remains stable throughout development ⁴¹. Noteworthy, early studies especially in mice, have identified the neonatal equivalents of cDC subsets solely based on expression profiles of surface markers used for adult cDCs. However, recent studies have started to reveal that in fact many hallmark adult cDC markers have an altered expression profile in early life. For example, in the first week of life murine cDC1 from the spleen and mesenteric lymph node retain expression of the hallmark adult markers CD24, CLEC9A, CD205 and XCR-1 but lack CD8 α and lung cDC1 have been documented

to exhibit reduced expression of the defining marker CD103 in early life ^{105,106}. Similarly, CD4 only reaches adult levels of expression in splenic cDC2 after the second week of life ¹⁵, while the age dependent distribution of cDC2 subsets based on ESAM expression remains yet unexplored. Consequently, due to the use of developmentally non conserved phenotypic markers the heterogeneity of early life cDC subsets still remains not completely characterized. Additionally, the use of such markers also hampers the complete functional characterization of these cells because their implementation in experimental designs can lead to isolation of mixed or partial populations, as would be the case when using solely CD8 α and CD4 to purify early life splenic cDC subsets, for example. In continuation, the reasons underlying the age dependent subset distribution and phenotype of cDCs in mice have yet to be identified. On the one hand, it is possible that the DC-poiesis during development is biased in generating an adapted cDC repertoire that fits the age specific needs, which could go in line, for example, with the dominance of cDC1 in early life tissues as this subset is considered more capable in inducing Treg formation in the periphery ⁵. On the other hand, however, age-specific changes in specific organ microenvironments could alter the skewing of cDC subset development and their phenotype. For example, this seems to be the case in lung where the decreased CD103 expression in cDC1 can be attributed to reduced levels of GM-CSF the tissue ¹⁰⁵.

Regarding the functional properties of cDCs in early life, the exhibited differences compared to their adult counterparts manifest in a seemingly conserved pattern in both humans and mice, although the underlying reasons remain yet undefined. For example, in both species neonatal cDCs express lower basal levels of MCH-II and co-stimulatory molecules ^{41,105,107-110}. This could lead to the assumption that they are less potent in activating antigen specific T cells and indeed, it was shown that splenic cDC subsets from 1-week-old mice were able to stimulate reduced proliferation of allogeneic CD4⁺ T cells *in vitro* compared to their counterparts isolated from 6-week-old mice ¹⁵. However, it should be noted that cDC subset discrimination in the latter study was performed using surface markers with poor expression profile in early life as was later shown. CD4⁺ T cell polarization instructed by neonatal cDCs is thought to be biased towards Th2 immune responses and is documented to manifest either during primary ¹¹¹ or recall responses ⁹¹. Mechanistically, in the lung the abundance of IL-33 in the microenvironment has been shown to induce expression of Th2 favorable co-stimulatory molecules in cDCs and thus directly instruct Th2 polarization ¹¹¹ while in spleen

the delayed production of IL-12p70 from neonatal cDC1 is the main driver of Th2 biased recall responses to neonatally encountered antigens⁹¹. Neonatal cDC1 were additionally shown to produce lower amounts of IL-12 after stimulation with pathogenic stimuli like CpG *in vitro* or poly I:C *in vivo*^{15,106}. The latter observation was very interesting when put into the context of neonatal infection with the bacteria *Listeria monocytogenes*. More specifically, in the first week of life, CD8 α ⁻ cDC1 are able to phagocytose the bacteria, process and present derived antigens to CD8⁺ T cells, however, compared to their adult counterparts not only they produce less IL-12 but additionally secrete the anti-inflammatory cytokine IL-10¹⁰⁶. This ultimately results in dampening of the pathogen specific CD8⁺ T cell effector response with life threatening implications for the neonatal mice. In another model of neonatal infection using respiratory syncytial virus, neonatal lung cDC1 were shown to preferentially present an altered epitope repertoire to antigen specific CD8⁺ T cells, compared to lung cDC1 in adults^{105,107}. Noteworthy, this observation hints the existence of age-specific antigen processing differences, but was also shown to stem from the lower levels of co-stimulatory molecules in neonatal lung cDC1 as co-administration of soluble co-stimulatory molecules during the infection partially shifted the elicited response to the immunodominant epitope in adults^{105,107}. Lower levels of co-stimulatory molecules in cDC1 could be a result of inefficient primary activation by the pathogen or/and to them being refractory to IFN- α signaling that is induced during viral infections¹¹². In contrast to cDC1, only few studies have examined in detail cDC2 in early life. Most of our knowledge in mice comes from studies in the lung, where cDC2 have been described to express lower levels of MHC-II and co-stimulatory molecules, promote Th2-mediated allergy and induce moderate CD8⁺ T cell proliferation after infection with respiratory syncytial virus^{105,107,111}. Additionally, a recent article studying the cDC compartment in human fetuses described that after stimulation with various pathogen associated molecular patterns fetal splenic cDC2 were characterized by production of an anti-inflammatory cytokine profile in contrast to their adult counterparts¹¹³. The same study highlighted the potential role of these cells in maintenance of fetomaternal tolerance, as despite their ability to induce allogeneic T cell proliferation fetal cDC2 limited the TNF- α production from activated T cells in an arginase-2 dependent manner and promoted differentiation of more Foxp3⁺ regulatory T cells¹¹³. The above data indicate that cDC2 in early life have the potential to induce T cell responses and even direct these responses distinctly depending on the tissue of origin. Therefore, from a functional perspective, the present

thesis focuses mainly on comparing the properties of cDC2 in young mice with those of their adult counterparts and uncovering the underlying reasons for the observed differences. In accordance with the dynamic role of cDC2 in inducing effector CD4⁺ T cell responses, detailed characterization of the unique early life cDC2 functional properties could also open possibilities for harnessing their potential and target them to boost early life immune responses.

1.6 Contribution to publication: “Clec9a-Mediated Ablation of Conventional Dendritic Cells Suggests a Lymphoid Path to Generating Dendritic Cells In Vivo.”

Conventional dendritic cells in adults have been documented to arise from a branch of bone marrow derived myeloid progenitors, as described above. Under certain experimental conditions lymphoid progenitors have been shown to differentiate in cells resembling DCs. However, these experiments mostly involved culturing of lymphoid progenitors *in vitro* or adoptively transferring them to irradiated recipients¹¹⁴⁻¹¹⁷. It is therefore considered that any lymphoid contribution to the pool of cDCs under steady state conditions is negligible and even restricted to specific peripheral organs like the thymus^{114,115}.

The initial aim of this published study was to generate a cDC deficient mouse model by using *Clec9a^{cre}Rosa^{DTA}* mice. The generated mouse model would take advantage of the *Clec9a* expression profile during cDC development and thus deplete the lineage already at the progenitor level. Experimental results showed that cDC progenitors and thus also their progeny were reliably and constitutively depleted. However, under these experimental conditions, leading to the impairment of myeloid-derived cDCs, cells resembling cDC2 were observed in lymphoid and non-lymphoid organs of *Clec9a^{cre}Rosa^{DTA}* mice. Therefore, this observation suggested that an alternative developmental pathway could serve as a source for DC-poiesis. Driven by the aforementioned published results, we hypothesized that lymphoid progenitors could be the alternative source for DC-poiesis when the conventional myeloid pathway is abrogated. Additionally, the study aimed to investigate whether a possible differential developmental pathway would pre-program the generated cDC-like cells with distinct functional properties compared to *bona fide* cDCs. Focusing on the splenic compartment, these cDC2-like cells were found to be almost indistinguishable from *bona fide* cDC2

in terms of their surface phenotype and transcriptional profile. These findings were in line with previously published results concerning *in vitro* generated DCs from lymphoid progenitors ¹¹⁷, however emphasized the need to use an additional approach to point the relatedness of cDC2-like cells in *Clec9a^{cre}Rosa^{DTA}* mice to the lymphoid branch of hematopoiesis. This was made possible by exhibiting that these cDC2-like cells contained D-J rearrangements at the immunoglobulin heavy chain (IgH) locus. Existence of such rearrangements serves as a fingerprint of RAG gene expression history, which is a hallmark of lymphoid primed progenitors even in the early stages of their development in the bone marrow ¹¹⁸. Thus, this study suggested that when the myeloid branch of hematopoiesis is impaired in generating cDCs, lymphopoiesis is capable to fill in this gap and contribute to DC-poiesis.

I established in our lab two published protocols for detecting D-J rearrangements. We chose to use both of these protocols because they are complementary and enable detection of rearrangements containing different D elements, more specifically of the Df16 and Dsp2 gene families and of the DHQ52 element. This approach increased the sensitivity of detecting the fingerprints of a lymphoid origin as only one D element participates in any given rearrangement event and its selection is stochastic. I performed and analyzed the experiments presented in Figures 5E, F and in Supplementary Figure 5. Results of the aforementioned experiments were essential in supporting the lymphoid origin of cDC2-like cells in *Clec9a^{cre}Rosa^{DTA}* mice. Additionally, I performed experiments shown in Supplementary Figure 3D. These results suggested that the lower expression of CD135 observed in splenic cDC2-like cells from *Clec9a^{cre}Rosa^{DTA}* mice, a hallmark phenotypic difference when compared to *bona fide* cDC2, could be attributed to receptor downregulation driven by increased systemic levels of its ligand, FLT3L, in these mice.

1.7 Contribution to publication: “Environmental signals rather than layered ontogeny imprint the function of type 2 conventional dendritic cells in young and adult mice.”

As mentioned in the introductory section, conventional dendritic cells in early life have been described to exhibit qualitative and quantitative differences when compared to their adult counterparts ⁸³. These observations have led to the impression that early life cDCs consist an immature version of adult cDCs with lesser ability to induce and

properly polarize immune responses. Aim of this research work was to elucidate the reasons shaping these age-dependent functional differences especially with regards to cDC2, due to a lack of studies focusing on this subset in early life. Additionally, the aforementioned question is approached with an ontogenetic scope, hypothesizing that a distinct developmental pathway of neonatal cDCs could pre-program them to function distinctly in early life than in adulthood. This hypothesis is driven by many publications describing such layered development in other immune populations like macrophages, T and B cells, mast cells and innate lymphoid cells (ILCs)^{9,13,87,92,119}. As a continuation of our findings using the *Clec9a^{cre}Rosa^{DTA}* mice which showed that lymphoid progenitors could compensate DC-poiesis when the myeloid branch was impaired, we more specifically questioned whether lymphopoiesis could be the source of early life cDCs, especially since observing that *bona fide* myeloid cDC committed progenitors in early life hematopoietic organs are present in scarce quantities. This study demonstrates for the first time that cDC2 exhibit a layered ontogeny during development with lymphoid progenitors having a major contribution to the pool early life cDC2. *Bona fide* myeloid cDC progenitors gradually replace the first wave of DC-poiesis and dominate in adulthood. Interestingly, these data suggest that ontogenetic origin does not have a major impact in cDC2 function as in early life, cells originating from either lymphoid or myeloid progenitors are inseparable in terms of their phenotype, transcriptional profile and function. Surprisingly, early life cDC2, irrespective of their ontogeny, are fully functional in inducing immune responses with distinct capacities in supporting certain effector polarization states. We also report that cDC2 transcriptional profiles, and in extension functional properties, are imprinted by distinct cytokine environments existing during development. Additionally, this study identified for the first time a new subset of cDC2 expressing the transcription factor ROR γ t, that is unique for early life and is currently subject of follow-up studies.

I performed and analyzed experiments shown in Figure 1, Figure 2 (a,b,d), Figure 3a, Figure 4, Figure 5 (a-c, e-i), Figure 6, Supplementary Figure 1 (A-C,E-G), Supplementary Figure 2, Supplementary Figure 3, Supplementary Figure 4 (A,B), Supplementary Figure 5 (A-G), Supplementary Figure 6 (A-G, I-J) and Supplementary Figure 7. I analyzed data generated by our international collaborators presented in Figure 2e and Supplementary Figure 5l. Additionally, I contributed to manuscript writing, creation of the figures and experimental design under the advice and guidance of my supervisor Prof. Dr. Barbara Schraml-Schotta.

2. Paper I



Clec9a-Mediated Ablation of Conventional Dendritic Cells Suggests a Lymphoid Path to Generating Dendritic Cells *In Vivo*

Johanna Salvermoser^{1,2}, Janneke van Blijswijk³, Nikos E. Papaioannou², Stephan Rambichler^{1,2}, Maria Pasztoi², Dalia Pakalniškytė^{1,2}, Neil C. Rogers³, Selina J. Keppler⁴, Tobias Straub^{2,5}, Caetano Reis e Sousa^{3*†} and Barbara U. Schraml^{1,2*†}

OPEN ACCESS

Edited by:

Simon Yona,
University College London,
United Kingdom

Reviewed by:

Charlotte Scott,
VIB-UGent Center for Inflammation
Research (IRC), Belgium
Dawn Shuiping Lin,
Walter and Eliza Hall Institute of
Medical Research, Australia
Ken Shortman,
Walter and Eliza Hall Institute of
Medical Research, Australia

*Correspondence:

Caetano Reis e Sousa
caetano@crick.ac.uk;
Barbara U. Schraml
barbara.schraml@med.
uni-muenchen.de

[†]These authors have contributed
equally to this work.

Specialty section:

This article was submitted to
Antigen Presenting Cell Biology,
a section of the journal
Frontiers in Immunology

Received: 07 February 2018

Accepted: 21 March 2018

Published: 16 April 2018

Citation:

Salvermoser J, van Blijswijk J,
Papaioannou NE, Rambichler S,
Pasztoi M, Pakalniškytė D,
Rogers NC, Keppler SJ, Straub T,
Reis e Sousa C and Schraml BU
(2018) Clec9a-Mediated Ablation of
Conventional Dendritic Cells
Suggests a Lymphoid Path to
Generating Dendritic Cells *In Vivo*.
Front. Immunol. 9:699.
doi: 10.3389/fimmu.2018.00699

¹Walter-Brendel-Centre for Experimental Medicine, University Hospital, LMU Munich, Planegg Martinsried, Germany,
²Biomedical Center, LMU Munich, Planegg Martinsried, Germany, ³Immunobiology Laboratory, The Francis Crick Institute,
London, United Kingdom, ⁴Technische Universität München, Klinikum Rechts der Isar, Institut für Klinische Chemie und
Pathobiochemie, Munich, Germany, ⁵Core Facility Bioinformatics, Biomedical Center (BMC), LMU Munich, Planegg
Martinsried, Germany

Conventional dendritic cells (cDCs) are versatile activators of immune responses that develop as part of the myeloid lineage downstream of hematopoietic stem cells. We have recently shown that in mice precursors of cDCs, but not of other leukocytes, are marked by expression of DNNGR-1/CLEC9A. To genetically deplete DNNGR-1-expressing cDC precursors and their progeny, we crossed *Clec9a-Cre* mice to Rosa-lox-STOP-lox-diphtheria toxin (DTA) mice. These mice develop signs of age-dependent myeloproliferative disease, as has been observed in other DC-deficient mouse models. However, despite efficient depletion of cDC progenitors in these mice, cells with phenotypic characteristics of cDCs populate the spleen. These cells are functionally and transcriptionally similar to cDCs in wild type control mice but show somatic rearrangements of Ig-heavy chain genes, characteristic of lymphoid origin cells. Our studies reveal a previously unappreciated developmental heterogeneity of cDCs and suggest that the lymphoid lineage can generate cells with features of cDCs when myeloid cDC progenitors are impaired.

Keywords: dendritic cell, development, CLEC9A/DNNGR-1, DC depletion, myelopoiesis, lymphopoiesis, fate mapping

INTRODUCTION

Conventional dendritic cells (cDCs) are remarkable activators of adaptive immune responses with a superior capacity to capture, process, and present antigens to T cells (1–4). Through the production of cytokines, cDCs further direct effector responses and play essential roles in immune homeostasis and innate immunity (5–10). This versatility of cDCs in immune responses is regulated in part through the functional specialization of cDC subpopulations. cDCs exist as two main developmentally distinct subsets that are found across lymphoid and non-lymphoid organs. cDC1 requires the transcription factors Batf3, IRF8, and ID2 for their development and are marked by expression of XCR1 and DNNGR-1 (a.k.a. CLEC9A) across tissues and species (1, 11, 12). They are exceptional activators of CD8 T cells owing to their superior capacity to take up dead cells and cross-present antigens (1–4). Through the production of IL-12, cDC1 promotes type-I immune responses hallmarked by expression of Th1 cytokines (1, 5). In contrast, the differentiation and function of the cDC2 subset is controlled by the transcription factors IRF4, KLF4, RelB, and ZEB2 (1, 11–14), although ZEB2 may predominantly control cDC2 differentiation in inflammatory conditions (15). Phenotypically

cDC2 can be distinguished from cDC1 by expression of CD11b, CD172a, and CLEC4A4 (DCIR2), as well as expression of IRF4 and concomitant lack of IRF8 (1, 11, 12, 16). cDC2 appears to play a more prominent role in CD4 T-cell activation and the promotion of Th2 and Th17 responses, particularly at mucosal surfaces (17, 18).

Although the existence of cDCs as independent cell type has been a matter of intense debate, lineage tracing and other studies in mice have established that cDCs develop as distinct hematopoietic cell lineage (12, 19, 20). Single-cell analyses have recently suggested that myeloid lineage decisions take place early in hematopoiesis but the production of lymphoid and myeloid lineages is thought to branch after the lymphoid-primed multipotent progenitor (LMPP) stage (20–24). Downstream of LMPP, in a stepwise differentiation process, common myeloid progenitors give rise to a lineage (lin) negative CD115⁺CD117^{hi}CD135⁺ fraction of bone marrow that generates monocytes, plasmacytoid DCs (pDCs), and cDCs and has therefore been termed macrophage and DC progenitor (MDP) (25, 26). Whether MDPs are a true bi-potent developmental intermediate for cDCs/pDCs and monocytes is controversial (27). MDPs further give rise to common monocyte progenitors that exclusively generate monocytes (28) and a lin[−]CD115⁺CD117^{low}CD135⁺ fraction of cells termed common DC progenitors (CDP) that lose monocyte potential but generate cDCs and pDCs (29, 30). Within CDPs the expression of the C-type lectin receptor DNNGR-1 (encoded by the *Clec9a* gene) distinguishes cells with exclusive cDC potential (19). CDPs further differentiate into pre-cDCs, which also express DNNGR-1 (19) and travel *via* blood to peripheral organs, where their terminal differentiation into cDC1 and cDC2 takes place in response to environmental cues (31–33). Some pre-cDCs exist as pre-committed subsets that can be already distinguished in bone marrow based on the expression of specific surface markers and transcription factors (32, 34, 35). The developmental steps of cDC differentiation appear conserved, as equivalent progenitors and transcriptional requirements for cDC differentiation have been identified in humans (12, 36–40).

By crossing mice expressing Cre recombinase (Cre) under the control of the endogenous *Clec9a* promoter to Rosa26-lox-STOP-lox-yellow fluorescent protein (YFP) reporter mice, we were able to demonstrate that *Clec9a* expression history faithfully traces the cDC lineage, including the main cDC1 and cDC2 subsets, but no other myeloid and lymphoid lineages in steady state as well as during inflammation (19). In this model, any cell-expressing Cre becomes irreversibly labeled with YFP, thereby allowing us to trace DNNGR-1-expressing CDP and pre-cDC irrespective of continuous DNNGR-1 expression (19). One exception to faithful tracing of the cDC lineage is pDCs, which do not arise from DNNGR-1-expressing cDC progenitors but express low levels of DNNGR-1 in their differentiated form (19). In pDCs *Clec9a* expression history, therefore, is not necessarily a measure of cell origin (19). The same applies to cDC1, which express high levels of DNNGR-1 and could become labeled with YFP because they express Cre in their differentiated form (19). However, cDC1 are CDP-derived (1, 11) and arise from DNNGR-1-expressing cDC progenitors upon adoptive transfer, confirming their classification as cDCs (19). Despite these limitations, *Clec9a-Cre* mice

offer a powerful means to identify cDCs as descendants from *Clec9a*-expressing cDC progenitors and to trace the cDC lineage, particularly the cDC2 subtype, which lacks DNNGR-1 in its differentiated form.

Although we have reached a consensus that cDCs arise as part of the myeloid lineage, several studies have suggested a lymphoid path to cDC development. Purified lymphoid progenitors can differentiate into cells resembling cDC1 and cDC2 after adoptive transfer and *in vitro* (41–47). This process appears to be driven by the same lineage promoting transcription factors that control cDC development from myeloid progenitors, such as IRF8 (46, 48). Additionally, B-cell receptor gene rearrangements at the IgH locus, indicative of a lymphoid past, can be found in populations of thymic cDCs, some splenic cDC1, and pDCs (49–52). Nevertheless, fate-mapping studies in steady-state mice have excluded a prominent contribution of lymphoid progenitors to the steady-state cDC pool (53, 54) and have confirmed a binary branching of lymphoid and myeloid lineages downstream of hematopoietic stem cells (21). However, whether lymphoid progenitors can serve as an alternative path to DC poiesis in conditions of inflammation or when myeloid cDC progenitors are absent has not been investigated. Because cDCs generated *in vitro* from purified human lymphoid or myeloid progenitors are indistinguishable by gene expression analysis (42), addressing this question requires faithful ontogeny-based fate-mapping models.

Here, we investigated cDC development in mice in conditions in which cDC progenitors are impaired. We crossed *Clec9a-Cre* mice to Rosa26-lox-STOP-lox-diphtheria toxin (DTA) reporter mice (55) (*Clec9a^{Cre}Rosa^{DTA}*) to constitutively deplete *Clec9a*-expressing cDC progenitors and their progeny. We found that *Clec9a^{Cre}Rosa^{DTA}* mice lack cDC progenitors and cDC1 but not cDC2. We show that in the absence of cDC progenitors, cells with features of cDC2 arise *via* an alternative developmental path. These cells show similarities to bona fide cDC2 in terms of transcriptional profile and inflammatory cytokine production but exhibit evidence of Ig receptor rearrangements, indicating a lymphoid origin. Thus, our data suggest a previously unrecognized role for lymphoid progenitors as an alternative source of cDC2, when the conventional myeloid path of cDC development is blocked.

MATERIALS AND METHODS

Mice

Clec9a-Cre (19), Rosa26-lox-STOP-lox-EYFP (56), Rosa26-lox-STOP-lox-DTA (55), Rosa26-lox-STOP-lox-DTR (57), C57BL/6J, and B6.SJL mice were bred at Cancer Research UK, at ENVIGO or the Biomedical Center in specific pathogen-free conditions. All animal experiments were performed in accordance with national and institutional guidelines for animal care and approved by the Francis Crick Institute Animal Ethics Committee, the UK Home Office, or the Regierung of Oberbayern.

Cell Isolation

Spleen and lymph nodes were cut into small pieces and digested with Collagenase IV (200 U/mL; Worthington) and DNase I (0.2 mg/mL Roche) in RPMI for 30 min at 37°C. Cells were

strained through 70- μ m cell strainers (BD Biosciences), washed with FACS buffer [PBS, 1% fetal calf serum (FCS), 2.5-mM EDTA, 0.02% sodium azide] and incubated for 2 min in red blood cell lysis buffer (Sigma). Cells were then washed and resuspended in FACS buffer. Bone marrow was isolated by flushing one femur with FACS buffer onto a cell strainer. Erythrocytes were lysed as above. Colonic single-cell suspensions were prepared as published (19).

Cell Culture

CD11c⁺ cells from spleen were enriched by positive selection using magnetic beads and LS-columns (Miltenyi), cultured in complete RPMI (10% FCS, penicillin/streptomycin, non-essential amino acids, sodium pyruvate, L-glutamine, 0.025-mM β -mercaptoethanol), and stimulated with LPS (100 ng/mL) or CpG (0.5 μ g/mL) for 2 h before addition of brefeldin A (5 μ g/mL) for an additional 4 h.

ELISA

FLT3L and G-CSF were measured with DuoSet mFLT3L (DY427) and Quantikine[®] ELISA kits (both R&D Systems) according to the manufacturer's recommendations. Other cytokines were measured by Legendplex (BioLegend).

Flow Cytometry

Data were collected on a LSR Fortessa (BD Biosciences) and analyzed with FlowJo software (Tree Star, Inc.). Cell sorting was performed on an Aria III Fusion (BD Biosciences). Antibodies used in this study can be found in Table S2 in Supplementary Material. For intracellular cytokine staining cells were fixed with 2% paraformaldehyde (15 min, room temperature), then washed in FACS buffer with 0.05% saponin and stained in 0.5% saponin. IRF8 and IRF4 were stained in Foxp3 transcription factor staining set (eBioscience-00-5523-00) and Zbtb46 in transcription factor buffer from BDBioscience-562574. Dead cells were identified with Dapi or live/dead fixable violet (Invitrogen) or zombie UV dye (Biolegend).

Microarray Analysis

CD11c⁺ cells were enriched using magnetic beads and LS columns (Miltenyi Biotec). Cells were then sorted as CD11c⁺ MHCII⁺CD11b⁺CD24⁺CD64⁺Gr-1⁻ cells from *Clec9a*^{cre/cre} *Rosa*^{DTA} mice or as YFP⁺CD11c⁺MHCII⁺CD11b⁺CD24⁺CD64⁺Gr-1⁻ cells from *Clec9a*^{cre/cre} *Rosa*^{YFP} mice. Total RNA was isolated using Qiagen RNeasy Micro Kit and prepared for hybridization on Affymetrix Mouse Gene 1.0 ST Arrays. We processed microarray data with R/bioconductor (R version 3.4.2) using the annotation package "mogene10sttranscriptcluster.db" version 8.7.0. The Robust Multichip Average (RMA) algorithm was used to extract raw expression values (library "oligo," version 1.42.0 and "pd.mogene.1.0.st.v1" version 3.14.1). We subsequently removed probe sets with zero variance and kept the ones with a median log₂ expression level higher than 4.5 in at least one condition. Many-to-one probe-sets-to-gene relationships were resolved by retaining per gene only the probe set with the highest interquartile range of expression levels across the samples. External data were merged and batch corrected using ComBat (library "sva," version 3.26.0). Principle component analysis (PCA) was

performed on 50% of the genes defined by highest variance across all samples. Heatmaps were generated using function pheatmap (library pheatmap, version 1.0.8) including gene-based scaling and clustering.

DJ-Rearrangement Polymerase Chain Reaction (PCR)

Genomic DNA was extracted by phenol chloroform extraction and 20-ng DNA were used per reaction. PCR for the IgH locus (Dfl16 and Dsp2 D gene families) (58) was split in two reactions for Germline (J3 & Mu0) and DJ-rearrangement (DH L & J3).

DHL-GGAATTTCG(AorC)TTTTTGT(CorG)AAGGGA TCTACTACTGTG;
Mu0-CCGCATGCCAAGGCTAGCCTGAAAGATTACC;
J3-GTCTAGATTCTCACAAGAGTCCGATAGACCCTGG.
IgH DJ-rearrangements for the D_HQ52 element were assessed by sequential PCRs with the following primers:
PCR-1: DHQ52-1-CACAGAGAATTCTCCATAGTTGATAGC T C A G ; D H Q 5 2 - 2 G C C T C A G A A T T C C T G T G G T C TCTGACTGGT; PCR-2: JH4-1-AGGCTCTGAGATCCCTAG ACAG; JH4-2- GGGTCTAGACTCTCAGCCGGCTCCCTC AGGG as previously described (51).

Diphtheria Toxin (DT)-Mediated Cell Ablation

Mice were injected intraperitoneally with 25 ng per gram body weight DT (SIGMA). Spleens were analyzed 24 h later.

Statistical Analysis

Statistical testing was performed using two-sided, unpaired Welch *t*-tests in GraphPad Prism 6 software (GraphPad, La Jolla, CA, USA). A *p* < 0.05 was considered significant.

RESULTS

Clec9a^{Cre/Cre} *Rosa*^{DTA} Mice Develop Myeloproliferative Disease

To generate mice lacking progeny derived from cDC-restricted progenitors, we crossed *Clec9a*-Cre mice to Rosa26-lox-STOP-lox-DTA reporter mice to induce apoptotic cell death in Cre-expressing cells and their progeny (55). We have previously shown that the penetrance of Cre-mediated recombination is increased in homozygous *Clec9a*-Cre mice without affecting specificity (19). For most experiments, we therefore generated mice homozygous for the *Clec9a*-Cre locus that were either heterozygous or homozygous for the Rosa26-lox-STOP-lox-DTA allele (henceforth referred to as *Clec9a*^{Cre/Cre} *Rosa*^{DTA} mice). *Clec9a*^{Cre/Cre} *Rosa*^{DTA} mice were born at Mendelian ratio and developed normally (not shown). With age, spleens from *Clec9a*^{Cre/Cre} *Rosa*^{DTA} mice appeared larger (not shown) and exhibited significantly increased cellularity compared to spleens from littermate controls (*Clec9a*^{+/+} *Rosa*^{DTA} or *Clec9a*^{Cre} *Rosa*^{+/+} mice, henceforth referred to as controls, **Figure 1A**). Despite prominent splenomegaly in mice 10 weeks or older, no difference in bone-marrow cellularity was observed (**Figure 1A**).

DC deficiency is associated with myeloproliferation leading to systemic neutrophilia and monocytosis (59–62). In 5-week-old mice, we observed no differences in the frequency and number of Ly-6C⁺CD11b⁺ myeloid cells but in mice 10 weeks or older Ly-6C⁺CD11b⁺ cells were significantly increased (Figures 1B,C). This age-dependent increase in Ly-6C⁺CD11b⁺ cells encompassed both neutrophils and monocytes, whereas red pulp macrophages were not affected (Figures S1A–C in Supplementary Material). Myeloproliferation in DC-deficient mice is thought to be secondary to dysregulation of growth factors, such as FLT3L, G-CSF, or GM-CSF (59, 61). *Clec9a*^{Cre/Cre} *Rosa*^{DTA} mice displayed increased serum levels of FLT3L, with a slight increase evident even before the onset of overt splenomegaly in 6-week-old mice (Figure 1D). Systemic levels of other

cytokines implicated in neutrophil and monocyte homeostasis were unaffected (Figure S1D in Supplementary Material). Of note, we could not detect GM-CSF in serum of control or *Clec9a*^{Cre/Cre} *Rosa*^{DTA} mice (unpublished observation). Therefore, *Clec9a*^{Cre/Cre} *Rosa*^{DTA} mice develop splenomegaly and exhibit increased levels of FLT3L, reminiscent of the myeloproliferative disease reported in other cDC-deficient animal models (59, 61–63).

Loss of cDC1 but Not cDC2 in *Clec9a*^{Cre/Cre} *Rosa*^{DTA} Mice

To analyze the efficiency of cDC depletion in *Clec9a*^{Cre/Cre} *Rosa*^{DTA} mice, we focused on steady-state spleen, where cDCs can reliably be identified as CD11c⁺MHCII⁺ cells and the two main cDC1 and cDC2 subsets can be distinguished as CD24⁺ and CD11b⁺ cells,

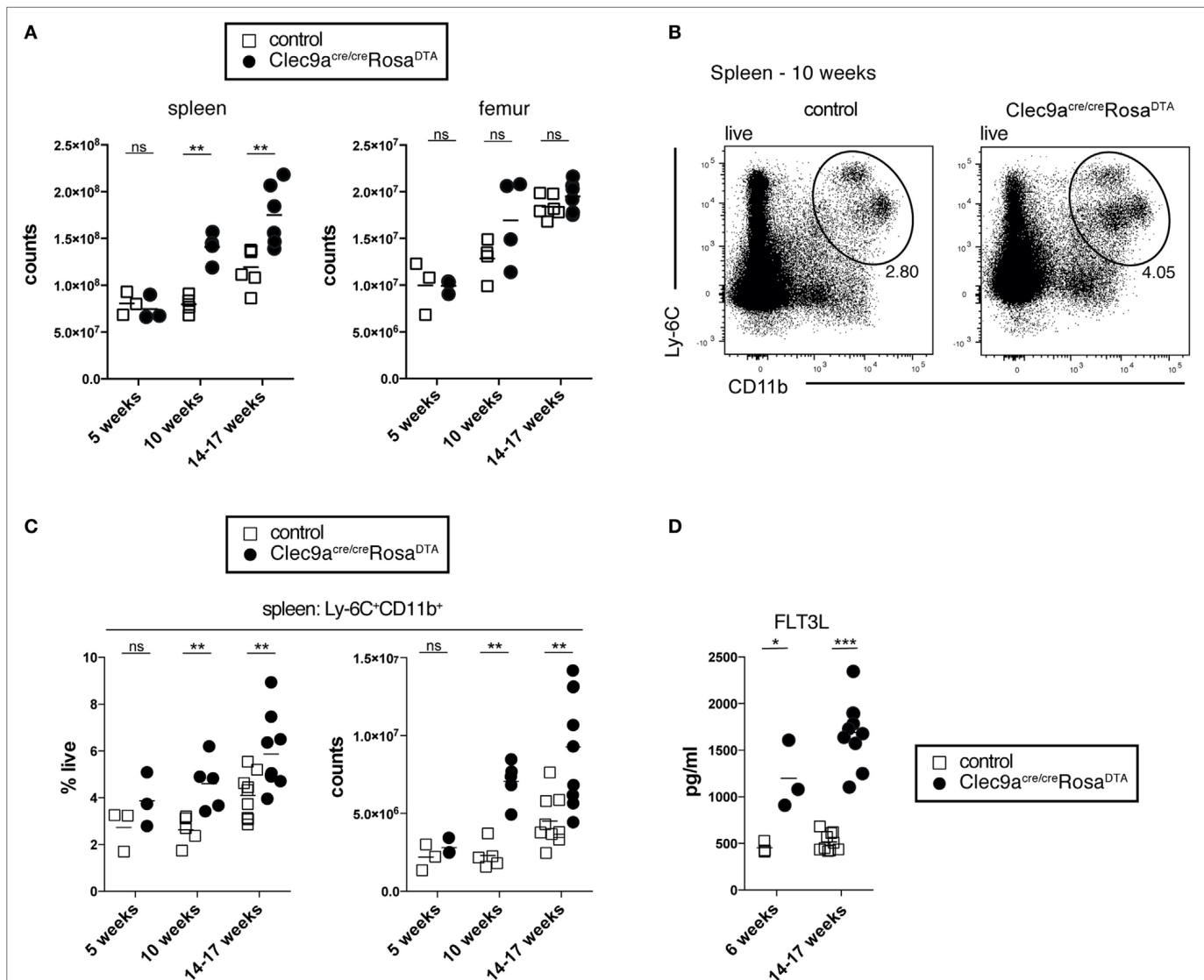


FIGURE 1 | *Clec9a*^{Cre/Cre} *Rosa*^{DTA} mice showing signs of age-dependent myeloproliferation. **(A)** The total number of leukocytes per spleen and femur from control and *Clec9a*^{Cre/Cre} *Rosa*^{DTA} mice of the indicated ages is shown. **(B,C)** Ly-6C⁺CD11b⁺ cells were identified by flow cytometry in spleen from control and *Clec9a*^{Cre/Cre} *Rosa*^{DTA} mice. **(B)** Representative gating strategy of Ly-6C⁺CD11b⁺ cells in 10-week-old mice. Plots are gated on DAPI⁺ live cells. **(C)** Frequency and total counts of Ly-6C⁺CD11b⁺ cells in mice of the indicated ages and genotypes. **(D)** Serum was collected from control and *Clec9a*^{Cre/Cre} *Rosa*^{DTA} mice at 6 and 14–17 weeks of age and the concentrations of FLT3L were determined by ELISA. Each symbol represents one mouse. ns, not significant; * $p < 0.05$, ** $p < 0.001$, and *** $p < 0.0001$.

respectively (Figure 2A) (12). At 10 weeks of age *Clec9a^{Cre/Cre}Rosa^{DTA}* mice showed a twofold reduction in the frequency of splenic cDCs compared to controls. Due to the increased organ cellularity, however, there was no effect on the absolute number of splenic CD11c⁺MHCII⁺ cells (Figures 2A,B). The same was observed in older *Clec9a^{Cre/Cre}Rosa^{DTA}* mice (14–17 weeks; Figure 2B). In 5-week-old mice that do not exhibit increased spleen cellularity, a reduction of splenic CD11c⁺MHCII⁺ cells was apparent in cell counts (Figure 2B), yet cell depletion was surprisingly inefficient (about 3.5-fold). When we further separated CD11c⁺MHCII⁺ cells into cDC1 and cDC2 using the surface markers CD24 and CD11b (Figure 2A), we found that cDC1 were completely depleted in spleens from *Clec9a^{Cre/Cre}Rosa^{DTA}* mice at all ages examined (Figure 2C and unpublished observations). In contrast, CD11b⁺cDC2 showed a significant but small reduction (Figure 2C) only in 5-week-old *Clec9a^{Cre/Cre}Rosa^{DTA}* mice and their frequency and absolute number was not reduced in mice 10 weeks or older (Figure 2C). This could be seen in other lymphoid organs, as well as in mice heterozygous for Cre expression, as the lymph nodes of *Clec9a^{+/-}Rosa^{DTA}* mice also lacked cDC1 but not resident cDC2 or migratory CD103⁺CD11b⁺ and CD103⁻CD11b⁺cDC2 (Figure S2F in Supplementary Material). Finally, these findings could be extended to non-lymphoid organs as cDC1 but not CD103⁺CD11b⁺ or CD103⁻CD11b⁺cDC2 were absent from colon of *Clec9a^{Cre/Cre}Rosa^{DTA}* mice (Figure S2G in Supplementary Material).

The lack of cDC2 depletion was surprising, as this population shows near complete fluorescent reporter labeling in *Clec9a^{Cre/Cre}Rosa^{YFP}* mice (19) and can be depleted with DT in *Clec9a-Cre* mice crossed to Rosa26-lox-STOP-lox-diphtheria toxin receptor mice (DTR; *Clec9a^{Cre/Cre}Rosa^{DTR}*) (64). We confirmed that a single injection of DT was sufficient to efficiently deplete pre-cDCs, cDC1, and cDC2 in *Clec9a^{Cre/Cre}Rosa^{DTR}* mice (Figures 2D,E; Figures S2A,B in Supplementary Material). Of note, 24 h after DT injection no increase in splenic neutrophils or monocytes was observed (Figure S2C in Supplementary Material), suggesting that *Clec9a^{Cre/Cre}Rosa^{DTR}* mice do not develop acute monocytosis and neutrophilia (62). Therefore, *Clec9a-Cre* mice serve as an efficient model to transiently deplete cDC1 and cDC2 when crossed to Rosa^{DTR} mice (64) but depletion of cDC2 is not seen when crossed to Rosa^{DTA} mice.

Fully differentiated pDCs express low levels of DNNGR-1 although they do not arise from DNNGR-1-expressing CDPs (19). Splenic pDC numbers were not altered in *Clec9a^{Cre/Cre}Rosa^{DTA}* mice (Figure S2D in Supplementary Material). However, pDCs that developed in *Clec9a^{+/-}Rosa^{DTA}* mice almost completely lacked DNNGR-1 (Figure S2E in Supplementary Material). These data suggest that DNNGR-1-expressing pDCs are depleted and replaced with DNNGR-1 negative pDCs. We conclude that constitutive depletion of DNNGR-1-expressing cells in *Clec9a^{Cre/Cre}Rosa^{DTA}* adult mice leads to a complete loss of cDC1 but not cDC2 or pDCs.

Efficient Depletion of Pre-cDCs in Bone Marrow and Spleen of *Clec9a^{Cre/Cre}Rosa^{DTA}* Mice

We next investigated whether cDC progenitors were depleted in *Clec9a^{Cre/Cre}Rosa^{DTA}* mice. As expected, *Clec9a^{Cre/Cre}*

Rosa^{DTA} mice showed no reduction in MDPs lin⁻CD11c⁻CD115⁺CD135⁺CD117^{hi} compared to control mice (Figures 3A,B). In contrast, CDPs (lin⁻CD11c⁻CD115⁺CD135⁺CD117^{low/-}) were significantly reduced in *Clec9a^{Cre/Cre}Rosa^{DTA}* mice (Figures 3A,B). High serum levels of FLT3L in *Clec9a^{Cre/Cre}Rosa^{DTA}* mice could have led to downregulation of CD135 in MDPs or CDPs, causing them to be missed in our gating. This was not the case because bone marrow lin⁻CD11c⁻CD115⁺CD117^{hi} and lin⁻CD11c⁻CD115⁺CD117^{low/-} cells from control and *Clec9a^{Cre/Cre}Rosa^{DTA}* mice expressed similar levels of CD135 (Figure 3C). Pre-cDCs, identified as lin⁻CD11c⁺CD135⁺CD172a^{low} cells, were also nearly absent in bone marrow of *Clec9a^{Cre/Cre}Rosa^{DTA}* mice when compared to controls (Figures 3A,B) and this was true when pre-cDC were also identified irrespective of the CD135 marker as the lin⁻CD11c⁺ fraction of bone marrow (Figure S3A in Supplementary Material). Similarly, in spleen, lin⁻CD11c⁺CD43⁺CD135⁺CD172a^{low} pre-cDCs were virtually absent in *Clec9a^{Cre/Cre}Rosa^{DTA}* mice, as well as heterozygous *Clec9a^{+/-}Rosa^{DTA}* mice (Figures 3D,E; Figure S3C in Supplementary Material). Although CD43⁺CD135⁻ cells were found in the splenic pre-cDC gate, those cells expressed reduced levels of CD11c, indicating that they were contaminants rather than bona fide pre-cDCs (Figures 3D–F; Figures S3B,C in Supplementary Material). A more efficient depletion of pre-cDCs compared with CDPs is to be expected because Cre-mediated DNA rearrangement in pre-cDCs is higher than in CDPs, reflecting the developmental hierarchy of DNNGR-1 expression in rapidly cycling progenitors (19). Thus, our data indicate efficient depletion of cDC progenitors in bone marrow and spleen of *Clec9a^{Cre/Cre}Rosa^{DTA}* mice and suggest that cells resembling cDC2 in *Clec9a^{Cre/Cre}Rosa^{DTA}* mice arise independently of the classical CDP and pre-cDC differentiation pathway.

cDC2 From *Clec9a^{Cre/Cre}Rosa^{DTA}* Mice Phenotypically and Functionally Resemble cDCs

Phenotypic analysis revealed that cDC2 from *Clec9a^{Cre/Cre}Rosa^{DTA}* mice showed no alterations in surface expression of the cDC markers CD172a, MHCII, CLEC4A4, and ESAM, although the expression of CD4 was slightly lower on cDC2 from *Clec9a^{Cre/Cre}Rosa^{DTA}* mice compared to controls (Figure 4A). cDC2 from *Clec9a^{Cre/Cre}Rosa^{DTA}* mice further showed normal expression of lineage defining transcription factors ZBTB46, IRF4 and IRF8 (Figure 4A). cDC2 from control and *Clec9a^{Cre/Cre}Rosa^{DTA}* mice responded similarly to stimulation with the TLR ligands lipopolysaccharide (LPS) and CpG oligonucleotides (Figure 4B). Interestingly, upon LPS treatment fewer cDC2 from *Clec9a^{Cre/Cre}Rosa^{DTA}* mice than from control mice produced TNF, whereas this was not the case for IL-12 (Figure 4B). Reduced TNF production after LPS stimulation was already present in cDC2 from young *Clec9a^{Cre/Cre}Rosa^{DTA}* mice that did not yet display myeloproliferation (Figure 4C) indicating that it was not merely a functional adaptation to the myeloproliferative environment. We conclude that cDC2 from *Clec9a^{Cre/Cre}Rosa^{DTA}* mice are broadly similar to cDC2 from control mice, other than a slight impairment in the production of TNF after LPS stimulation.

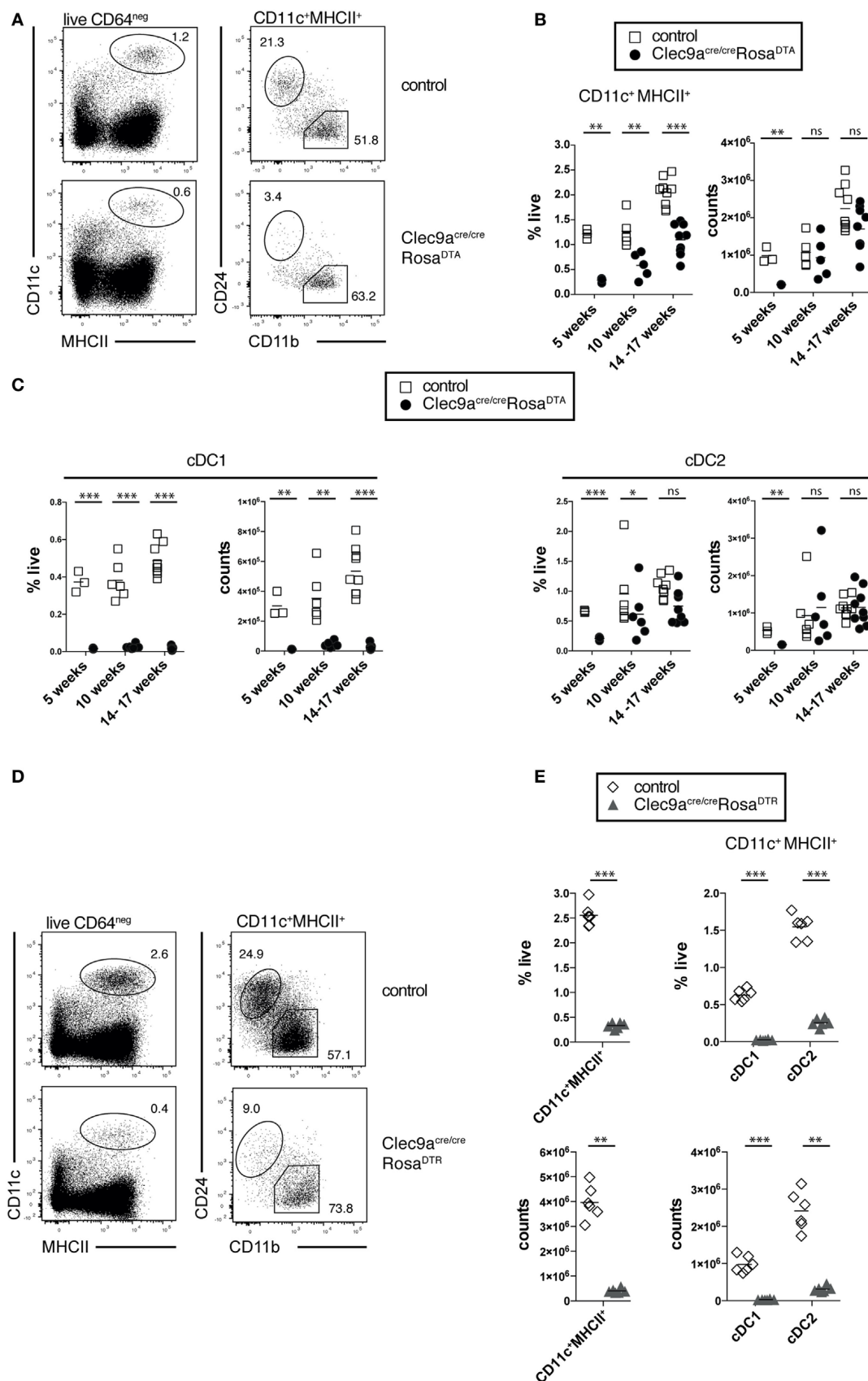


FIGURE 2 | Continued

FIGURE 2 | Loss of cDC1 but not cDC2 in spleen from *Clec9a^{Cre/Cre}Rosa^{DTA}* mice. **(A–C)** CD11c⁺MHCII⁺ conventional dendritic cells (cDCs) were identified by flow cytometry in spleen from *Clec9a^{Cre/Cre}Rosa^{DTA}* and control mice and further analyzed for CD24 and CD11b expression, to identify cDC1 and cDC2, respectively. **(A)** Representative gating strategy to identify CD11c⁺MHCII⁺ cDCs, CD24⁺ cDC1, and CD11b⁺ cDC2. **(B)** Frequency and total counts of CD11c⁺MHCII⁺ cells in spleen from control and *Clec9a^{Cre/Cre}Rosa^{DTA}* mice of the indicated ages. **(C)** Frequency and total counts of CD24⁺ cDC1 and CD11b⁺ cDC2 in mice of the indicated ages. **(D,E)** *Clec9a^{Cre/Cre}Rosa^{DTA}* and control mice were injected i.p. with DT and 24 h later spleens were analyzed by flow cytometry to identify CD11c⁺MHCII⁺ cells, as well CD24⁺ cDC1 and CD11b⁺ cDC2 **(D)**. **(E)** The frequency and counts of total cDCs and cDC subsets identified as in **(D)**. Each symbol represents one mouse. ns, not significant; * $p < 0.05$, ** $p < 0.001$, and *** $p < 0.0001$.

cDC2 From *Clec9a^{Cre/Cre}Rosa^{DTA}* Mice Are Transcriptionally Similar to Bona Fide cDC2 but Exhibit Somatic Rearrangements of Lymphoid Receptor Genes

We next performed whole transcriptome profiling by microarray of cDC2 from *Clec9a^{Cre/Cre}Rosa^{DTA}* mice. To this end, we sorted splenic CD11c⁺MHCII⁺CD11b⁺ cDC2 from *Clec9a^{Cre/Cre}Rosa^{DTA}* mice (CD11b⁺ *DTA*) and compared their mRNA profile to that of cDC2 sorted as YFP⁺CD11c⁺MHCII⁺CD11b⁺ cells from *Clec9a^{Cre/Cre}Rosa^{YFP}* mice (YFP⁺; **Figure 5**; Figure S3 and Table S1 in Supplementary Material). We chose this experimental strategy to ensure comparison to bona fide cDC2 arising from *Clec9a*-expressing myeloid cDC progenitors. Our analysis revealed surprisingly few differences in gene expression, indicating that cDC2 from *Clec9a^{Cre/Cre}Rosa^{DTA}* mice are very similar to YFP⁺ cDC2. Interestingly, among the 50 most significantly differentially expressed genes, only 11 showed more than a twofold difference and we found CD135 as a top hit (Table S1 in Supplementary Material). The expression of CD135 was about twofold lower in cDC2 from *Clec9a^{Cre/Cre}Rosa^{DTA}* mice than in YFP⁺ cDC2 (Table S1 in Supplementary Material), raising the possibility that expression of the lineage defining marker CD135 may be dysregulated at the mRNA level. Consistent with that notion, staining for CD135 was reduced on cDC2 from *Clec9a^{Cre/Cre}Rosa^{DTA}* mice (**Figure 4A**). However, incubation of cDCs with FLT3L inhibited CD135 staining intensity, even in conditions in which endocytosis should be blocked (Figure S3D in Supplementary Material), suggesting that, when occupied by FLT3L, CD135 may no longer be freely available for antibody binding. Therefore, decreased CD135 staining on cDC2 from *Clec9a^{Cre/Cre}Rosa^{DTA}* mice may reflect the fact that the receptor is engaged by FLT3L, as well as a possible reduction in gene expression. We next used cDC and macrophage core gene signatures (65) and performed unsupervised hierarchical clustering of cDC2 from *Clec9a^{Cre/Cre}Rosa^{DTA}* mice and YFP⁺ cDC2 in the context of published datasets for cDC and macrophage populations from the Immgen database. When compared in this manner cDC2 from *Clec9a^{Cre/Cre}Rosa^{DTA}* mice and YFP⁺ cDC2 showed greater similarity to splenic cDC2 than to cDC1 or red pulp macrophages (**Figures 5A,B**; Figure S3 in Supplementary Material). cDC2 from *Clec9a^{Cre/Cre}Rosa^{DTA}* mice did not display a migratory cDC signature (Figure S4 in Supplementary Material), suggesting that they are not cDC2 that have aberrantly migrated from the periphery.

We next performed principal component analysis (PCA) in the context of published datasets for splenic cDCs, thymic cDCs, migratory cDCs, splenic pDCs, macrophages, and monocytes.

Notably, cDC2 from *Clec9a^{Cre/Cre}Rosa^{DTA}* mice were most closely related to YFP⁺ cDC2 and splenic cDC2 and clustered far away from monocytes/macrophages, thymic cDCs, or pDCs (**Figure 5C**). In humans, a subset of cDC2 has been identified that appears to be related to pDCs (66). These cells can be distinguished from cDC2 and pDCs by expression of signature genes, including *Axl*, *Pp1rb*, *Dab2*, *CD22*, and *IL3Ra* (66). However, we found no enrichment of the *Axl* gene signature in cDC2 from *Clec9a^{Cre/Cre}Rosa^{DTA}* mice compared with YFP⁺ cDC2 (**Figure 5D**). Taken together, these data demonstrate that cDC2 from *Clec9a^{Cre/Cre}Rosa^{DTA}* mice do not show a comprehensive loss of cDC identity and resemble cDC2 from wild type mice.

CLPs can give rise to cDCs *in vivo* and *in vitro* under certain conditions (41–48) and pDCs in normal mice can originate from myeloid or lymphoid progenitors that appear phenotypically indistinguishable except for a history of RAG expression in those originating from the latter (50, 67–69). We therefore sorted CD11b⁺CD11c⁺MHCII⁺ cells from control and *Clec9a^{Cre/Cre}Rosa^{DTA}* mice (**Figures 5E,F**; Figures S5A–C in Supplementary Material) and performed PCR analysis for Ig gene rearrangements indicative of historical RAG activity. Sorted pDCs from control mice exhibited prominent Ig gene rearrangements (**Figures 5E,F**; Figure S5C in Supplementary Material), as reported (49, 50), serving as a positive control. Strikingly, cDC2 from *Clec9a^{Cre/Cre}Rosa^{DTA}* mice also showed clear evidence of Ig gene rearrangements, which were completely absent in cDC2 from control mice (**Figures 5E,F**; Figure S5C in Supplementary Material). In summary, cDC2 that arise in the absence of *Clec9a*-expressing cDC progenitors are transcriptionally similar to bona fide cDC2 but they exhibit RAG gene expression history in the form of D–J somatic rearrangements, indicating a putative lymphoid origin.

DISCUSSION

Although the existence of a lymphoid path to cDC development in mice has been suggested (43, 47, 49, 50, 70), in steady-state cDCs arise primarily from myeloid progenitors (53). Here, we report the generation of *Clec9a^{Cre/Cre}Rosa^{DTA}* mice as a model to constitutively deplete *Clec9a*-expressing cDC progenitors and their progeny. We show that in the absence of these myeloid-derived cDC progenitors, cells that are phenotypically and transcriptionally similar to bona fide cDC2 develop in spleen. These cells show RAG gene expression history in the form of D–J rearrangements at the IgH locus indicating a relation to the lymphoid branch of hematopoiesis. Therefore, our study suggests that lymphopoiesis can contribute to the generation of cDC-like cells in a situation in which myeloid cDC progenitors are impaired. This observation opens an interesting conundrum, namely, whether such cells

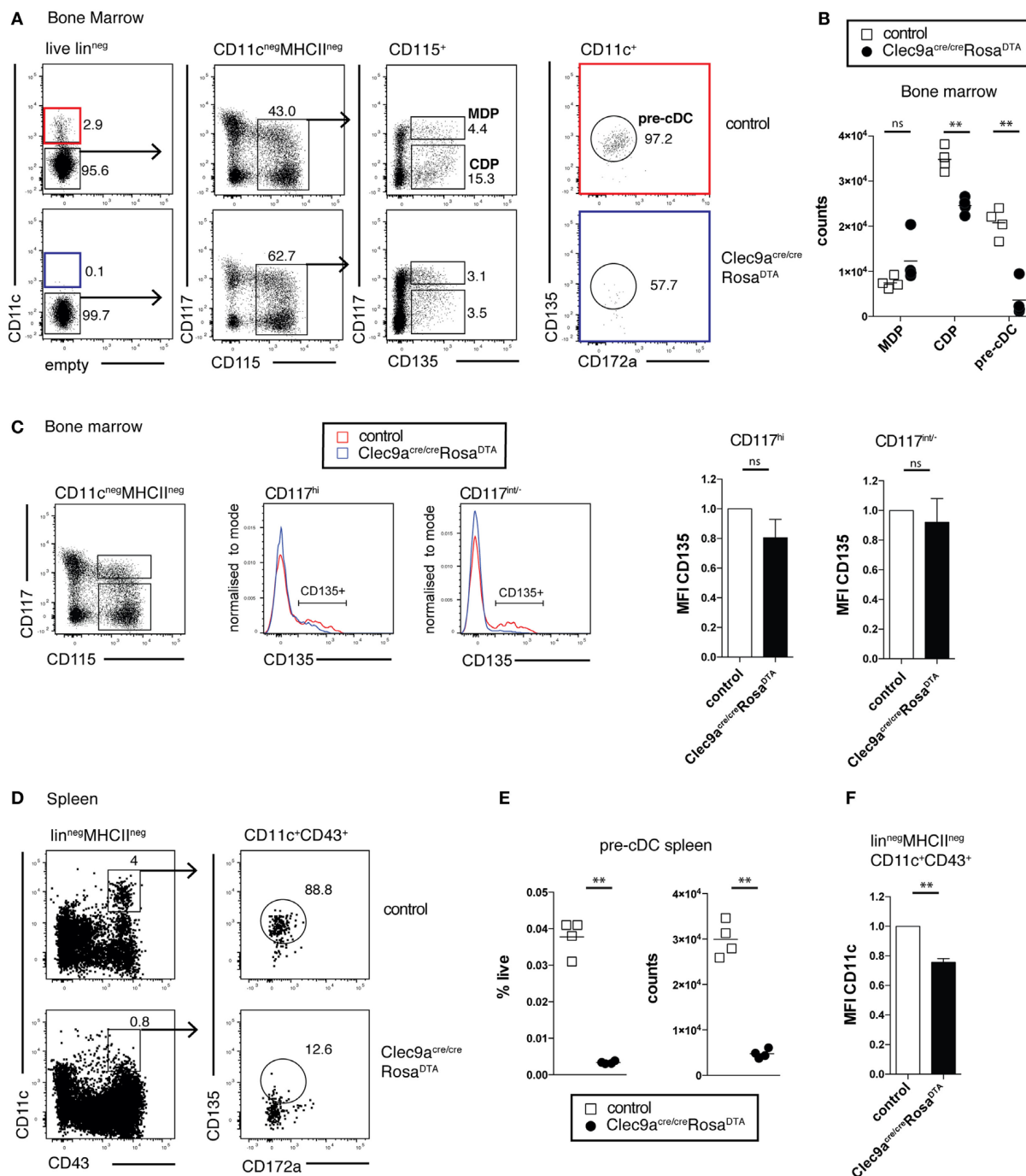


FIGURE 3 | Efficient depletion of conventional dendritic cell (cDC) progenitors in bone marrow and spleen. **(A,B)** cDC progenitors were identified by flow cytometry in the bone marrow of 10-week-old control and *Clec9a^{cre/cre}Rosa^{DTA}* mice. **(A)** Live lineage negative (lin⁻; CD3, CD4, CD8, CD11b, MHCII, Ter119, NK1.1, and B220) cells were gated and further analyzed for CD11c, CD117, CD115, CD172a, and CD135 expression. Macrophage and DC progenitor (MDPs) were identified as CD11c⁻CD115⁺CD135⁺CD117^{hi} cells, common DC progenitors (CDPs) as CD11c⁻CD115⁺CD135⁺CD117^{int/-} cells, and pre-cDCs as CD11c⁺CD172a^{int}CD135⁺ cells. **(B)** The number of MDP, CDP, and pre-cDC per femur is shown. **(C)** Lin⁻CD115⁺CD117^{hi} and lin⁻CD115⁺CD117^{int/-} bone-marrow cells from control and *Clec9a^{cre/cre}Rosa^{DTA}* mice were gated and further analyzed for CD135 expression. Mean fluorescence intensity (MFI) ($n = 4$) of the CD135⁺ cell fraction, as gated in the histogram overlays, is shown. It was normalized to MFI on the same population from control mice, which is set as 1. **(D–F)** Pre-cDCs in spleen from control and *Clec9a^{cre/cre}Rosa^{DTA}* mice 10 weeks of age were identified as lin⁻CD11c⁺CD43⁺CD172a^{int}CD135⁺ cells by flow cytometry **(D)**. **(E)** The frequency and number of pre-cDCs per spleen is shown. **(F)** CD11c MFI on splenic lin⁻MHCII⁻CD11c⁺CD43⁺ cells from *Clec9a^{cre/cre}Rosa^{DTA}* mice is shown. It was normalized to MFI on the same population from control mice, which is set as 1 ($n = 4$). Each symbol represents one mouse. ns, not significant; * $p < 0.05$, ** $p < 0.001$, and *** $p < 0.0001$.

should be considered part of the cDC lineage. We and others have proposed that mononuclear phagocytes should predominantly be defined on the basis of their ontogeny (12, 71, 72). However,

environmental imprinting appears to be a major identity determining criterion for mononuclear phagocytes (73–77). Therefore, an ontogenetic view to cell definition may be less tenable if cell

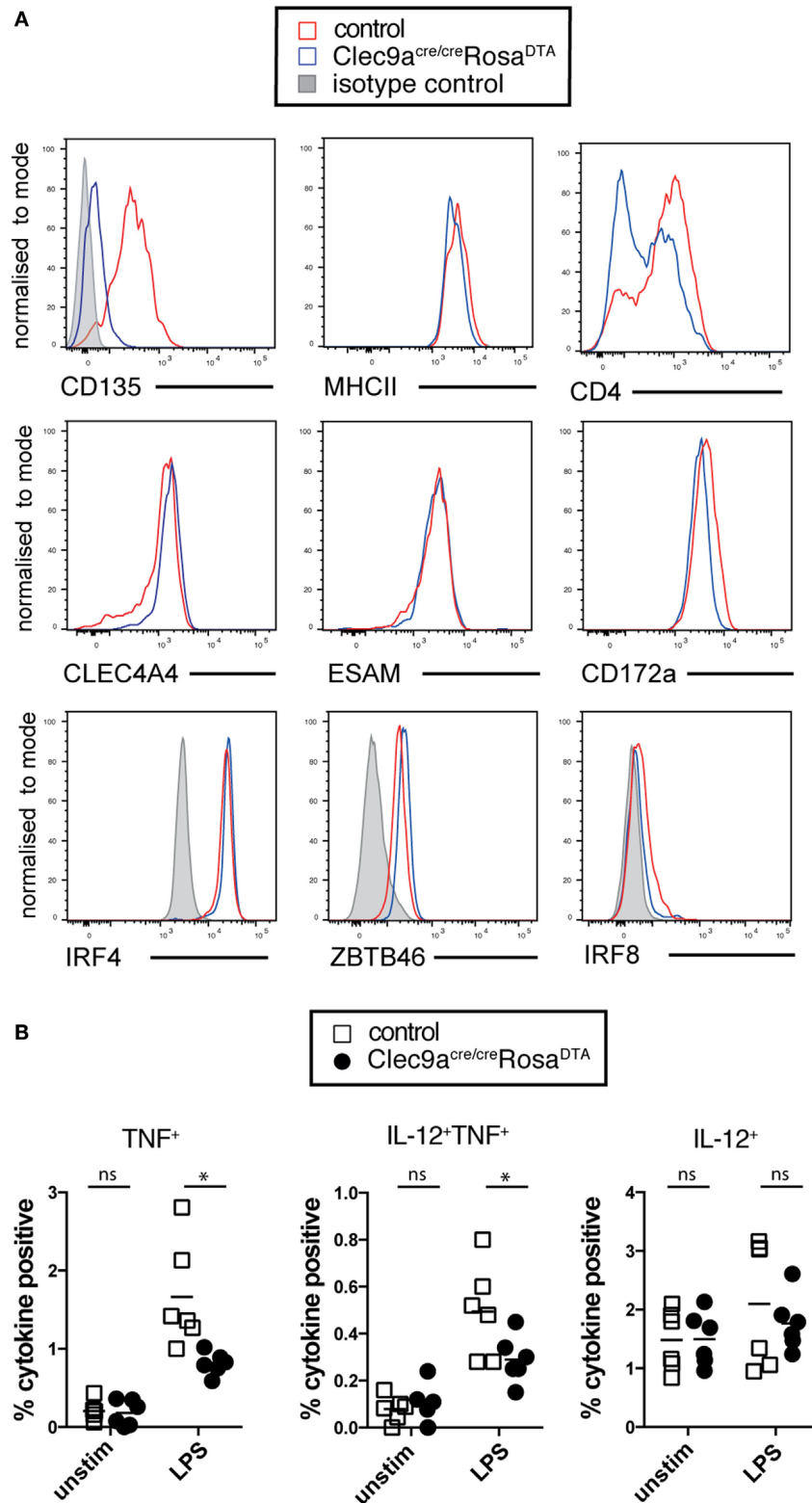


FIGURE 4 | Continued

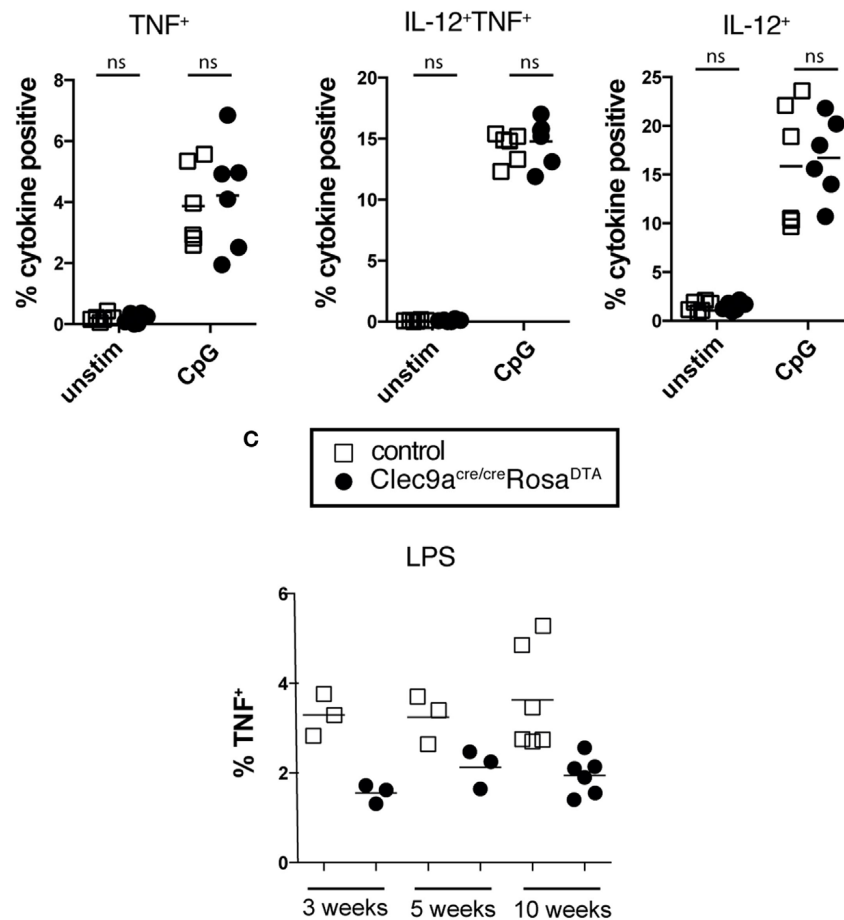


FIGURE 4 | cDC2 from *Clec9a^{Cre/Cre}Rosa^{DTA}* mice phenotypically and functionally resemble cDCs. **(A)** Splenic CD11c⁺MHCII⁺CD11b⁺ cells from control (red) and *Clec9a^{Cre/Cre}Rosa^{DTA}* (blue) mice were analyzed for the expression of indicated surface markers or transcription factors (lower line) by flow cytometry. Gray traces represent staining with isotype matched control antibody. **(B,C)** CD11c⁺ cells from control and *Clec9a^{Cre/Cre}Rosa^{DTA}* mice of the indicated ages were enriched using magnetic beads, stimulated with lipopolysaccharide (LPS) (100 ng/mL) or CpG (0.5 µg/mL) for 6 h followed by intracellular cytokine staining. CD11c⁺MHCII⁺CD11b⁺ cDC2 were identified by flow cytometry and TNF and IL-12 production was analyzed. **(B)** The frequency of cytokine positive cDC2 is shown. **(C)** Frequency of TNF producing cDC2 from mice of the indicated ages stimulated with LPS. Each data point represents one mouse. Data are compiled from two independent experiments. * $p < 0.05$.

populations with different origins turn out to be identical by all measures examined. Because cDC2 in *Clec9a^{Cre/Cre}Rosa^{DTA}* mice are not CDP-derived but show lymphoid gene expression history, we suggest to refer to these cells as lymphoid DC2 for the time being (12). Although we find strong similarities between cDC2 and lymphoid DC2, additional studies are necessary to further define the transcriptional and growth factor requirements, as well as functional properties of lymphoid DC2 to firmly establish their lineage affiliation and determine whether these cells should be considered a new type of mononuclear phagocyte (12).

As cDC differentiation from precursors is thought to be homeostatically regulated by the size of the mature cDC pool (78, 79), we cannot formally exclude at this point that some CDPs escape deletion in *Clec9a^{Cre/Cre}Rosa^{DTA}* mice to preferentially expand and contribute to the cDC2 population. However, our data demonstrate that at least part of the cDC2 pool in *Clec9a^{Cre/Cre}Rosa^{DTA}* mice derives from a cell type that has undergone Ig gene rearrangement and that pool is therefore qualitatively distinct from CDP-derived cDC2. Whether these ontogenetically

distinct cDC2s arise from early lymphoid-committed progenitors, such as CLPs, is an attractive possibility that will need to be explored. However, it is worth mentioning that some myeloid progenitors reportedly express RAG1 and can generate pDCs with D-J rearrangements *in vitro* (50). Such RAG1-expressing myeloid progenitors, which would presumably lack DNCR-1, could contribute to cDC2 generation in *Clec9a^{Cre/Cre}Rosa^{DTA}* mice, in which case our designation of these cells as “lymphoid cDC2” would be incorrect. Finally, it is possible that pDCs, some of which have a lymphoid past (49, 50), could convert to lymphoid cDC2 in the FLT3L-rich environment of *Clec9a^{Cre/Cre}Rosa^{DTA}* mice, although this is difficult to reconcile with the fact that we failed to find any pDC-specific transcripts in lymphoid DC2 (Figure 5 and unpublished observations). Another intriguing observation is that lymphoid DC2 display decreased surface staining for CD135. Gene expression analysis suggests that CD135 may be dysregulated at the RNA level (Figure 5). However, it is equally possible that CD135 could be downregulated upon continuous receptor engagement by FLT3L (80) or may no longer be available



FIGURE 5 | cDC2 from *Clec9a^{Cre/Cre}Rosa^{DTA}* mice are transcriptionally similar to bona fide cDC2 but exhibit somatic rearrangements of lymphoid receptor genes. Splenic CD11c⁺MHCII⁺CD11b⁺ cDC2 from *Clec9a^{Cre/Cre}Rosa^{DTA}* mice (CD11b⁺ DTA) and CD11c⁺MHCII⁺CD11b⁺YFP⁺ cDC2 (YFP⁺) from *Clec9a^{Cre/Cre}Rosa^{YFP}* mice were sorted and subjected to microarray analysis. **(A,B)** Population clustering and heat map display of the relative expression values for core conventional dendritic cells (cDC) signature genes **(A)** and core CD8^{neg} cDC signature genes **(B)** comparing cDC2 from *Clec9a^{Cre/Cre}Rosa^{DTA}* mice and YFP⁺ cDC2 to the indicated murine cDC and macrophage populations from the Immgen database. **(C)** Principle component analysis (PCA) was performed on 50% of the genes defined by highest variance across all samples. Each dot of the same color represents a replicate sample. For each cluster, normal confidence ellipses are indicated. **(D)** Box plots of the log₂ expression values of the indicated genes in cDC2 from *Clec9a^{Cre/Cre}Rosa^{DTA}* mice and YFP⁺ cDC2. **(E,F)** CD11c⁺MHCII⁺CD11b⁺ cDC2 from control and *Clec9a^{Cre/Cre}Rosa^{DTA}* mice were sorted and genomic DNA was isolated. **(E)** Polymerase chain reaction (PCR) was performed using primers for the germline (GL) locus and primer mixtures homologous for regions of the Df116 and Dsp2 D gene families for detecting D–J rearrangements of the IgH chain. DJ rearrangements in pDCs (SiglecH⁺B220⁺) and neutrophils (Ly-6G⁺) are shown as control. * indicates an unspecific band. **(F)** Genomic PCR was performed using primers for the GL locus and primer sets for the D_HQ52 element for detecting D–J rearrangements of the IgH chain. DJ rearrangements in pDCs (SiglecH⁺B220⁺), CD205⁺ cDC1, and neutrophils (Ly-6G⁺) are shown as control. Each lane in E and F represents independent replicates from different mice.

for antibody binding (Figure S3D in Supplementary Material). As FLT3L-deficient mice lack all cDCs (33, 81), it is unlikely that lymphoid DC2 arise independently of FLT3L. It will be important to determine whether different growth factors may preferentially promote the differentiation of lymphoid and myeloid progenitors into cDCs.

The fact that lymphoid DC2 are strikingly similar to bona fide cDC2 of myeloid origin in terms of transcriptional profile is in agreement with data demonstrating that *in vitro* generated human myeloid-derived cDC1 are indistinguishable from ones derived from human lymphoid-committed progenitors (42). These data suggest a primary role for the environment in the functional imprinting of cDCs, similar to observations made for macrophages and monocytes (73–76). Despite functional similarities between lymphoid DC2 and cDC2 *in vitro*, these cells respond somewhat differently to the TLR ligand LPS. These data raise the possibility that lymphoid DC2 are not fully functionally equivalent to cDC2, which needs to be addressed experimentally in more detail. In this context, it is noteworthy that *Clec9a^{Cre/Cre}Rosa^{DTA}* mice develop signs of systemic myeloproliferation, which is typical of mice lacking both cDC1 and cDC2 but has not been reported in mice lacking only the cDC1 subset (82, 83).

It will be important to determine whether additional situations exist where a lymphoid path may contribute to generating or replacing bona fide cDC2, either to ensure functional redundancy or to mediate specific immune functions. Notably, RAG-expressing immune-restricted progenitors contribute to embryonic myelopoiesis in the fetal liver and, although this occurs before the onset of definitive hematopoiesis (84), it indicates that lymphoid and myeloid lineage decisions are not always binary. During emergency hematopoiesis distinct monocyte progenitors have been suggested to respond to inflammatory stimuli on a per need basis, yielding a situation-adapted repertoire of inflammatory monocytes (85). It is intriguing to speculate that, in a similar manner, lymphoid and myeloid progenitors may be differentially

triggered in certain conditions of inflammation to generate lymphoid DC2 and cDC2, respectively.

ETHICS STATEMENT

All animal experiments were performed in accordance with national and institutional guidelines for animal care and approved by the Francis Crick Institute Animal Ethics Committee, the UK Home Office, or the Regierung of Oberbayern.

AUTHOR CONTRIBUTIONS

JS and BS planned and performed experiments. JB, NP, SR, MP, DP, NR, and SJK performed experiments. TS performed Microarray analysis. JS, BS, and CRS wrote the manuscript. BS and CRS designed the study.

ACKNOWLEDGMENTS

We thank members of the Schraml lab for helpful discussions and critical reading of the manuscript. We also thank members of the Brouck and Krug laboratories for technical help. This work was supported by the German Research Foundation Emmy Noether Grant: Schr 1444/1-1 (to BS) and SFB914- project A11 (to BS), by The Francis Crick Institute (to CRS), which receives core funding from Cancer Research UK (FC001136), the UK Medical Research Council (FC001136), and the Wellcome Trust (FC001136), by an ERC Starting Grant awarded to BS (ERC-2016-STG-715182), and an ERC Advanced Investigator grant awarded to CRS (2010-AdG-268670).

SUPPLEMENTARY MATERIAL

The Supplementary Material for this article can be found online at <https://www.frontiersin.org/articles/10.3389/fimmu.2018.00699/full#supplementary-material>.

REFERENCES

- Merad M, Sathe P, Helft J, Miller J, Mortha A. The dendritic cell lineage: ontogeny and function of dendritic cells and their subsets in the steady state and the inflamed setting. *Annu Rev Immunol* (2013) 31:563–604. doi:10.1146/annurev-immunol-020711-074950
- Steinman RM, Idoyaga J. Features of the dendritic cell lineage. *Immunol Rev* (2010) 234:5–17. doi:10.1111/j.0105-2896.2009.00888.x
- Schlitzer A, Ginhoux F. Organization of the mouse and human DC network. *Curr Opin Immunol* (2014) 26:90–9. doi:10.1016/j.coi.2013.11.002
- Durai V, Murphy KM. Functions of murine dendritic cells. *Immunity* (2016) 45:719–36. doi:10.1016/j.immuni.2016.10.010

5. Briseño CG, Murphy TL, Murphy KM. Complementary diversification of dendritic cells and innate lymphoid cells. *Curr Opin Immunol* (2014) 29:69–78. doi:10.1016/j.coi.2014.04.006
6. Satpathy AT, Briseño CG, Briseño GC, Lee JS, Ng D, Manieri NA, et al. Notch2-dependent classical dendritic cells orchestrate intestinal immunity to attaching-and-effacing bacterial pathogens. *Nat Immunol* (2013) 14:937–48. doi:10.1038/ni.2679
7. Kinnebrew MA, Buffie CG, Diehl GE, Zenewicz LA, Leiner I, Hohl TM, et al. Interleukin 23 production by intestinal CD103(+)CD11b(+) dendritic cells in response to bacterial flagellin enhances mucosal innate immune defense. *Immunity* (2012) 36:276–87. doi:10.1016/j.immuni.2011.12.011
8. Arora P, Baena A, Yu KO, Saini NK, Kharkwal SS, Goldberg ME, et al. A single subset of dendritic cells controls the cytokine bias of natural killer T cell responses to diverse glycolipid antigens. *Immunity* (2014) 40:105–16. doi:10.1016/j.immuni.2013.12.004
9. Loschko J, Schreiber HA, Rieke GJ, Esterházy D, Meredith MM, Pedicord VA, et al. Absence of MHC class II on cDCs results in microbial-dependent intestinal inflammation. *J Exp Med* (2016) 213:517–34. doi:10.1084/jem.20160062
10. Naik S, Bouladoux N, Linehan JL, Han S-J, Harrison OJ, Wilhelm C, et al. Commensal-dendritic-cell interaction specifies a unique protective skin immune signature. *Nature* (2015) 520:104–8. doi:10.1038/nature14052
11. Murphy TL, Grajales-Reyes GE, Wu X, Tussiwand R, Briseño CG, Iwata A, et al. Transcriptional control of dendritic cell development. *Annu Rev Immunol* (2015) 34:93–119. doi:10.1146/annurev-immunol-032713-120204
12. Guillems M, Ginhoux F, Jakubczak C, Naik SH, Onai N, Schraml BU, et al. Dendritic cells, monocytes and macrophages: a unified nomenclature based on ontogeny. *Nat Rev Immunol* (2014) 14:571–8. doi:10.1038/nri3712
13. Tussiwand R, Everts B, Grajales-Reyes GE, Kretzer NM, Iwata A, Bagaitkar J, et al. Klf4 expression in conventional dendritic cells is required for T helper 2 cell responses. *Immunity* (2015) 42:916–28. doi:10.1016/j.immuni.2015.04.017
14. Scott CL, Soen B, Martens L, Skrypek N, Saelens W, Taminiau J, et al. The transcription factor Zeb2 regulates development of conventional and plasmacytoid DCs by repressing Id2. *J Exp Med* (2016) 213(6):897–911. doi:10.1084/jem.20151715
15. Wu X, Briseño CG, Grajales-Reyes GE, Haldar M, Iwata A, Kretzer NM, et al. Transcription factor Zeb2 regulates commitment to plasmacytoid dendritic cell and monocyte fate. *Proc Natl Acad Sci U S A* (2016) 113:14775–80. doi:10.1073/pnas.1611408114
16. Guillems M, Dutertre C-A, Scott CL, McGovern N, Sichien D, Chakarov S, et al. Unsupervised high-dimensional analysis aligns dendritic cells across tissues and species. *Immunity* (2016) 45:669–84. doi:10.1016/j.immuni.2016.08.015
17. Schlitzer A, McGovern N, Teo P, Zelante T, Atarashi K, Low D, et al. IRF4 transcription factor-dependent CD11b+ dendritic cells in human and mouse control mucosal IL-17 cytokine responses. *Immunity* (2013) 38:970–83. doi:10.1016/j.immuni.2013.04.011
18. Persson EK, Uronen-Hansson H, Semmrich M, Rivollier A, Hägerbrand K, Marsal J, et al. IRF4 transcription-factor-dependent CD103(+)CD11b(+) dendritic cells drive mucosal T helper 17 cell differentiation. *Immunity* (2013) 38:958–69. doi:10.1016/j.immuni.2013.03.009
19. Schraml BU, van Blijswijk J, Zelenay S, Whitney PG, Filby A, Acton SE, et al. Genetic tracing via DNGR-1 expression history defines dendritic cells as a hematopoietic lineage. *Cell* (2013) 154:843–58. doi:10.1016/j.cell.2013.07.014
20. Naik SH, Perié L, Swart E, Gerlach C, van Rooij N, de Boer RJ, et al. Diverse and heritable lineage imprinting of early haematopoietic progenitors. *Nature* (2013) 496:229–32. doi:10.1038/nature12013
21. Pei W, Feyerabend TB, Rössler J, Wang X, Postrach D, Busch K, et al. Polylox barcoding reveals haematopoietic stem cell fates realized in vivo. *Nature* (2017) 548:456–60. doi:10.1038/nature23653
22. Paul F, Arkin Y, Giladi A, Jaitin DA, Kenigsberg E, Keren-Shaul H, et al. Transcriptional heterogeneity and lineage commitment in myeloid progenitors. *Cell* (2015) 163:1663–77. doi:10.1016/j.cell.2015.11.013
23. Perié L, Duffy KR, Kok L, de Boer RJ, Schumacher TN. The branching point in erythro-myeloid differentiation. *Cell* (2015) 163:1655–62. doi:10.1016/j.cell.2015.11.059
24. Schultze JL, Beyer M. Myelopoiesis reloaded: single-cell transcriptomics leads the way. *Immunity* (2016) 44:18–20. doi:10.1016/j.immuni.2015.12.019
25. Fogg DK, Sibon C, Miled C, Jung S, Aucouturier P, Littman DR, et al. A clonogenic bone marrow progenitor specific for macrophages and dendritic cells. *Science* (2006) 311:83–7. doi:10.1126/science.1117729
26. Auffray C, Fogg DK, Narni-Mancinelli E, Senechal B, Trouillet C, Saederup N, et al. CX3CR1+ CD115+ CD135+ common macrophage/DC precursors and the role of CX3CR1 in their response to inflammation. *J Exp Med* (2009) 206:595–606. doi:10.1084/jem.20081385
27. Sathe P, Metcalf D, Vremec D, Naik SH, Langdon WY, Huntington ND, et al. Lymphoid tissue and plasmacytoid dendritic cells and macrophages do not share a common macrophage-dendritic cell-restricted progenitor. *Immunity* (2014) 41:104–15. doi:10.1016/j.immuni.2014.05.020
28. Hettinger J, Richards DM, Hansson J, Barra MM, Joschko A-C, Krijgsvelde J, et al. Origin of monocytes and macrophages in a committed progenitor. *Nat Immunol* (2013) 14:821–30. doi:10.1038/ni.2638
29. Onai N, Obata-Onai A, Schmid MA, Ohteki T, Jarrossay D, Manz MG. Identification of clonogenic common Flt3+M-CSFR+ plasmacytoid and conventional dendritic cell progenitors in mouse bone marrow. *Nat Immunol* (2007) 8:1207–16. doi:10.1038/ni1518
30. Naik SH, Sathe P, Park H-Y, Metcalf D, Proietto AI, Dakic A, et al. Development of plasmacytoid and conventional dendritic cell subtypes from single precursor cells derived in vitro and in vivo. *Nat Immunol* (2007) 8:1217–26. doi:10.1038/ni1522
31. Liu K, Victoria GD, Schwickert TA, Guernonprez P, Meredith MM, Yao K, et al. In vivo analysis of dendritic cell development and homeostasis. *Science* (2009) 324:392–7. doi:10.1126/science.1170540
32. Naik SH, Metcalf D, Van Nieuwenhuijze A, Wicks I, Wu L, O’Keeffe M, et al. Intrasplenic steady-state dendritic cell precursors that are distinct from monocytes. *Nat Immunol* (2006) 7:663–71. doi:10.1038/ni1340
33. Ginhoux F, Liu K, Helft J, Bogunovic M, Greter M, Hashimoto D, et al. The origin and development of nonlymphoid tissue CD103+ DCs. *J Exp Med* (2009) 206:3115–30. doi:10.1084/jem.20091756
34. Grajales-Reyes GE, Iwata A, Albringer J, Wu X, Tussiwand R, Kc W, et al. Batf3 maintains autoactivation of Irf8 for commitment of a CD8 α (+) conventional DC clonogenic progenitor. *Nat Immunol* (2015) 16:708–17. doi:10.1038/ni.3197
35. Schlitzer A, Sivakamasundari V, Chen J, Sumatoh HRB, Schreuder J, Lum J, et al. Identification of cDC1- and cDC2-committed DC progenitors reveals early lineage priming at the common DC progenitor stage in the bone marrow. *Nat Immunol* (2015) 16:718–28. doi:10.1038/ni.3200
36. Breton G, Lee J, Zhou YJ, Schreiber JJ, Keler T, Pühr S, et al. Circulating precursors of human CD1c+ and CD141+ dendritic cells. *J Exp Med* (2015) 212:401–13. doi:10.1084/jem.20141441
37. Breton G, Zheng S, Valieris R, Tojal da Silva I, Satija R, Nussenzweig MC. Human dendritic cells (DCs) are derived from distinct circulating precursors that are precommitted to become CD1c+ or CD141+ DCs. *J Exp Med* (2016) 213:2861–70. doi:10.1084/jem.20161135
38. Lee J, Breton G, Oliveira TYK, Zhou YJ, Aljoufi A, Pühr S, et al. Restricted dendritic cell and monocyte progenitors in human cord blood and bone marrow. *J Exp Med* (2015) 212:385–99. doi:10.1084/jem.20141442
39. Poulin LF, Reyat Y, Uronen-Hansson H, Schraml BU, Sancho D, Murphy KM, et al. DNGR-1 is a specific and universal marker of mouse and human Batf3-dependent dendritic cells in lymphoid and nonlymphoid tissues. *Blood* (2012) 119:6052–62. doi:10.1182/blood-2012-01-406967
40. Collin M, Bigley V, Haniiffa M, Hambleton S. Human dendritic cell deficiency: the missing ID? *Nat Rev Immunol* (2011) 11:575–83. doi:10.1038/nri3046
41. Manz MG, Traver D, Miyamoto T, Weissman IL, Akashi K. Dendritic cell potentials of early lymphoid and myeloid progenitors. *Blood* (2001) 97:3333–41. doi:10.1182/blood.V97.11.3333
42. Helft J, Anjos-Afonso F, Van der Veen AG, Chakravarty P, Bonnet D, Reis e Sousa C. Dendritic cell lineage potential in human early hematopoietic progenitors. *Cell Rep* (2017) 20:529–37. doi:10.1016/j.celrep.2017.06.075
43. Izon D, Rudd K, DeMuth W, Pear WS, Clendenin C, Lindsley RC, et al. A common pathway for dendritic cell and early B cell development. *J Immunol* (2001) 167:1387–92. doi:10.4049/jimmunol.167.3.1387
44. Ardavin C, Wu L, Li CL, Shortman K. Thymic dendritic cells and T cells develop simultaneously in the thymus from a common precursor population. *Nature* (1993) 362:761–3. doi:10.1038/362761a0
45. Welner RS, Esplin BL, Garrett KP, Pelayo R, Luche H, Fehling HJ, et al. Asynchronous RAG-1 expression during B lymphopoiesis. *J Immunol* (2009) 183:7768–77. doi:10.4049/jimmunol.0902333
46. Becker AM, Michael DG, Satpathy AT, Sciammas R, Singh H, Bhattacharya D. IRF-8 extinguishes neutrophil production and promotes dendritic cell lineage

- commitment in both myeloid and lymphoid mouse progenitors. *Blood* (2012) 119:2003–12. doi:10.1182/blood-2011-06-364976
47. Wu L, D'Amico A, Hochrein H, O'Keeffe M, Shortman K, Lucas K. Development of thymic and splenic dendritic cell populations from different hemopoietic precursors. *Blood* (2001) 98:3376–82. doi:10.1182/blood.V98.12.3376
 48. Lee J, Zhou YJ, Ma W, Zhang W, Aljoufi A, Luh T, et al. Lineage specification of human dendritic cells is marked by IRF8 expression in hematopoietic stem cells and multipotent progenitors. *Nat Immunol* (2017) 18:877–88. doi:10.1038/ni.3789
 49. Corcoran L, Ferrero I, Vremec D, Lucas K, Waithman J, O'Keeffe M, et al. The lymphoid past of mouse plasmacytoid cells and thymic dendritic cells. *J Immunol* (2003) 170:4926–32. doi:10.4049/jimmunol.170.10.4926
 50. Sathe P, Vremec D, Wu L, Corcoran L, Shortman K. Convergent differentiation: myeloid and lymphoid pathways to murine plasmacytoid dendritic cells. *Blood* (2013) 121:11–9. doi:10.1182/blood-2012-02-413336
 51. Bar-On L, Birnberg T, Lewis KL, Edelson BT, Bruder D, Hildner K, et al. CX3CR1+ CD8alpha+ dendritic cells are a steady-state population related to plasmacytoid dendritic cells. *Proc Natl Acad Sci U S A* (2010) 107:14745–50. doi:10.1073/pnas.1001562107
 52. Shigematsu H, Reizis B, Iwasaki H, Mizuno S-I, Hu D, Traver D, et al. Plasmacytoid dendritic cells activate lymphoid-specific genetic programs irrespective of their cellular origin. *Immunity* (2004) 21:43–53. doi:10.1016/j.immuni.2004.06.011
 53. Schlenner SM, Madan V, Busch K, Tietz A, Läufler C, Costa C, et al. Fate mapping reveals separate origins of T cells and myeloid lineages in the thymus. *Immunity* (2010) 32:426–36. doi:10.1016/j.immuni.2010.03.005
 54. Luche H, Ardouin L, Teo P, See P, Henri S, Merad M, et al. The earliest intrathymic precursors of CD8alpha(+) thymic dendritic cells correspond to myeloid-type double-negative 1c cells. *Eur J Immunol* (2011) 41:2165–75. doi:10.1002/eji.201141728
 55. Ivanova A, Signore M, Caro N, Greene NDE, Copp AJ, Martinez-Barbera JP. In vivo genetic ablation by Cre-mediated expression of diphtheria toxin fragment A. *Genesis* (2005) 43:129–35. doi:10.1002/gene.20162
 56. Srinivas S, Watanabe T, Lin CS, William CM, Tanabe Y, Jessell TM, et al. Cre reporter strains produced by targeted insertion of EYFP and ECFP into the ROSA26 locus. *BMC Dev Biol* (2001) 1:4. doi:10.1186/1471-213X-1-4
 57. Buch T, Heppner FL, Tertilt C, Heinen TJAJ, Kremer M, Wunderlich FT, et al. A Cre-inducible diphtheria toxin receptor mediates cell lineage ablation after toxin administration. *Nat Methods* (2005) 2:419–26. doi:10.1038/nmeth762
 58. Schlissel MS, Corcoran LM, Baltimore D. Virus-transformed pre-B cells show ordered activation but not inactivation of immunoglobulin gene rearrangement and transcription. *J Exp Med* (1991) 173:711–20. doi:10.1084/jem.173.3.711
 59. Birnberg T, Bar-On L, Sapozhnikov A, Caton ML, Cervantes-Barragan L, Makia D, et al. Lack of conventional dendritic cells is compatible with normal development and T cell homeostasis, but causes myeloid proliferative syndrome. *Immunity* (2008) 29:986–97. doi:10.1016/j.immuni.2008.10.012
 60. Sichien D, Scott CL, Martens L, Vanderkerken M, Van Gassen S, Plantinga M, et al. IRF8 transcription factor controls survival and function of terminally differentiated conventional and plasmacytoid dendritic cells, respectively. *Immunity* (2016) 45:626–40. doi:10.1016/j.immuni.2016.08.013
 61. Jiao J, Dragomir A-C, Kocabayoglu P, Rahman AH, Chow A, Hashimoto D, et al. Central role of conventional dendritic cells in regulation of bone marrow release and survival of neutrophils. *J Immunol* (2014) 192:3374–82. doi:10.4049/jimmunol.1300237
 62. Tittel AP, Heuser C, Ohliger C, Llanto C, Yona S, Hämmerling GJ, et al. Functionally relevant neutrophilia in CD11c diphtheria toxin receptor transgenic mice. *Nat Methods* (2012) 9:385–90. doi:10.1038/nmeth.1905
 63. Holtschke T, Löhler J, Kanno Y, Fehr T, Giese N, Rosenbauer F, et al. Immunodeficiency and chronic myelogenous leukemia-like syndrome in mice with a targeted mutation of the ICSBP gene. *Cell* (1996) 87:307–17. doi:10.1016/S0092-8674(00)81348-3
 64. van Blijswijk J, Schraml BU, Rogers NC, Whitney PG, Zelenay S, Acton SE, et al. Altered lymph node composition in diphtheria toxin receptor-based mouse models to ablate dendritic cells. *J Immunol* (2015) 194:307–15. doi:10.4049/jimmunol.1401999
 65. Miller JC, Brown BD, Shay T, Gautier EL, Jojic V, Cohain A, et al. Deciphering the transcriptional network of the dendritic cell lineage. *Nat Immunol* (2012) 13:888–99. doi:10.1038/ni.2370
 66. Villani A-C, Satija R, Reynolds G, Sarkizova S, Shekhar K, Fletcher J, et al. Single-cell RNA-seq reveals new types of human blood dendritic cells, monocytes, and progenitors. *Science* (2017) 356:eaah4573. doi:10.1126/science.aah4573
 67. Shortman K, Sathe P, Vremec D, Naik S, O'Keeffe M. Plasmacytoid dendritic cell development. *Adv Immunol* (2013) 120:105–26. doi:10.1016/B978-0-12-417028-5.00004-1
 68. Reizis B. Regulation of plasmacytoid dendritic cell development. *Curr Opin Immunol* (2010) 22:206–11. doi:10.1016/j.coi.2010.01.005
 69. Pelayo R, Hirose J, Huang J, Garrett KP, Delogu A, Busslinger M, et al. Derivation of 2 categories of plasmacytoid dendritic cells in murine bone marrow. *Blood* (2005) 105:4407–15. doi:10.1182/blood-2004-07-2529
 70. Vremec D, Shortman K. What's in a name? Some early and current issues in dendritic cell nomenclature. *Front Immunol* (2015) 6:267. doi:10.3389/fimmu.2015.00267
 71. Schraml BU, Reis e Sousa C. Defining dendritic cells. *Curr Opin Immunol* (2015) 32:13–20. doi:10.1016/j.coi.2014.11.001
 72. Ginhoux F, Guillemin M, Naik S. Dendritic cell and macrophage nomenclature and classification. *Front Immunol* (2016). doi:10.3389/fimmu.2016.00001
 73. Lavin Y, Winter D, Blecher-Gonen R, David E, Keren-Shaul H, Merad M, et al. Tissue-resident macrophage enhancer landscapes are shaped by the local microenvironment. *Cell* (2014) 159:1312–26. doi:10.1016/j.cell.2014.11.018
 74. Gosselin D, Link VM, Romanoski CE, Fonseca GJ, Eichenfield DZ, Spann NJ, et al. Environment drives selection and function of enhancers controlling tissue-specific macrophage identities. *Cell* (2014) 159:1327–40. doi:10.1016/j.cell.2014.11.023
 75. Gosselin D, Skola D, Coufal NG, Holtman IR, Schlachetzki JCM, Sajti E, et al. An environment-dependent transcriptional network specifies human microglia identity. *Science* (2017) 1617:eaal3222. doi:10.1126/science.aal3222
 76. van de Laar L, Saelens W, De Prijck S, Martens L, Scott CL, Van Isterdael G, et al. Yolk sac macrophages, fetal liver, and adult monocytes can colonize an empty niche and develop into functional tissue-resident macrophages. *Immunity* (2016) 44:1–27. doi:10.1016/j.immuni.2016.02.017
 77. Gibbings SL, Goyal R, Desch AN, Leach SM, Prabagar M, Atif SM, et al. Transcriptome analysis highlights the conserved difference between embryonic and postnatal-derived alveolar macrophages. *Blood* (2015) 126:1357–66. doi:10.1182/blood-2015-01-624809
 78. Hochweller K, Miloud T, Striegler J, Naik S, Hämmerling GJ, Garbi N. Homeostasis of dendritic cells in lymphoid organs is controlled by regulation of their precursors via a feedback loop. *Blood* (2009) 114:4411–21. doi:10.1182/blood-2008-11-188045
 79. Kabashima K, Banks TA, Ansel KM, Lu TT, Ware CF, Cyster JG. Intrinsic phototoxicity-beta receptor requirement for homeostasis of lymphoid tissue dendritic cells. *Immunity* (2005) 22:439–50. doi:10.1016/j.immuni.2005.02.007
 80. Tussiwand R, Onai N, Mazzucchelli L, Manz MG. Inhibition of natural type I IFN-producing and dendritic cell development by a small molecule receptor tyrosine kinase inhibitor with Flt3 affinity. *J Immunol* (2005) 175:3674–80. doi:10.4049/jimmunol.175.6.3674
 81. McKenna HJ, Stocking KL, Miller RE, Brasel K, De Smedt T, Maraskovsky E, et al. Mice lacking flt3 ligand have deficient hematopoiesis affecting hematopoietic progenitor cells, dendritic cells, and natural killer cells. *Blood* (2000) 95:3489–97.
 82. Hildner K, Edelson BT, Purtha WE, Diamond M, Matsushita H, Kohyama M, et al. Batf3 deficiency reveals a critical role for CD8alpha+ dendritic cells in cytotoxic T cell immunity. *Science* (2008) 322:1097–100. doi:10.1126/science.1164206
 83. Ohta T, Sugiyama M, Hemmi H, Yamazaki C, Okura S, Sasaki I, et al. Crucial roles of XCR1-expressing dendritic cells and the XCR1- XCL1 chemokine axis in intestinal immune homeostasis. *Sci Rep* (2016) 6:1–11. doi:10.1038/srep23505
 84. Böiers C, Carrelha J, Lutteropp M, Luc S, Green JCA, Azzoni E, et al. Lymphomyeloid contribution of an immune-restricted progenitor emerging prior to definitive hematopoietic stem cells. *Cell Stem Cell* (2013) 13:535–48. doi:10.1016/j.stem.2013.08.012

85. Yáñez A, Coetzee SG, Olsson A, Muench DE, Berman BP, Hazelett DJ, et al. Granulocyte-monocyte progenitors and monocyte- dendritic cell progenitors independently produce functionally distinct monocytes. *Immunity* (2017) 47:890–902.e4. doi:10.1016/j.immuni.2017.10.021

Conflict of Interest Statement: The authors declare that the research was conducted in the absence of any commercial or financial relationships that could be construed as a potential conflict of interest.

Copyright © 2018 Salvermoser, van Blijswijk, Papaioannou, Rambichler, Pasztoi, Pakalniškytė, Rogers, Keppeler, Straub, Reis e Sousa and Schraml. This is an open-access article distributed under the terms of the Creative Commons Attribution License (CC BY). The use, distribution or reproduction in other forums is permitted, provided the original author(s) and the copyright owner are credited and that the original publication in this journal is cited, in accordance with accepted academic practice. No use, distribution or reproduction is permitted which does not comply with these terms.

Supplementary Material

Clec9a-mediated ablation of conventional dendritic cells suggests a lymphoid path to generating dendritic cells *in vivo*

Johanna Salvermoser^{1,2}, Janneke van Blijswijk³, Nikos E. Papaioannou², Stephan Rambichler^{1,2}, Maria Pasztoi², Dalia Pakalniškytė^{1,2}, Neil C. Rogers³, Selina J. Keppler⁴, Tobias Straub^{2,5}, Caetano Reis e Sousa^{3*}, Barbara U. Schraml^{1,2*}

¹*Walter-Brendel-Centre for Experimental Medicine, University Hospital, LMU Munich, Großhaderner Str. 9, 82152 Planegg Martinsried, Germany*

²*Biomedical Center, LMU Munich, Großhaderner Str. 9, 82152 Planegg Martinsried, Germany*

³*Immunobiology Laboratory, The Francis Crick Institute, 1 Midland Road, London NW1 1AT, United Kingdom*

⁴*Technische Universität München, Klinikum Rechts der Isar, Institut für Klinische Chemie und Pathobiochemie, Ismaningerstr. 22, 81675 Munich, Germany*

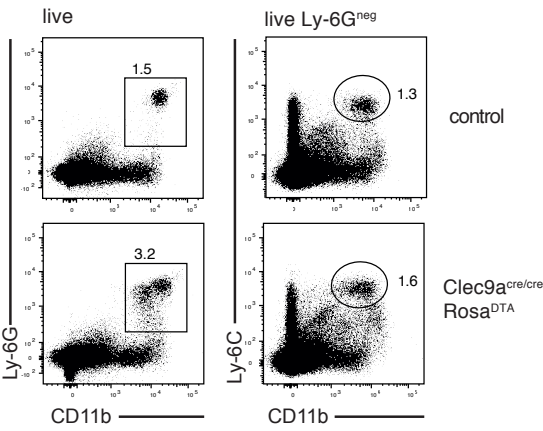
⁵*Core Facility Bioinformatics, Biomedical Center (BMC), LMU Munich, Großhaderner Str. 9 82152 Planegg Martinsried*

**These authors contributed equally*

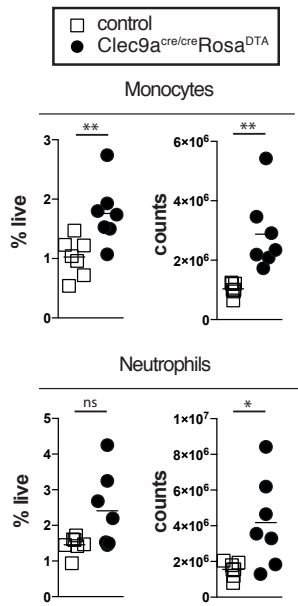
correspondence: barbara.schraml@med.uni-muenchen.de , caetano@crick.ac.uk

Supplementary Figure 1

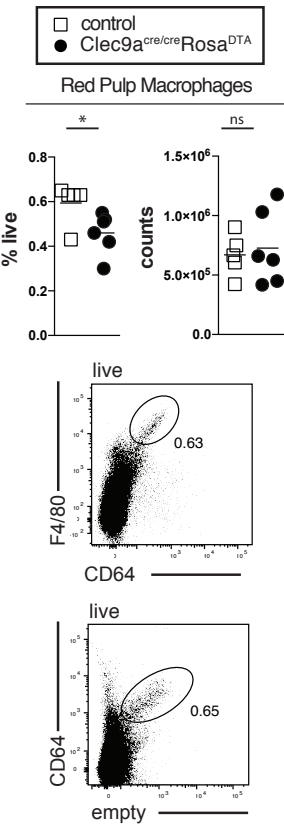
A Spleen



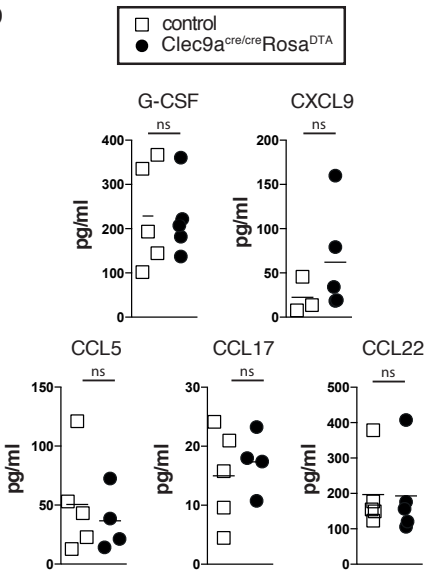
B Spleen 8-15 weeks



C



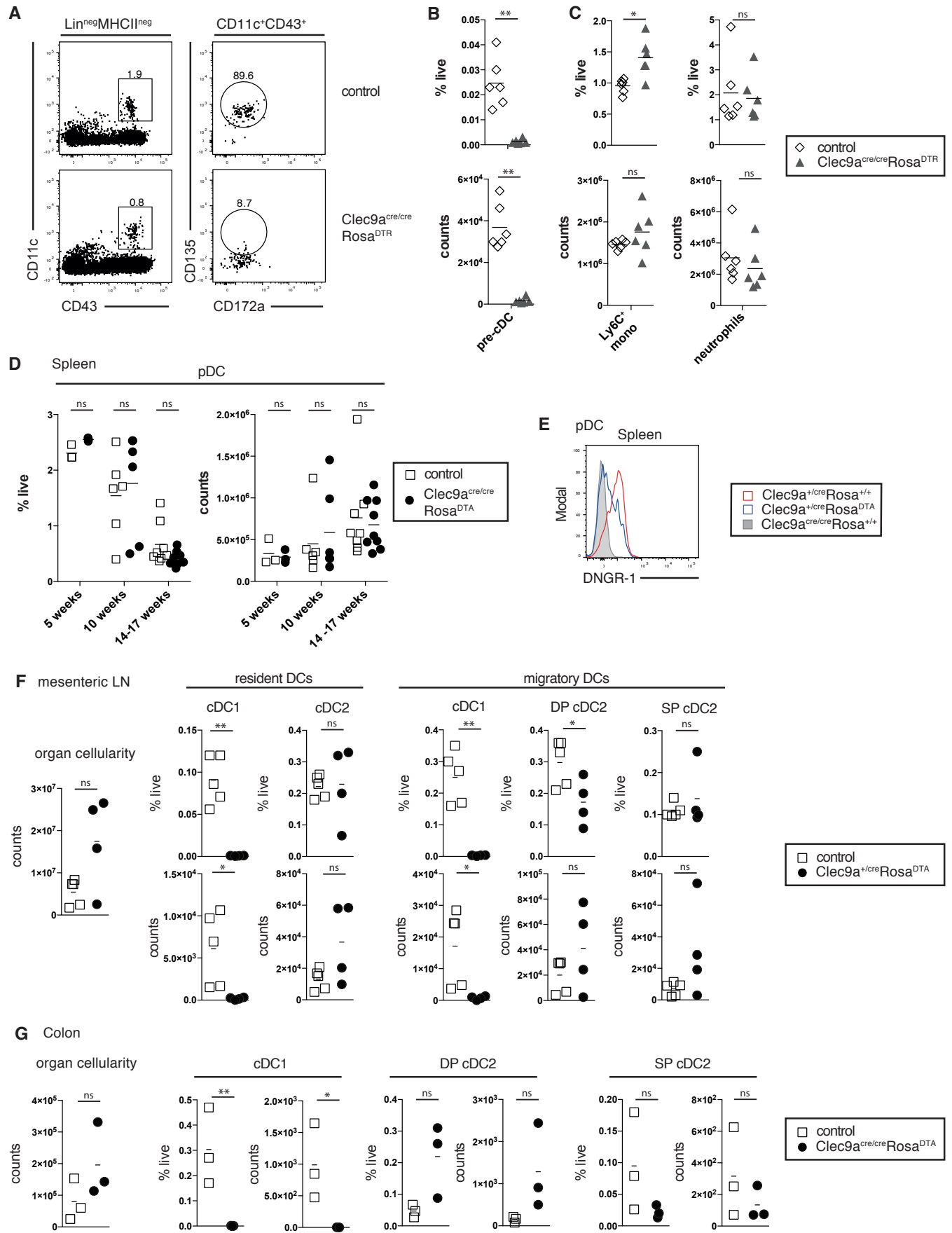
D



Supplementary Figure 1: *Clec9a^{cre/cre}Rosa^{DTA}* mice develop signs of age-dependent myeloproliferation

A, B. Neutrophils and monocytes were identified by flow cytometry in spleen from control and *Clec9a^{cre/cre}Rosa^{DTA}* mice. **A.** Representative gating strategy in 14-week-old mice. Neutrophils were identified as live CD11b⁺Ly-6G⁺ cells. Monocytes were identified as live Ly-6G⁺Ly-6C⁺CD11b⁺ cells. **B.** The frequency and total counts of splenic Ly-6G⁺ neutrophils and Ly-6C⁺ monocytes are plotted. **C.** Frequency and counts of red pulp macrophages (RPM) identified as autofluorescent CD64⁺F4/80^{hi} cells or as autofluorescent CD64⁺ cells in spleen from *Clec9a^{cre/cre}Rosa^{DTA}* and control mice. Representative gating strategies to identify red pulp macrophages are shown. **D.** Serum was collected from control and *Clec9a^{cre/cre}Rosa^{DTA}* mice older than 10 weeks and the concentrations of G-CSF, CXCL9, CCL5, CCL17, and CCL22 were determined by ELISA or cytometric bead array as described in the materials and methods. Data are compiled from at least two independent experiments. Each symbol represents one mouse. * p<0.05, ** p<0.001.

Supplementary Figure 2

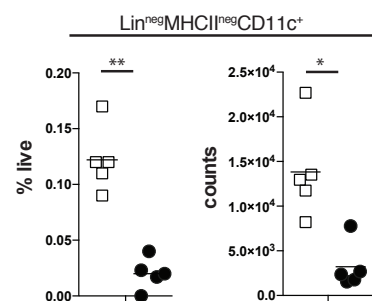


Supplementary Figure 2: Analysis of pDCs in spleen from *Clec9a^{cre/cre}Rosa^{DTA}* mice and loss of pre-cDCs in *Clec9a^{cre/cre}Rosa^{DTR}* mice

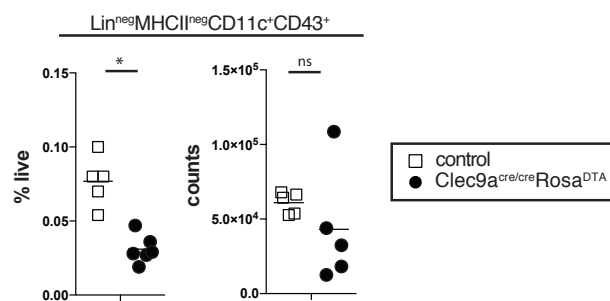
A, B, C. *Clec9a^{cre/cre}Rosa^{DTR}* and control mice were injected i.p. with 25 ng/g of diphtheria toxin (DT). 24 hours later spleens were analysed by flow cytometry. **A.** Representative gating strategy of splenic lin^- (CD3, CD4, CD8, Ter119, NK1.1, B220, CD11b, MHCII) $\text{CD11c}^+\text{CD43}^+\text{CD135}^+\text{CD172a}^{\text{low}}$ pre-cDCs. **B.** Frequency and total counts of pre-cDCs were identified as in (A). **C.** The frequency and total counts of neutrophils ($\text{Ly-6G}^+\text{CD11b}^+$) and Ly-6C^+ monocytes ($\text{Ly-6G}^-\text{Ly-6C}^+\text{CD11b}^+$) are shown. **D.** Splenic pDCs were identified as $\text{SiglecH}^+\text{B220}^+$ cells by flow cytometry in *Clec9a^{cre/cre}Rosa^{DTA}* and control mice. The frequency and counts of splenic pDCs in *Clec9a^{cre/cre}Rosa^{DTA}* and control mice of the indicated ages are shown. **E.** Analysis of DNNGR-1 protein expression on pDCs from *Clec9a^{+cre}Rosa^{DTA}* mice. DNNGR-1 protein levels were analysed by flow cytometry on splenic $\text{B220}^+\text{SiglecH}^+$ pDCs from *Clec9a^{+cre}Rosa^{+/+}* control mice and compared to levels on pDCs from *Clec9a^{+cre}Rosa^{DTA}* mice. Homozygous *Clec9a^{cre/cre}Rosa^{+/+}* mice serve as a negative control for DNNGR-1 protein staining. **F, G.** mesenteric LN from *Clec9a^{+cre}Rosa^{DTA}* and control mice (**F**) and colon from *Clec9a^{cre/cre}Rosa^{DTA}* and control mice (**G**) were analysed for total organ cellularity, as well as for the presence of the indicated DC subsets. **F.** Resident and migratory cDCs were distinguished as $\text{CD11c}^+\text{MHCII}^+$ and $\text{CD11c}^{\text{int}}\text{MHCII}^{\text{hi}}$ cells respectively. cDC1 were identified as $\text{XCR-1}^+\text{CD11b}^-$ cells and cDC2 were identified as $\text{XCR-1}^-\text{CD11b}^+$ or $\text{CD103}^+\text{CD11b}^+$ (DP) and $\text{CD103}^-\text{CD11b}^+$ (SP) cDC2. **F.** Colonic cDCs were identified as $\text{CD11c}^+\text{MHCII}^+\text{CD64}^-$ cells and distinguished as $\text{XCR-1}^+\text{CD172a}^-$ cDC1, as well as $\text{CD103}^+\text{CD11b}^+\text{CD172a}^+$ (DP) and $\text{CD103}^-\text{CD11b}^+\text{CD172a}^+$ (SP) cDC2. Each symbol represents one mouse. ns - not significant, * $p < 0.05$, ** $p < 0.001$.

Supplementary Figure 3

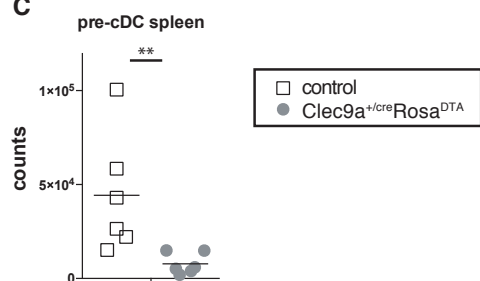
A bone marrow



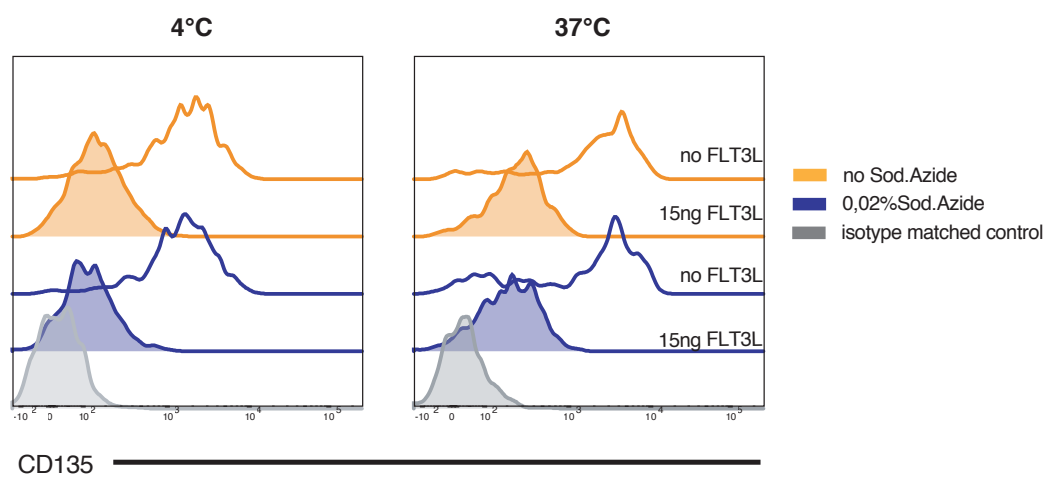
B spleen



C



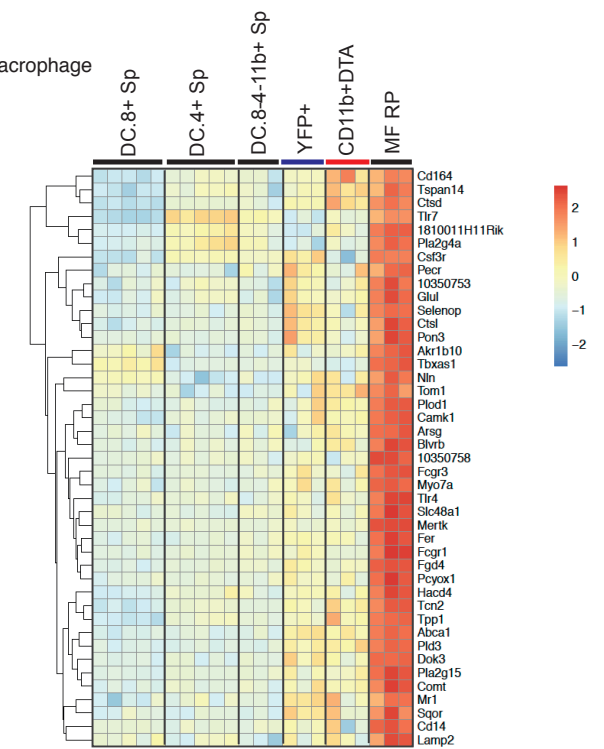
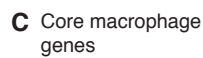
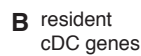
D



Supplementary Figure 3. Loss of cDC progenitors in *Clec9a^{cre/cre}Rosa^{DTA}* and *Clec9a^{+/-cre}Rosa^{DTA}* mice.

A, B. cDC progenitors were identified by flow cytometry in the bone marrow and spleen of 10-week-old control and *Clec9a^{cre/cre}Rosa^{DTA}* mice. **A.** Live lineage negative (lin⁻; CD3, CD4, CD8, CD11b, MHCII, Ter119, NK1.1, B220) CD11c⁺ cells from bone marrow of *Clec9a^{cre/cre}Rosa^{DTA}* and control mice were gated and quantified. The frequency and total counts per femur are shown. **B.** Lin⁻CD11c⁺CD43⁺ splenocytes, containing pre-cDCs, were identified in control and *Clec9a^{cre/cre}Rosa^{DTA}* mice 10 weeks of age. Frequency and total counts per spleen are shown. **C.** Lin⁻CD11c⁺CD43⁺CD135⁺CD172a^{low} pre-cDCs were quantified in spleen from *Clec9a^{+/-cre}Rosa^{DTA}* mice 9-12 weeks of age. **D.** CD11c⁺ splenocytes were cultured with or without 15ng/ml FLT3L for 2 hours at 37°C or 4°C in the presence or absence of 0,02% sodium azide to interfere with endocytosis. Cells were then washed and analysed for CD135 expression. CD135 staining on CD11c⁺MHCII⁺CD11b⁺ splenocytes is shown.

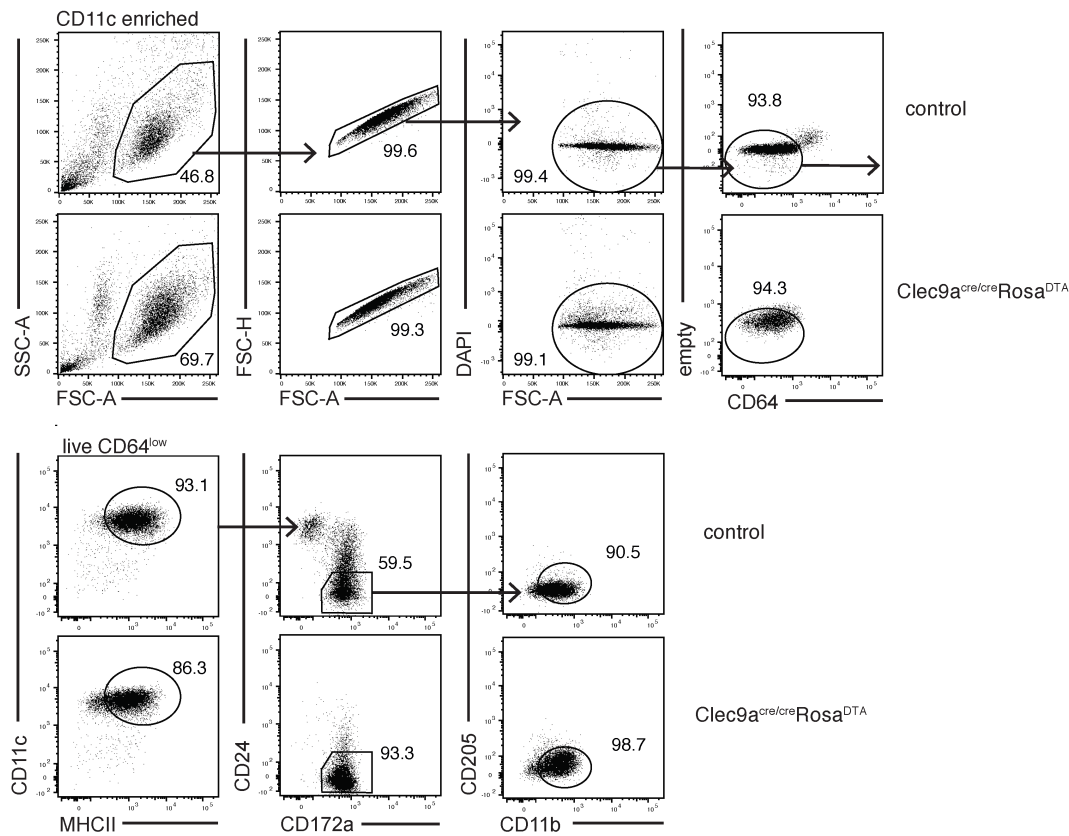
A migratory
cDC genes



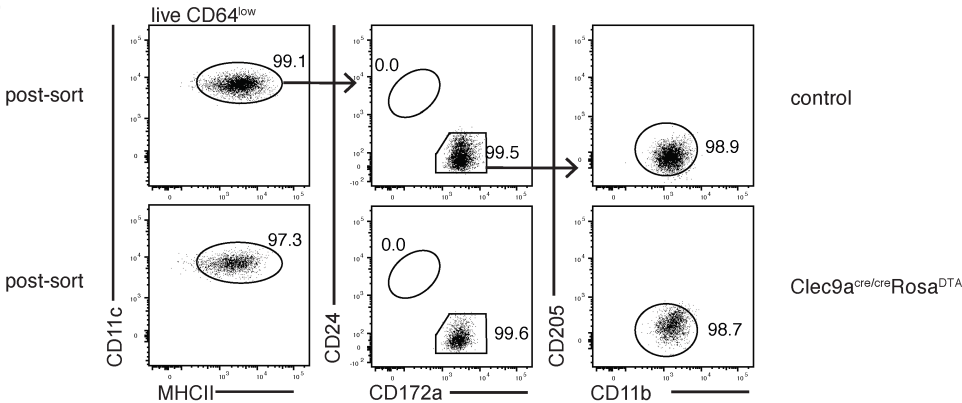
Supplementary Figure 4: Transcriptional profiling of cDC2 from *Clec9a^{cre/cre}Rosa^{DTA}* mice reveals no major loss in cDC identity.

Splenic CD11c⁺MHCII⁺CD11b⁺ cDC2 *Clec9a^{cre/cre}Rosa^{DTA}* mice (CD11b⁺ DTA) and cDC2 (identified as CD11c⁺MHCII⁺CD11b⁺YFP⁺ cells from *Clec9a^{cre/cre}Rosa^{YFP}* mice; YFP⁺) were sorted and subjected to microarray analysis. Population clustering and heat map display of the relative expression values for migratory cDC signature genes (**A**), resident cDC signature genes (**B**), and core macrophage signature genes (**C**) in CD11b⁺ DTA and YFP⁺ cDC2 samples compared to the indicated murine cDC and macrophage populations from the Immgen database.

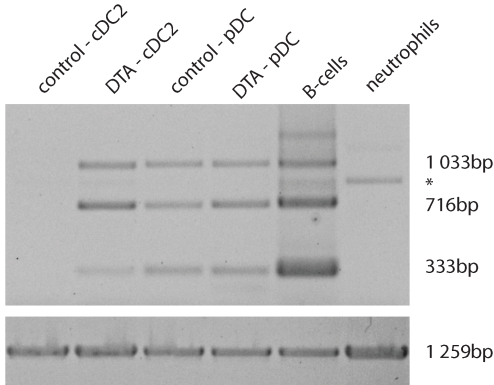
A Sort strategy for cDC2



B



C



Supplementary Figure 5: cDC2 from *Clec9a^{cre/cre}Rosa^{DTA}* mice exhibit somatic rearrangements of lymphoid receptor genes.

A, B. Gating strategy and purity check for DJ- rearrangement PCR. **A.** CD11c⁺MHCII⁺CD11b⁺ cDC2 from control and *Clec9a^{cre/cre}Rosa^{DTA}* mice were sorted according to the indicated gating strategy. **B.** The purity of the sorted cDC2 populations from control and *Clec9a^{cre/cre}Rosa^{DTA}* mice is shown. **C.** CD11c⁺MHCII⁺CD11b⁺ cDC2 from control and *Clec9a^{cre/cre}Rosa^{DTA}* mice were sorted and genomic DNA was isolated. Genomic PCR was performed using primers for the germline (GL) locus and primer mixtures homologous for regions of the Dfl16 and Dsp2 D gene families for detecting D–J rearrangements of the IgH chain. DJ rearrangements in pDCs (SiglecH⁺B220⁺), splenic B-cells and neutrophils (Ly-6G⁺) are shown as control. * indicates an unspecific band.

3. Paper II

ARTICLE


<https://doi.org/10.1038/s41467-020-20659-2>

OPEN

Environmental signals rather than layered ontogeny imprint the function of type 2 conventional dendritic cells in young and adult mice

Nikos E. Papaioannou^{1,2}, Natallia Salei^{1,2}, Stephan Rambichler^{1,2}, Kaushikk Ravi^{1,2}, Jelena Popovic^{1,2}, Vanessa Küntzel^{1,2}, Christian H. K. Lehmann^{3,4}, Remi Fiancette⁵, Johanna Salvermoser^{1,2}, Dominika W. Gajdasik⁵, Ramona Mettler^{1,2}, Denise Messerer⁶, Joana Carrelha⁷, Caspar Ohnmacht⁸, Dirk Haller^{9,10}, Ralf Stumm¹¹, Tobias Straub¹², Sten Eirik W. Jacobsen^{7,13}, Christian Schulz^{6,14}, David R. Withers⁵, Gunnar Schotta^{15,16}, Diana Dudziak^{3,4,17,18} & Barbara U. Schraml^{1,2}✉

Conventional dendritic cells (cDC) are key activators of naive T cells, and can be targeted in adults to induce adaptive immunity, but in early life are considered under-developed or functionally immature. Here we show that, in early life, when the immune system develops, cDC2 exhibit a dual hematopoietic origin and, like other myeloid and lymphoid cells, develop in waves. Developmentally distinct cDC2 in early life, despite being distinguishable by fate mapping, are transcriptionally and functionally similar. cDC2 in early and adult life, however, are exposed to distinct cytokine environments that shape their transcriptional profile and alter their ability to sense pathogens, secrete cytokines and polarize T cells. We further show that cDC2 in early life, despite being distinct from cDC2 in adult life, are functionally competent and can induce T cell responses. Our results thus highlight the potential of harnessing cDC2 for boosting immunity in early life.

¹Faculty of Medicine, Biomedical Center, Institute for Cardiovascular Physiology and Pathophysiology, LMU Munich, 82152 Planegg-Martinsried, Germany.

²Walter-Brendel-Centre of Experimental Medicine, University Hospital Munich, LMU Munich, 82152 Planegg-Martinsried, Germany. ³Laboratory of Dendritic Cell Biology, Department of Dermatology, University Hospital Erlangen, Friedrich-Alexander University of Erlangen-Nürnberg, Erlangen, Germany.

⁴Medical Immunology Campus Erlangen, University Hospital of Erlangen, Friedrich-Alexander-University (FAU) of Erlangen-Nürnberg, Erlangen, Germany.

⁵Institute of Immunology and Immunotherapy, College of Medical and Dental Sciences, University of Birmingham, Birmingham, UK. ⁶Medizinische Klinik und Poliklinik I, University Hospital Munich, LMU Munich, 81377 Munich, Germany. ⁷Haematopoietic Stem Cell Biology Laboratory, MRC Molecular

Haematology Unit, MRC Weatherall Institute of Molecular Medicine, Radcliffe Department of Medicine, University of Oxford, Oxford, UK. ⁸Center of Allergy and Environment, Helmholtz Center and Technical University of Munich, 80802 Munich, Germany. ⁹ZIEL-Institute for Food and Health, Technische

Universität München, Freising, Germany. ¹⁰Chair of Nutrition and Immunology, Technische Universität München, Freising, Germany. ¹¹Institute of

Pharmacology and Toxicology, Jena University Hospital, Jena, Germany. ¹²Core Facility Bioinformatics, Biomedical Center, LMU Munich, 82152 Planegg-

Martinsried, Germany. ¹³Department of Medicine Huddinge, Center for Hematology and Regenerative Medicine and Department of Cell and Molecular

Biology, Karolinska Institutet, Stockholm, Sweden. ¹⁴DZHK (German Center for Cardiovascular Research), Partner Site Munich Heart Alliance, 80802

Munich, Germany. ¹⁵Faculty of Medicine, Center for Integrated Protein Science Munich, LMU Munich, 82152 Planegg-Martinsried, Germany. ¹⁶Faculty of

Medicine, Division of Molecular Biology, Biomedical Center, LMU Munich, 82152 Planegg-Martinsried, Germany. ¹⁷Deutsches Zentrum Immuntherapie

(DZI), Erlangen, Germany. ¹⁸Comprehensive Cancer Center Erlangen-European Metropolitan Area of Nuremberg (CCC ER-EMN), Erlangen, Germany.

✉email: barbara.schraml@bmc.med.lmu.de

Vaccination is a reliable means of inducing protective immunity but it can have limited efficacy in infants¹. The newborn immune system exhibits quantitative and qualitative differences compared to adult hosts that ultimately result in dampened immune responses in early life, which are necessary to tolerate the sudden encounter with commensal microbes and environmental antigens^{2,3}. The unique features of the early life immune system also leave infants at increased risk of infection³. Antigen presentation and priming of T cells are pre-requisites for adaptive immune responses and the establishment of protective immunity. Improving T-cell priming by tailoring the design of vaccines towards the age-specific immune parameters of neonates and infants has therefore been suggested as a possibility to boost vaccination efficacy and immunity in early life^{3,4}.

Classical or conventional dendritic cells (cDCs) are potent activators of naive T cells that have successfully been targeted to induce adaptive immune responses in adults^{5–8}. In early life, however, these cells are considered under-developed or functionally immature. In murine and human neonates, the cDC compartment is smaller than that of adults^{9–11} and cDCs from both human and murine neonates express lower basal levels of major histocompatibility complex II (MHCII) and costimulatory molecules rendering them less potent at stimulating T cells^{12–15}. The early life murine cDC compartment further exhibits an intrinsic bias to generate T-helper type 2 (Th2) immune responses due to delayed production of IL-12p70^{16,17}. Such Th2 bias is also evident in cord blood cDCs, which exhibit reduced IL-12p70 production and upregulation of costimulatory molecules following pathogenic stimulation compared to cDCs from peripheral blood of adults^{13,14,18}. However, expansion of cDCs in early life by administration of the DC growth factor fms tyrosine kinase 3 ligand (FLT3L) can improve innate and adaptive immune defense in mice^{19,20}, indicating a potential of early life cDCs to initiate functional immune responses.

The cDC compartment is composed of developmentally distinct subsets with unique functions in immunity^{5,6,21}. cDC1 are potent cross-presenters and activators of CD8⁺ T cells and promote Th1 differentiation through the production of interleukin-12 (IL-12) and interferon- γ (IFN- γ)^{22–24}. In contrast, cDC2 are considered more potent activators of CD4⁺ T cells and inducers of Th2, Th17, and T-follicular helper cell differentiation^{25–29}. The neonatal cDC compartment in mice is dominated by cDC1, whereas cDC2 constitute the main cDC subtype in most adult organs^{9,10,30,31}. Considering the predominant role of cDC1 in producing IL-12 and IFN- γ in adults^{23,24}, it is unlikely that subset distribution can account for the observed Th2 bias of the cDC compartment in early life and in most human tissues the relative frequency of cDC1 and cDC2 remains stable throughout life¹⁵. These data suggest that an additional layer of age-dependent regulation influences cDC function. This is highlighted by the fact that neonatal cDC1 are refractory to IFN- α signaling, produce less IL-12 but more IL-10 than their adult counterparts and have a reduced capacity to activate CD4⁺ T cells and select epitopes for presentation to CD8⁺ T cells during viral infection^{9,16,17,32,33}.

Few studies have investigated cDC2 in early life. In neonatal mouse spleen, CD8⁺ cDCs show lower production of IFN- γ and reduced activation of alloreactive T cells than their adult counterparts⁹. Although CD8 expression does not reliably distinguish cDC1 and cDC2 in neonatal spleen^{17,34}, these data suggest a reduced ability of neonatal cDC2 to activate T cells. Similarly, cDC2 in neonatal lung express lower costimulatory molecules than adult cDC2^{32,35–37}, although they can promote Th2-mediated allergy and induce some CD8⁺ T-cell proliferation when infected with respiratory syncytial virus^{30,32,38}. These data indicate that in early life, cDC2 have the potential to activate T cells in some circumstances, raising the question whether this

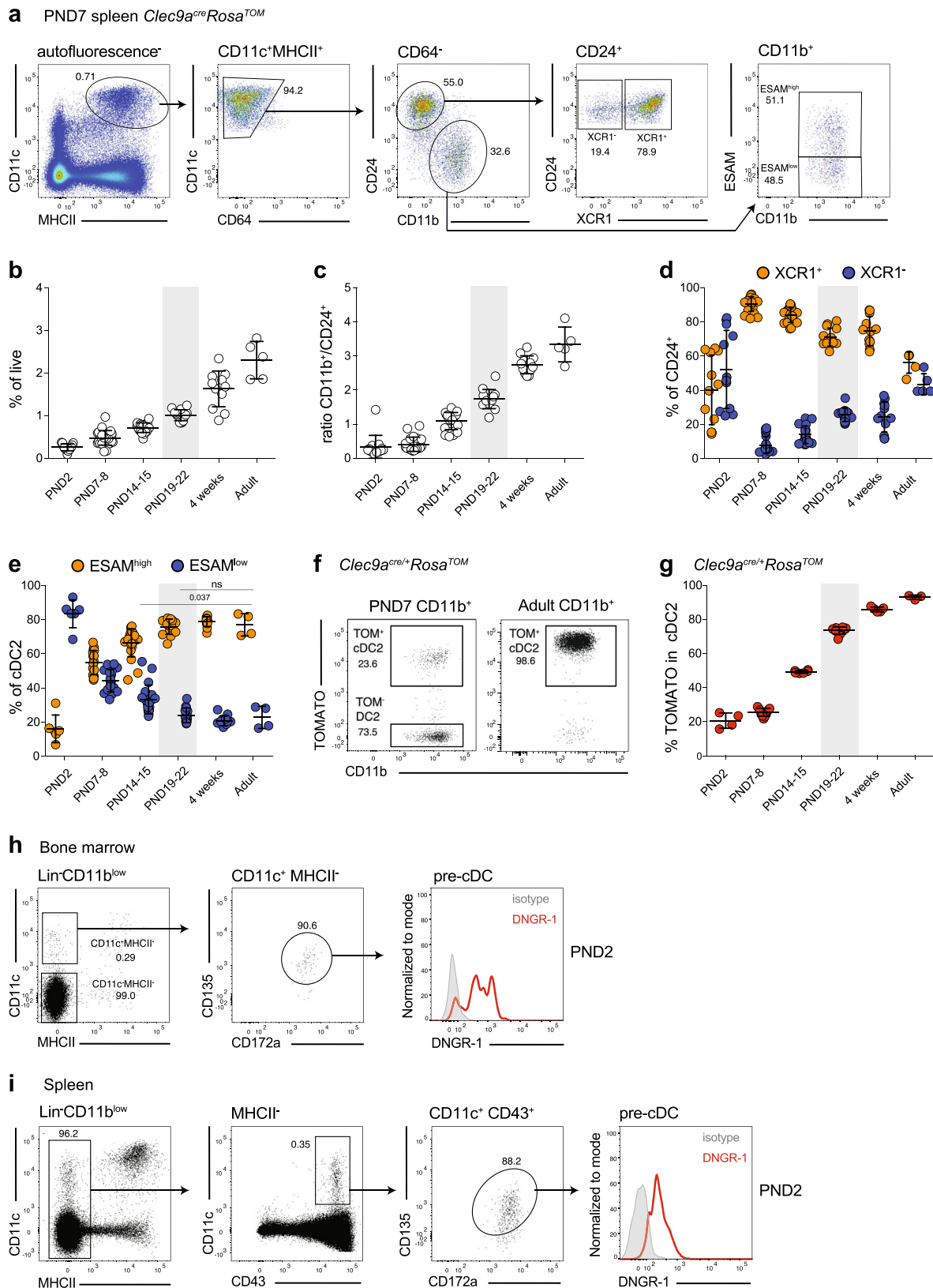
capacity could be harnessed in a broader sense, for instance to initiate T-cell responses in the spleen, which is a major site for antibody production³⁹.

The first blood and immune cells arise from extra-embryonic yolk sac progenitors and for some cell types, such as macrophages or mast cells, yolk sac-derived cells can persist in tissues for extended periods of time after birth^{40–42}. cDCs first arise during embryogenesis in mice and humans, when they are thought to critically contribute to fetomaternal tolerance^{9,10,40,43}. However, the origins of cDCs in early life have not been investigated. In adults, cDCs develop downstream of hematopoietic stem cells (HSCs) from a fraction of myeloid bone marrow progenitors capable of generating plasmacytoid DCs (pDCs) and cDCs that has been termed common DC progenitor (CDP)^{44–47}. Within CDPs in mice, expression of the C-type lectin receptor DNGR-1 (encoded by the *Clec9a* gene) distinguishes cDC-restricted progenitors⁴⁸. CDPs further differentiate into pre-cDCs, which continue to express DNGR-1⁴⁸, exit the bone marrow and terminally differentiate into cDC subtypes in peripheral organs and in response to environmental cues⁴⁹. The *Clec9a* promoter is also active in cDC1 and to a lower extent on pDCs but it is not active in cDC2 and other lymphoid or myeloid cells^{48,50–52}. By crossing mice expressing CRE-recombinase under the *Clec9a* promoter to *Rosa^{lox-stop-lox}*-yellow fluorescent protein (YFP) or *Rosa^{lox-stop-lox}*-TOMATO mice, we have generated mice that faithfully track cells belonging to the cDC lineage in steady state and under inflammatory conditions^{48,53,54}. Using these mice, we have found that cDC2 in adult spleen are predominantly derived from CDP/pre-cDC^{48,53,54}, which is consistent with other studies^{55,56}.

Here we set out to investigate the differences between cDC2 in early and adult life and clarify the reasons underlying age-dependent functional regulation of cDC2. We reveal that cDC2, analogous to other lymphoid and myeloid cell types, develop in waves. cDC2 arising from distinct hematopoietic sources in early life are phenotypically and transcriptionally similar, and functionally capable to induce T-cell responses. cDC2 in early and adult life, however, have a distinct ability to sense pathogens, produce cytokines and induce T-cell differentiation that is transcriptionally imprinted by distinct cytokine signaling in early and adult life. Exploiting the unique aspects of cDC2 in early life may thus provide an efficient means to boost vaccination efficacy and protective immunity.

Results

Early-life cDC2 exhibit ontogenetic diversity. To investigate phenotype and origin of cDCs in early life, we first profiled these cells in *Clec9a^{cre/+}Rosa^{TOM}* mice. In this context, we defined the neonatal period as the first 10 days after birth⁵⁷. In the steady-state mouse spleen, cDCs, identified as CD11c⁺MHCII⁺ cells⁵, could be found as early as embryonic day 16 (E16, Fig. 1a, b and Supplementary Fig. 1). The frequency of CD11c⁺MHCII⁺ cells increased steadily with age and reached adult levels at around 4 weeks of age (Fig. 1a, b and Supplementary Fig. 1), confirming results of previous studies^{9,10}. CD11c⁺MHCII⁺ cells could further be divided into CD24⁺ and CD11b⁺ cells⁵. CD24⁺ cDCs include XCR-1⁺ BATF3-dependent cDC1, as well as a subset of non-canonical BATF3-independent CD8⁺ cDCs that expresses CD172a and CX3CR1 but lacks XCR-1 (Fig. 1a)^{58–60}. As expected, CD24⁺ cDCs dominated the splenic cDC compartment in early life but became less frequent with age, whereas the proportion of CD11b⁺ cDC2 increased with age⁹ (Fig. 1c). Notably, XCR-1⁺ cDC1 were the more frequent cell type within CD24⁺ cells at most ages examined, although in 2-day-old and adult mice non-canonical CD8⁺ cDC and cDC1 were present at equal



proportions (Fig. 1d). In the spleen, CD11b⁺ cDC2 can be divided into NOTCH2- and RUNX3-dependent ESAM^{high} cDC2 and ESAM^{low} cDC2, which develop independent of these transcription factors^{61–63} (Fig. 1a and Supplementary Fig. 1A, B). Notably, ESAM^{high} cells were less frequent within the cDC2 compartment of neonatal compared to adult mice; however, the proportion of ESAM^{high} cells within the cDC2 compartment reached adult

levels between 2 and 3 weeks of age (Fig. 1e and Supplementary Fig. 1A, B), which coincides with the organization of the splenic architecture.

We next assessed *Clec9a*-expression history with age by profiling TOMATO expression in splenic leukocytes from *Clec9a^{cre/+}Rosa^{TOM}* mice. cDC2 lack DNGR-1 expression and therefore TOMATO labeling in this population is a true indicator

Fig. 1 Developmental heterogeneity of early life cDC2. **a–e** Spleens from *Clec9a^{cre/+}Rosa^{TOM}* and *Clec9a^{cre/cre}Rosa^{TOM}* mice of the indicated ages were analyzed by flow cytometry. **a** Single live autofluorescence-negative cells were gated and cDCs identified as CD11c⁺MHCII⁺CD64[−] cells. cDCs were further divided into CD24⁺ and CD11b⁺ cells, and analyzed for XCR-1 and ESAM expression, respectively. **b** Frequency of CD11c⁺MHCII⁺ cDCs in total splenocytes ($n = 13$, PND2; $n = 25$, PND7–8; $n = 20$, PND14–15; $n = 14$, PND19–22; $n = 12$, 4 weeks; $n = 5$, adult). **c** Ratio of CD11b⁺ to CD24⁺ cells within CD11c⁺MHCII⁺ cDCs ($n = 13$, PND2; $n = 21$, PND7–8; $n = 20$, PND14–15; $n = 14$, PND19–22; $n = 12$, 4 weeks; $n = 5$, adult). **d** The percentage of XCR-1⁺ and XCR-1[−] cells within CD24⁺ cDC1 is shown ($n = 12$, PND2; $n = 21$, PND7–8; $n = 20$, PND14–15; $n = 14$, PND19–22; $n = 12$, 4 weeks; $n = 5$, adult). **e** The percentage of ESAM^{high} and ESAM^{low} cells within CD11b⁺ cDC2 is shown ($n = 6$, PND2; $n = 11$, PND7–8; $n = 18$, PND14–15; $n = 14$, PND19–22; $n = 11$, 4 weeks; $n = 4$, adult). **f** Representative flow cytometry gating for TOMATO expression in splenic cDC2 from 1-week-old and adult *Clec9a^{cre/+}Rosa^{TOM}* mice. **g** The frequency of TOMATO⁺ cells within splenic CD11b⁺ cDC2 of *Clec9a^{cre/+}Rosa^{TOM}* mice with age ($n = 4$, PND2; $n = 11$, PND7–8; $n = 6$, PND14–15; $n = 10$, PND19–22; $n = 5$, 4 weeks; $n = 3$, adult). Each dot represents one mouse, horizontal bars represent mean, error bars represent SD, gray rectangles indicate weaning. ns: not significant. Statistical analysis was performed using two-tailed *t*-test. **h, i** Bone marrow (**h**) and spleen (**i**) from 2-day-old wild-type mice were analyzed by flow cytometry. Lin[−](CD3, B220, NK1.1, CD4, CD8 α , TER119) cells were gated, pre-cDCs were identified as indicated and stained with anti-DNGR-1 (red) or isotype-matched control antibodies (gray). Source data are provided as a Source Data file.

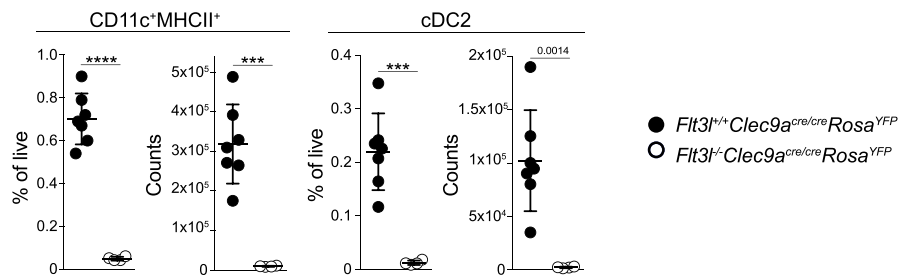
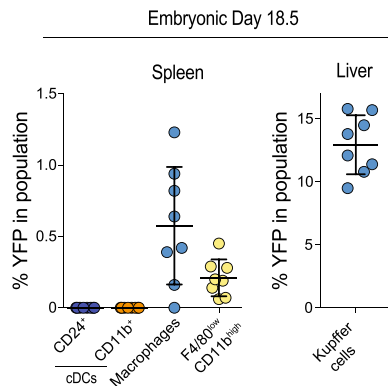
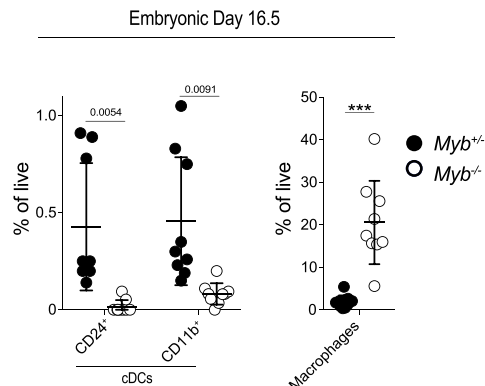
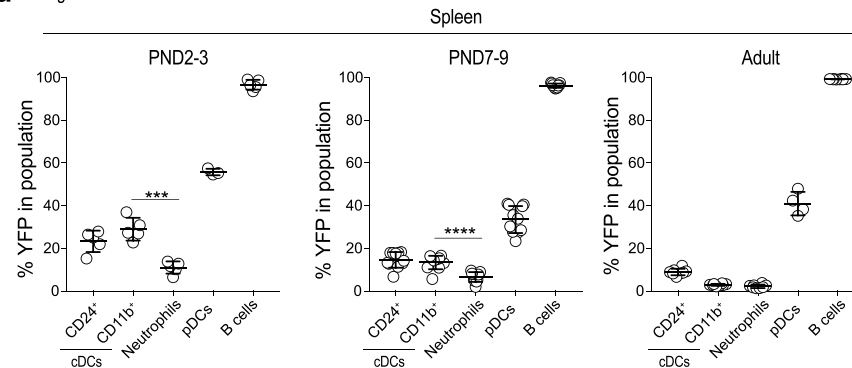
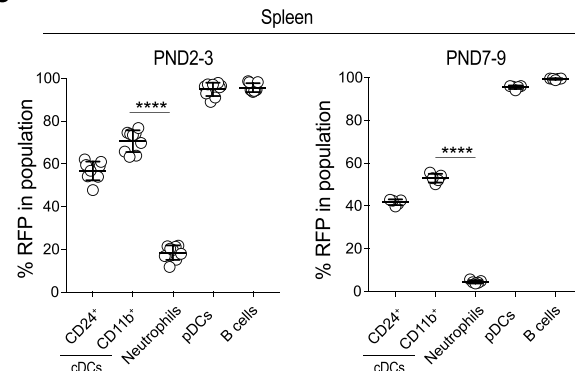
of cell origin⁴⁸. Consistent with our previous observations and their CDP origin^{5,48,54–56}, cDC2 from adult spleen showed near-complete labeling with TOMATO in *Clec9a^{cre/+}Rosa^{TOM}* mice ($93 \pm 1.28\%$). Notably, in neonatal mice TOMATO labeling in cDC2 was strongly reduced ($20.6 \pm 4.48\%$), indicating ontogenetic heterogeneity. The frequency of TOMATO⁺ cells within cDC2 increased with age until adult labeling was reached at around 4 weeks of age ($86 \pm 1.4\%$; Fig. 1f, g).

We have previously shown that increased CRE levels (in homozygous *Clec9a^{cre}* mice) leads to markedly increased labeling of DC precursors and differentiated cDCs, because a fraction of precursors “escapes” labeling in a stochastic fashion⁴⁸. In addition, the choice of fate reporter can influence labeling efficiency due to differences in the distance between the loxP sites⁶⁴. To exclude that reduced labeling of neonatal cDC2 was an artifact of the specific fate reporter used or due to “progenitor escape” in mice heterozygous for *cre*, we analyzed homozygous *Clec9a^{cre/cre}Rosa^{TOM}* mice and *Clec9a^{cre/cre}Rosa^{YFP}* mice. In both models, a relative lack of *Clec9a^{cre}*-mediated fate labeling in neonatal cDC2 was observed (Supplementary Fig. 1C, D). Importantly, TOMATO labeling did not correlate with either of the two cDC2 subsets, as ESAM^{high} or ESAM^{low} cells showed similar labeling frequency at all ages examined (Supplementary Fig. 1E). Comparable to observations in adult mice^{48,54}, *Clec9a^{cre}*-mediated TOMATO labeling in young mice remained restricted to CD11c⁺MHCII⁺ cDCs and cells resembling pDCs or pre-cDCs based on low CD11c and MHCII expression (Supplementary Fig. 1F, G).

As most of our work on DC ontogeny stems from studies in adult mice, we next confirmed that DNGR-1-expressing cDC progenitors were present in early life bone marrow and spleen. Cells resembling macrophage dendritic cell progenitors (MDPs) (lineage (lin)[−]CD11c[−]MHCII[−]CD11b^{low}CD115⁺CD135⁺CD117^{high}), CDPs (lin[−]CD11c[−]MHCII[−]CD11b^{low}CD115⁺CD135⁺CD117^{low}), and pre-cDCs (lin[−]MHCII[−]CD11b^{low}CD11c⁺CD135⁺CD172a^{int}) could be found in bone marrow from neonatal mice (Supplementary Fig. 2A, B). Notably, putative MDPs were more frequent, whereas CDP and pre-cDC-like cells were less frequent in neonatal compared to adult bone marrow (Supplementary Fig. 2B). Importantly, pre-cDC-like cells in bone marrow from 2-day- and 1-week-old mice uniformly expressed DNGR-1 (Fig. 1h and Supplementary Fig. 2C). Accordingly, TOMATO was detected in CDPs and pre-cDCs, but not MDPs or common lymphoid progenitors (CLPs) of 1- and 2-week-old *Clec9a^{cre/cre}Rosa^{TOM}* mice, as defined phenotypically (Supplementary Fig. 2E). These data confirm that *Clec9a*-driven CRE was active in DC precursors in early life. Importantly, pre-cDCs from 1- and 2-week-old mice labeled with TOMATO to a similar extent as their counterparts from adult mice, although labeling at 1 week of age had not completely reached adult levels (Supplementary Fig. 2E;

$81.15 \pm 2.77\%$ PND7, $94.67 \pm 1.72\%$ 2 weeks, $93.61 \pm 2.93\%$ adult). Pre-cDC-like cells with unimodal DNGR-1 expression were also found in spleen from 2-day- and 1-week-old mice (Fig. 1i and Supplementary Fig. 2D), and labeled with TOMATO at similar levels as their bone marrow counterparts (Supplementary Fig. 2E, F), indicating that CRE-mediated labeling of pre-cDCs completes in bone marrow. Actively cycling progenitor cells can escape labeling because of a time lag between CRE protein synthesis and DNA recombination^{45,48,49}. If cDC2 in neonates escaped labeling because of such rapid transition through their precursor stage, we would expect higher labeling in differentiated cDC2 than in their immediate progenitors. However, splenic pre-cDC labeled with TOMATO to a larger extent than differentiated cDC2 from the same mice at one and 2 weeks of age (Supplementary Fig. 2F). This is in contrast to adult mice, where labeling of splenic cDC2 and pre-cDCs was similar (Supplementary Fig. 2f). To further exclude the possibility that cDC2 in early life lack detectable TOMATO, because they have had insufficient time to accumulate enough fluorescent protein, we sorted TOMATO⁺ and TOMATO[−] CD11c⁺MHCII⁺CD11b⁺ cells from 1-week-old *Clec9a^{cre/cre}Rosa^{TOM}* mice and cultured them in the presence of the DC survival factors FLT3L and Granulocyte-macrophage colony-stimulating factor (GM-CSF). After 24 h, TOMATO[−] cells had remained TOMATO[−], supporting the notion that these cells arise independently of *Clec9a*-expressing progenitors (Supplementary Fig. 2G). Thus, cells resembling bona fide *Clec9a*-expressing cDC progenitors exist in early life and *Clec9a^{cre}* mice can be used to trace cDCs in early life.

Fate mapping reveals a lymphoid contribution to cDC2 in early life. To address the origin of cDC2 in early life, we first crossed *Clec9a^{cre/cre}Rosa^{YFP}* mice to mice lacking the growth factor FLT3L, which is required for the development of all DCs⁶⁵. In 2-week-old *Clec9a^{cre/cre}Rosa^{YFP}Flt3l^{−/−}* mice, both cDC1 and cDC2 were strongly reduced (Fig. 2a). Thus, early-life cDC2 require FLT3L for their development, independent of whether they arise from *Clec9a*-expressing progenitors or not. Hematopoiesis begins before birth and, in mice, yolk sac progenitors contribute to the generation of lymphoid and myeloid immune cells^{41,42,66,67}. To assess the contribution of yolk sac erythromyeloid progenitors to the cDC2 compartment in early life, we treated pregnant *Csf1r^{Mer-iCre}MerRosa^{YFP}* dams at E8.5 with 4OH-tamoxifen^{41,67} and analyzed spleens from offspring mice at E18.5, as well as 2 and 4 weeks after birth. Importantly, neither CD24⁺ nor CD11b⁺ cDCs labeled with YFP at any ages examined, when compared to liver Kupffer cells and splenic macrophages, which served as positive controls (Fig. 2b and Supplementary Fig. 3A). The transcription factor c-Myb is dispensable for yolk sac hematopoiesis but essential for the

a PND14 spleen**b** *Csf1r^{Meri-Cre-Mer}Rosa^{YFP}***c** Spleen**d** *Rag1^{cre}Rosa^{YFP}***e** *Il7^{cre}Rosa^{RFP}*

development of definitive HSCs⁶⁸. *Myb*-deficient mice are embryonically lethal but survive until E16.5. At this time CD24⁺ and CD11b⁺ cDCs, but not splenic macrophages, were reduced in spleens from *Myb*^{-/-} compared to littermate control embryos (Fig. 2c). Thus, CD11c⁺MHCI⁺ cells arise independent of yolk

sac-derived erythromyeloid progenitors and in late embryogenesis require c-Myb for their development, suggesting that they arise from definitive hematopoiesis.

CLPs can generate cDC-like cells in adoptive transfer^{69–73} and we have shown that lymphopoiesis contributes to cDC generation

Fig. 2 Fate mapping reveals a lymphoid contribution to cDC2 in early life. **a** Spleens from 2-week-old *Flt3l^{-/-}Clec9a^{cre/cre}Rosa^{YFP}* ($n = 7$) and *Flt3l^{+/+}Clec9a^{cre/cre}Rosa^{YFP}* ($n = 4$) mice were analyzed by flow cytometry. Shown are the frequency and number of CD11c⁺MHCII⁺ cells (left) and of cDC2 (middle). **b** *Csf1r^{Mer-iCre-Mer}* dams were mated with male *Rosa^{YFP}* mice and injected with 4OH-tamoxifen on E8.5. Spleen and liver from offspring mice were analyzed by flow cytometry on E18.5. The percentage of YFP⁺ cells in the indicated populations is plotted ($n = 8$). **c** Spleens from *Myb^{-/-}* and *Myb^{+/-}* littermate control mice were analyzed on E16.5. The frequency of the indicated populations was calculated and plotted ($n = 9$). **d** The percentage of YFP⁺ cells within the respective populations in spleen from *Rag1^{cre}Rosa^{YFP}* mice at the indicated ages ($n = 5$, PND2–3; $n = 11$ PND7–9; $n = 8$ adult; $n = 3$ and 4 for pDCs in PND2–3 and adult mice). **e** The percentage of RFP⁺ cells within the indicated populations in spleen from *Il7r^{cre}Rosa^{RFP}* mice at the indicated ages ($n = 9$, PND2–3; $n = 5$, PND7–9). Each dot represents one mouse, horizontal bars represent mean, error bars represent SD. *** $p < 0.001$, **** $p < 0.0001$. Statistical analysis in **a**, **c–e** was performed using two-tailed *t*-test. Source data are provided as a Source Data file.

when myeloid cDC progenitors are impaired⁷⁴. When cultured in vitro with FLT3L CLPs from *Clec9a^{cre/+}Rosa^{TOM}* mice gave rise to CD11c⁺MHCII⁺ cDC-like cells that predominantly resembled cDC1. However, few cDC2-like cells were also generated. These remained TOMATO negative, suggesting that CLP can generate TOM[−] cDC2 (Supplementary Fig. 3B). Expression of recombination-activating gene-1 is first detected in CLPs and required for the development of B and T cells by promoting somatic rearrangements of antigen receptor genes⁷⁵. Therefore, we profiled YFP labeling of splenic leukocytes in neonatal *Rag1^{cre}Rosa^{YFP}* mice at 2–3 and 7–9 days after birth, as well as in adulthood. As lineage decisions are stochastic, fate mapping with constitutive Cre is not absolute and should be considered at the population level and in the context of positive and negative control populations. Although B cells exhibited near-complete labeling with YFP at all ages examined (Fig. 2d), labeling in neutrophils ($11 \pm 2.86\%$ PND2–3, $6.63 \pm 2.32\%$ PND7–9, $2.27 \pm 0.82\%$ adults, Fig. 2d) and bone marrow erythroid cells ($5.32 \pm 1.88\%$ PND2–3, $1.87 \pm 0.8\%$ PND7–9) (Supplementary Fig. 3C), which served as negative controls, was low as expected⁶⁶. Notably, in 2- to 3-day- and 7- to 9-day-old *Rag1^{cre}Rosa^{YFP}* mice cDC2 labeled with YFP at $29 \pm 5.30\%$ and $13.43 \pm 3.16\%$, respectively (Fig. 2d and Supplementary Fig. 3C), whereas in cDC2 from adult spleen *Rag1^{cre}*-mediated YFP labeling did not exceed labeling of negative control populations (Fig. 2d and Supplementary Fig. 3C). Importantly, YFP labeling was comparable between ESAM^{high} ($16.15 \pm 1.01\%$) and ESAM^{low} ($15.21 \pm 1.07\%$) cDC2 in 7- to 9-day-old mice (Supplementary Fig. 3D), again supporting similar early life heterogeneity in both subsets. Of note, CD24⁺ cDC1 showed greater evidence of *Rag1^{cre}* expression history compared to cDC2 in neonatal and adult mice (Fig. 2d). IL-7 receptor (*Il7r*)-cre mice have been used to demonstrate that lymphoid progenitors do not contribute to cDCs in adult mice⁷⁶. We therefore used these mice as independent model to map the fate of lymphoid-restricted progenitors. Importantly, cDC2 from 2-day- and 1-week-old *Il7r^{cre}Rosa^{RFP}* mice labeled strongly with RFP, although labeling was lower in cDC2 from 1 week compared to 2-day-old mice (Fig. 2e).

Cxcr4^{creER} mice label consecutive stages of definitive hematopoiesis in embryonic and adult mice, while not labeling yolk sac progenitors⁷⁷. We therefore pulsed *Cxcr4^{creER}Rosa^{mTmG}* mice with tamoxifen at E12.5, reasoning that fetal liver HSCs would be labeled, allowing us to assess their contribution to splenic DCs. At E18.5, microglia, which served as negative control, exhibited no green fluorescent protein (GFP) labeling, as expected⁷⁷. In contrast, we observed labeling of monocytes and macrophages in E18.5 spleen, consistent with their descent from fetal liver HSCs (Supplementary Fig. 3E). Importantly, cDCs labeled with GFP to a similar extent, supporting the notion that fetal liver-resident progenitors contribute to cDC2 in early life (Supplementary Fig. 3E).

Thus, fate mapping indicates a lymphoid contribution to the steady-state cDC2 pool in early life, but not adulthood. Coupled

to the observation that cDC2 acquire *Clec9a^{cre}* expression history with age, these data suggest that cDC2 development is regulated in waves, with fetal liver-resident lymphoid progenitors contributing early but being gradually replaced with age by bona fide cDCs arising from *Clec9a*-expressing progenitors. Henceforth, we will refer to CD11c⁺MHCII⁺CD11b⁺ cells from *Clec9a^{cre}Rosa^{TOM}* mice that lack TOMATO expression as TOM[−] DC2 (Fig. 1f).

TOM⁺ cDC2 and TOM[−] DC2 in early life are phenotypically similar. Phenotypic analysis revealed no obvious differences in the expression of the prototypical cDC2 markers CLEC4A4, CD172a, CD26, ESAM, or CD4 on TOM⁺ cDC2 and TOM[−] DC2 from 1-week-old *Clec9a^{cre/cre}Rosa^{TOM}* mice (Fig. 3a). Expression of MHCII and the costimulatory molecule CD80 were also similar between TOM⁺ and TOM[−] cells (Fig. 3a). Using cytospin analyses we found cells with the typical dendritic morphology of cDCs, as well as cells with round morphology and little cytoplasm within TOM⁺ cDC2 and TOM[−] DC2 (Supplementary Fig. 3F). TOM⁺ cDC2 and TOM[−] DC2 in spleens from 1-week-old mice were located in the developing white pulp and in close proximity to CD3⁺ T cells (Fig. 3b). Thus, *Clec9a*-negative progenitors generate cDC2-like cells with similar phenotype and tissue localization to bona fide cDC2 arising from *Clec9a*-expressing progenitors.

TOM⁺ cDC2 and TOM[−] DC2 in early life are transcriptionally identical. Although environment strongly impacts cell identity, myeloid and lymphoid cell types arising from distinct hematopoietic sources at specified times during development can differ transcriptionally and functionally^{42,78–82}. To address if ontogeny transcriptionally imprints cDC2, we compared the gene expression profile of TOM⁺ cDC2 and TOM[−] DC2 from 1-week-old *Clec9a^{cre/cre}Rosa^{TOM}* mice to that of TOM⁺ cDC2 from adult mice. We used homozygous *Clec9a^{cre/cre}Rosa^{TOM}* mice to ensure highest penetrance *Clec9a^{cre}* and the 1-week time point, because ontogenetic heterogeneity was prominent enough to sort sufficient cells of both populations (Supplementary Fig. 1C), although ESAM^{high} to ESAM^{low} subset distribution at this age was still slightly lower than in adult mice (Fig. 1e). In principal component analysis (PCA) TOM⁺ cDC2 and TOM[−] DC2 from 1-week-old mice segregated away from adult TOM⁺ cDC2, identifying age as a major contributor to variation (Fig. 4a). Principle component 2 allowed some segregation between TOM⁺ cDC2 from TOM[−] DC2 from young mice, indicating differences in gene expression correlating with differential ontogeny (Fig. 4a). Using unsupervised hierarchical k-means clustering of differentially expressed genes we defined 14 clusters with distinct expression characteristics (Supplementary Fig. 4A). Of these, most clusters identified differences between cells from young and adult mice independent of *Clec9a^{cre}* expression history (Supplementary Fig. 4A), again highlighting that the biggest differences in gene expression are related to age. Clusters 8 and 14 identified genes

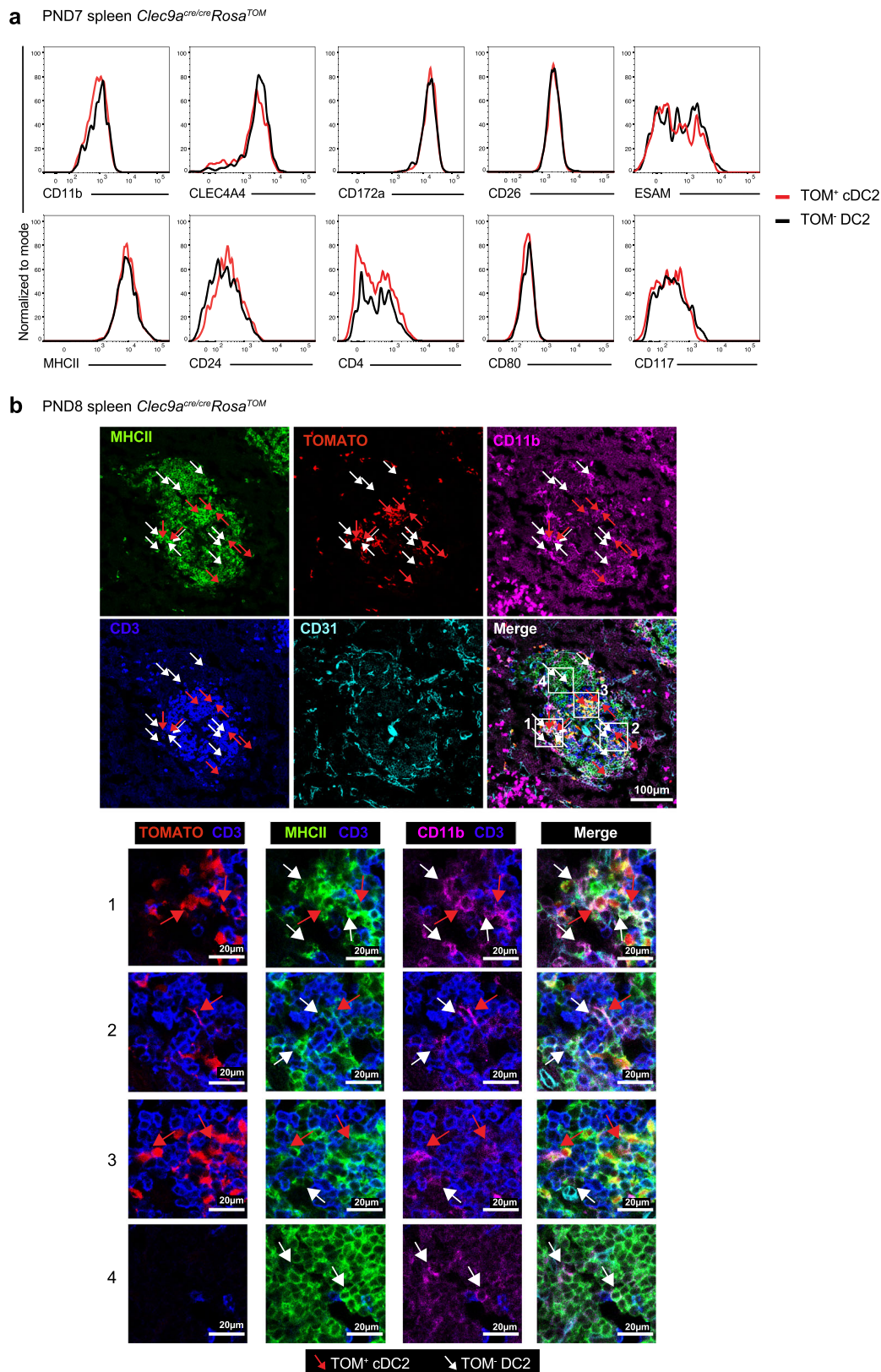
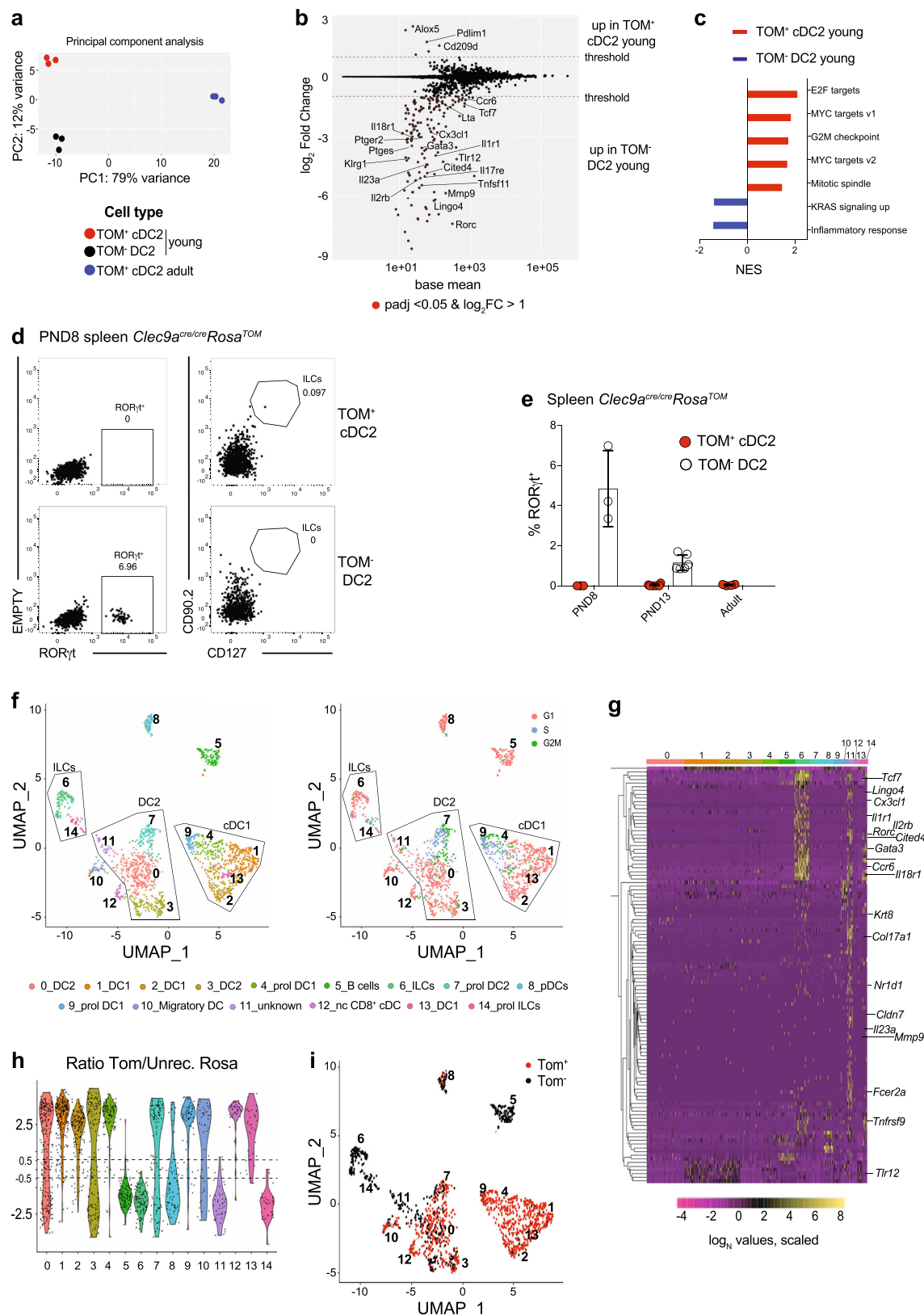


Fig. 3 TOM[−] DC2 phenotypically resemble TOM⁺ cDC2. **a** TOM⁺ cDC2 and TOM[−] DC2 from 1-week-old *Clec9a^{cre}/creRosa^{TOM}* mice were analyzed for expression of the indicated surface markers. Data are representative of at least two independent experiments with four to seven mice. **b** Splens from PND8 *Clec9a^{cre}/creRosa^{TOM}* mice were analyzed for expression of CD31 (cyan), CD3 (blue), MHCII (green), TOMATO (red), and CD11b (magenta) by microscopy. Numbered inset squares were magnified on the bottom panels TOM⁺ cDC2 (red arrows) or TOM[−] DC2 (white arrows) were identified. Data are representative of two independent experiments with three biological replicates.



with distinct expression characteristics in TOM⁻ DC2 compared to TOM⁺ cDC2 from young and adult mice (Supplementary Fig. 4A), identifying putative variation caused by ontogeny.

Pairwise comparison of TOM⁺ cDC2 and TOM⁻ DC2 from young mice identified 167 differentially expressed genes (log₂ fold change (log₂FC) > 1, adjusted *p*-value (padj) < 0.05) (Fig. 4b and Supplementary Data 1). In this comparison, TOM⁺ cDC2 showed

an enrichment of cell cycle genes (Fig. 4c), possibly reflecting the fact that these cells expand in number and gradually replace TOM⁻ DC2 with age. Most notable, several genes implicated in the biology of innate lymphoid cells (ILCs), such as *Rorc*, *Tcf7*, *Il18r1*, *Ccr6*, *Lingo4*, and *Lta*, showed higher expression in TOM⁻ DC2 than TOM⁺ cDC2 (Fig. 4b). Using flow cytometry, we detected a fraction of RORγt-expressing cells in TOM⁻ DC2 but

Fig. 4 TOM⁺ cDC2 and TOM⁻ DC2 in early life are transcriptionally identical. **a–c** TOM⁻ DC2 and TOM⁺ cDC2 from 8-day-old and TOM⁺ cDC2 from adult *Clec9a^{cre/cre}Rosa^{TOM}* mice were sorted and analyzed by mRNA sequencing. **a** Principal component analysis (PCA) of the top 500 most variable genes across all samples. Dots represent biological replicates. **b** Pairwise comparison of TOM⁺ cDC2 and TOM⁻ DC2 from 8-day-old mice. **c** Normalized enrichment score (NES) of gene sets enriched in TOM⁺ cDC2 (red) and TOM⁻ DC2 (blue) from 8-day-old mice. **d** TOM⁻ DC2 and TOM⁺ cDC2 from 8-day-old *Clec9a^{cre/cre}Rosa^{TOM}* mice were analyzed by flow cytometry for RORyt, CD90.2, and CD127 expression. Data are representative of three biological replicates. **e** The percentage of RORyt⁺ cells within TOM⁺ cDC2 and TOM⁻ DC2 in *Clec9a^{cre/cre}Rosa^{TOM}* mice at the indicated ages is shown ($n = 3$, PND8; $n = 6$, PND13; $n = 4$, adult). Each dot represents one mouse, horizontal bars represent mean, error bars represent SD. **f, g** CD19⁻MHCII⁺ cells from spleen of 9-day-old *Clec9a^{cre/cre}Rosa^{TOM}* mice were sorted after gating out F4/80^{high} macrophages and subjected to scRNA-Seq. **f** UMAP display of 1788 cells analyzed by unsupervised graph-based clustering with Seurat algorithm to indicate cluster identity (left) and cell cycle status (right) within clusters. **g** Heatmap displaying expression of genes enriched in TOM⁻DC2 compared to TOM⁺ cDC2 in bulk mRNA sequencing (Fig. 4b) among scRNA-Seq clusters. **h, i** The ratio of normalized *Tomato* reads per cell to normalized reads per cell of the predicted transcript of the unrecombined ROSA locus was calculated (**h**) and cells with a ratio > 0.5 were identified as *Tom*⁺, whereas cells with a ratio < -0.5 were identified as *Tom*⁻. **i** *Tom*⁺ and *Tom*⁻ cells visualized on the UMAP display. Source data are provided as a Source Data file.

not in TOM⁺ cDC2 from 1-week-old *Clec9a^{cre/cre}Rosa^{TOM}* mice (Fig. 4d, E). These cells lacked the canonical ILC markers CD127 and CD90^{83–85} and expressed typical cDC2 markers, including CD11c, MHCII, CD172a, CLEC4A4, ESAM and CD26, unlike ILCs (lin⁻CD11b⁻CD90⁺CD127⁺), which are CD11c negative (Supplementary Fig. 4B, C). Notably, the frequency of RORyt⁺ cells within the TOM⁻ DC2 population decreased with age and RORyt⁺ cells were not found in the adult cDC2 pool (Fig. 4e), raising the possibility that these RORyt⁺ cells may constitute a unique population of DC2 that is transiently present in early life and disappears with age.

To address this, we next performed droplet-based single-cell RNA-sequencing (scRNA-seq). We sort-purified splenic MHCII⁺ cells from 9-day-old *Clec9a^{cre/cre}Rosa^{TOM}* mice, after excluding CD19⁺ B cells and F4/80^{high} macrophages (Supplementary Fig. 5A). Using this approach, we expected to identify all main DC subsets, including cDC1, non-canonical CD8⁺ cDCs, TOM⁺ cDC2, and TOM⁻ DC2 and CD11c^{low}MHCII^{low} pDCs, as well as a fraction of RORyt-expressing type 3 ILCs that expresses MHCII but lacks CD11c (Supplementary Figs. 4B and 5a). Unsupervised graph-based clustering identified 15 clusters as visualized by dimensionality reduction using Uniform Manifold Approximation and Projection (UMAP) (Fig. 4f)^{86,87}. We identified some proliferating cells (being in G2M and S phase) in all clusters, but excluded clusters 4, 7, 9, and 14 from comparative analyses, as they consisted predominantly of proliferating cells (Fig. 4f). The identity of each cluster was determined using the top differentially expressed genes in combination with a priori knowledge about signature genes of cDCs and other immune cells (Supplementary Fig. 5B–E). Cluster 5 identified a contamination with *Cd19*-expressing B cells (Supplementary Fig. 5B), indicating a possible sort impurity or a discord between RNA and protein expression⁸⁸. cDC1 were partitioned across 5 clusters (1, 2, 4, 9, and 13) based on expression of *Xcr1*, *Cd24a*, *Irf8*, and *Tlr3* (Supplementary Fig. 5B, C). We further added the sequence of *cre* as inserted in the *Clec9a* locus^{48,89} into the reference transcriptome and found *cre* expression exclusively in clusters 1, 2, 4, 9, and 13, consistent with *Clec9a* expression in early life cDC1¹⁷. Cluster 8 constituted *Siglech* and *Ccr9* expressing pDCs and clusters 6 and 14 showed high expression of *Rorc*, *Rora*, *Il7r*, *Il18r1*, and *Tox*, identifying them as ILC3s^{83,84}. Cluster 12 resembled E2-2-dependent non-canonical CD8⁺ cDCs based on *Cx3cr1*, *Cd24a*, *Sirpa* (CD172a), and *Tcf4* (encoding for E2-2) expression^{58,60} (Supplementary Fig. 5B, C). cDC2 were spread across clusters 0, 3, and 7 based on expression of *Sirpa*, *Itgam*, *Irf4*, and published signature genes⁹⁰ (Supplementary Fig. 5B, D). Notably, cluster 3 more closely resembled ESAM^{low}, whereas cluster 0 resembled ESAM^{high} cDC2⁵⁹ (Supplementary Fig. 5F). In addition, we identified cluster 10 as cells resembling migratory cDCs⁹⁰ (Supplementary Fig. 5E). We were

not able to assign a clear identity to cluster 11, although this cluster showed expression of core cDC2 and ESAM^{high} cDC2 signature genes (Supplementary Fig. 5D, F). Notably, *Rorc* was found among the genes characteristic for cluster 11 and this population showed an enrichment of genes with higher expression in TOM⁻ DC2 in the pairwise comparison of TOM⁺ cDC2 and TOM⁻ DC2 in bulk RNA-seq (Fig. 4g and Supplementary Fig. 5B).

We next identified TOM⁺ cDC2 and TOM⁻ DC2 by adding the sequence of *Tomato* and the predicted transcript of the unrecombined *Rosa* locus into the reference transcriptome⁹¹. Forming the ratio of normalized *Tomato* reads per cell to normalized reads per cell of the predicted transcript of the unrecombined *Rosa* locus (ratio *Tom*/unrec. *Rosa*) clearly separated B cells (cluster 5) and cDC1 (clusters 1, 2, 4, 9, and 13), which served as negative and positive controls for *Tomato* expression, respectively (Fig. 4h). Accordingly, we set a threshold and identified *Tom*⁻ (ratio *Tom*/unrec. *Rosa* < -0.5) and *Tom*⁺ cells (ratio *Tom*/unrec. *Rosa* > 0.5, Fig. 4h). *Tom*⁺ and *Tom*⁻ cells distributed evenly within the UMAP of cDC2 clusters 0, 3, and 7 (Fig. 4i), and pairwise comparison of *Tom*⁺ and *Tom*⁻ cells within clusters 0 and 3 revealed few differences in gene expression, indicating that these cells are transcriptionally similar (Supplementary Data 2). Notably, cells within cluster 11 were predominantly *Tom*⁻, again indicating that this cluster corresponds to RORyt-expressing TOM⁻ DC2 (Fig. 4i).

In adults, cDC2 can be divided into T-bet expressing cDC2A and T-bet-negative cDC2B, putatively controlled by RORyt and C/EBPα⁹². This division appeared to hold up in early life as cluster 0 showed an enrichment of T-bet⁺ cDC2A signature genes (Supplementary Fig. 5G), whereas cluster 3 more closely resembled T-bet⁻ cDC2B (Supplementary Fig. 5G). Interestingly, cells in cluster 11 did not correspond to T-bet⁻ cDC2B but more closely resembled T-bet⁺ cDC2A (Supplementary Fig. 5G), consistent with the high expression of ESAM on RORyt⁺ DC2 (Supplementary Fig. 4C). To gain insights into a putative developmental hierarchy between *Rorc*-expressing cluster 11, cDC2 (clusters 0, 3, and 7), and ILC3 (clusters 6 and 14), we applied Palantir algorithm⁹³. Setting the starting point within cluster 11 identified two terminal states, one in ILC cluster 14 and one in cDC2 cluster 0 (Supplementary Fig. 5H). However, differentiation potential diminished quickly upon exit from cluster 11 and the branch probability that cells from cluster 11 reach the terminal states was low (Supplementary Fig. 5H). Accordingly, fate mapping in *Rorc^{cre}Rosa^{RFP}* mice⁹⁴ identified only few RFP⁺ cDC2 in 2-week-old mice that included a fraction that also stained positive for RORyt (Supplementary Fig. 5I). As RFP⁺ cells were only a minor fraction of the total splenic DC2 compartment in young mice, RORyt⁺ cells are unlikely to act as progenitors for TOM⁻ DC2 in early life.

Thus, in concordance with fluorescence-activated cell sorting (FACS) analyses, scRNA-seq revealed that cDC2 in 1-week-old mice contain the two main cDC2 subtypes also found in adults, and that, despite their distinct origin, TOM⁺ cDC2 and TOM[−] DC2 distribute evenly across cDC2 clusters, indicating they constitute transcriptionally identical cells. Differences in gene expression between TOM⁺ cDC2 and TOM[−] DC2 from 1-week-old mice in bulk RNA-seq correlated to a unique *Rorc*-expressing cluster of cDC2 that transcriptionally closely resembles but is distinct from ESAM^{high} cDC2 and present exclusively in early life.

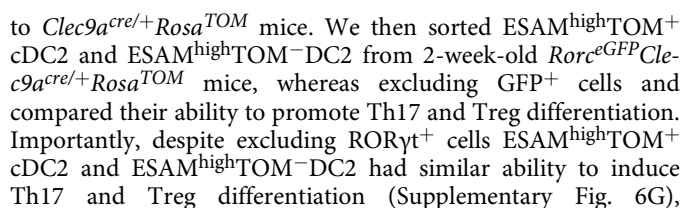
Age defines the strongest differences in gene expression. Having established ontogeny as a minor contributor to transcriptional variation, we next focused on differences in gene expression caused by age. Pairwise comparison of TOM⁺ cDC2 from 1-week-old and adult mice identified 1490 differentially expressed genes (log₂FC > 1, padj < 0.05) (Fig. 5a and Supplementary Data 3). TOM⁺ cDC2 from 1-week-old mice showed an enrichment of genes involved in cell cycle (Fig. 5b), possibly reflecting increased homeostatic proliferation within the expanding DC pool. TOM⁺ cDC2 from adults were enriched for genes implicated in the inflammatory response, which could indicate an increased level of activation or functional maturation of adult cDC2¹⁵. Most notable was the identification of genes involved in signaling downstream of IFN-γ, tumor necrosis factor-α (TNF-α), IL-2, and IFN-α (Fig. 5b) enriched in cDC2 from adult mice. As expression of receptors for these cytokines was comparable in 1-week-old and adult mice (Supplementary Data 3), these data suggested a distinct cytokine environment acting on cDC2 in spleen from neonatal and adult mice. We confirmed higher expression of PD-L1 (encoded by the *Cd274* gene) and CD38 (*Cd38*), which are regulated by type I and II IFN signaling^{95,96}, on TOM⁺ cDC2 from adult compared to 2-week-old mice (Fig. 5c). Importantly, expression of these markers was reduced on cDC2 from adult *Ifnar*^{−/−} compared to wild-type control mice (Fig. 5d), supporting the notion that distinct cytokine environments act on splenic cDC2 in early and adult life and indicating that age-dependent differences in gene expression are at least in part caused by IFN-α.

Among genes differentially expressed with age, we identified several pattern recognition receptors (PRRs) with higher expression in TOM⁺ cDC2 from adults, including *Clec7a* (encoding for Dectin-1), *Tlr7*, and *Tlr5* (Supplementary Fig. 6A). In contrast, expression of *Clec4n* (encoding for Dectin-2), *Tlr4*, and *Tlr2* was higher in early life (Supplementary Fig. 6A), whereas expression of other PRRs, such as *Tlr6*, *Tlr9*, and *Nod1* was comparable in cDC2 from 1-week-old and adult mice (Supplementary Fig. 6A). In line with previous observations in the lung^{32,35–37}, cDC2 from adult mice showed higher expression of several costimulatory molecules, including *Cd80*, *Cd40*, *Cd274* (encoding for PD-L1) and *Tnfsf4* (encoding for OX40L) (Fig. 5a). Lower expression of costimulatory molecules could indicate a reduced ability of early-life cDC2 to activate T cells but costimulatory signals also balance effector T-cell responses. *Tnfsf4* and *Cd274* for instance can suppress IL-17A production in T cells^{97,98}. Interestingly, adult cDC2 further showed higher expression of bone morphogenic protein 2 (*Bmp2*), which also suppresses IL-17A production from T cells⁹⁹ (Supplementary Fig. 6B). On the contrary, TOM⁺ cDC2 from 1-week-old mice showed higher levels of factors that promote Th17 and Treg differentiation, such as *Lgals3*, *Il6ra*, *Lgals1*, and *Sema4a*^{100–106} (Supplementary Fig. 6B). In line with age being the foremost contributor to transcriptional variation, expression of the aforementioned genes was similar between TOM⁺ cDC2 and TOM[−] DC2 from 1-week-old mice. Taken

together, these data suggest that distinct cytokine environments in early and adult life act on cDC2 to shape their transcriptional profile and ability to induce immune responses.

Early-life cDC2 induce distinct T-cell responses in vitro compared to adult-life cDC2. The above data suggested that cDC2 in early and adult life may differ in their ability to induce effector T-cell differentiation. To address this possibility in vitro, we sort-purified TOM⁺ cDC2 and TOM[−] DC2 from young and TOM⁺ cDC2 from adult mice, and pulsed them with Ovalbumin (OVA) peptide 323–339 (OVA_{323–339}). cDC2 populations were sorted from two to 2.5-week-old mice, because at this age ESAM^{high} to ESAM^{low} subset distribution had reached adult levels and ESAM^{high} cells dominated the cDC2 compartment (Fig. 1e). Although DNNGR-1 has no known function in DC development and is not expressed in cDC2, we used mice heterozygous for *cre* in functional assays, because *Clec9a*^{cre/cre} mice lack functional DNNGR-1⁴⁸. Peptide pulsed DC2 populations were subsequently cultured with naive OT-II transgenic T cells from adult mice in the absence or presence of T-cell polarizing cytokines. Adult T cells were chosen as responders, because neonatal T cells exhibit an intrinsic Th2 bias². Notably, TOM⁺ cDC2 and TOM[−] DC2 from young mice and TOM⁺ cDC2 from adult mice stimulated similar proliferation of naive T cells in all conditions tested (Fig. 5e, f and Supplementary Fig. 6C, D), indicating that adult cDC2 do not exhibit an increased level of activation in terms of their ability to stimulate T cells. Compared to adult cDC2, TOM⁺ cDC2, and TOM[−] DC2 from young mice also induced similar effector differentiation of OT-II cells under non-polarizing (Th0) and Th1 conditions, as assessed by IFN-γ production (Fig. 5g and Supplementary Fig. 6D). We did not observe IL-4 production from T cells stimulated under Th0 conditions by intracellular staining but Th2 cytokine levels in culture supernatants from T cells stimulated with cDC2 from young and adult mice were similar (Supplementary Fig. 6F). Thus, early life splenic cDC2 do not exhibit an intrinsic Th2 bias, which is in contrast to neonatal cDC2 from lung³⁰. In line with higher expression of positive regulators of Th17 differentiation, TOM⁺ cDC2 and TOM[−] DC2 from young mice induced twofold higher IL-17A production from T cells under Th17 conditions than cDC2 from adult mice (Fig. 5f, g). Similarly, under Treg conditions more OT-II T cells were positive for Foxp3 when stimulated with DC populations from young mice (Fig. 5f, g). Thus, despite exhibiting increased expression of proliferation related genes (Fig. 5b), cDC2 from young mice induce similar proliferation of T cells as their adult counterparts, whereas inducing higher Th17 and Treg differentiation, indicating qualitative, rather than quantitative differences in the ability to polarize T cells.

As ESAM^{high} and ESAM^{low} cDC2 have different transcriptional programs and may stimulate different types of T-cell responses⁶², we next addressed whether both subsets have different functions with age. We therefore sorted ESAM^{high} and ESAM^{low} TOM⁺ cDC2 from 2-week-old and adult mice and assessed their ability to stimulate Th17 and Treg differentiation as above. ESAM^{high} and ESAM^{low} cDC2 from young mice induced higher Th17 differentiation than their counterparts from adult mice (Fig. 5h). Similarly, ESAM^{high} cDC2 from young mice induced higher Treg differentiation than their adult counterparts, whereas ESAM^{low} cDC2 from young and adult mice induced similar Treg differentiation (Fig. 5h). Thus, functional differences between early and adult life exist for ESAM^{high} and ESAM^{low} cDC2, although there appears to be some level of subset specific functional regulation. As ESAM^{high} TOM[−] DC2 contain a unique fraction RORγt-expressing cells of unknown function (1.15 ± 0.38%, Fig. 4e), we next crossed *Rorc-eGFP* mice



To determine whether early-life cDC2 are also capable of antigen uptake and processing, we first cultured TOM⁺ cDC2 and TOM⁻ DC2 from 2-week-old and TOM⁺ cDC2 from adult *Clec9a^{cre/+}Rosa^{Tom}* mice with fluorescently labeled latex beads in vitro for 2 h in the presence or absence of cytochalasin D. All

Fig. 5 Age causes strongest differences in gene expression and cell function. **a, b** Bulk mRNA sequencing performed as in Fig. 4A–C. **a** Pairwise comparison of TOM⁺ cDC2 from 8-day-old and adult mice indicating genes with a $\log_2FC > 1$ and $padj < 0.05$ in red. **b** NES of gene sets enriched in TOM⁺ cDC2 from 8-day-old (red) or in cDC2 from adult mice (blue). **c** TOM⁺ cDC2 from 2-week-old and adult *Clec9a^{cre/+}Rosa^{TOM}* mice were analyzed for expression of PD-L1 ($n = 5$, 2-week-old; $n = 4$, adult) and CD38 ($n = 7$, 2-week-old; $n = 6$, adult) (MFI = mean fluorescence intensity). **d** Splenic cDC2 from adult wild-type and *Ifnar^{-/-}* mice were profiled for expression of PD-L1 and CD38 ($n = 5$). Expression levels are depicted as MFI. Each dot represents one mouse, horizontal bars represent mean, error bars represent SD. **e–g** TOM[−] DC2 and TOM⁺ cDC2 from 2-week-old and TOM⁺ cDC2 from adult *Clec9a^{cre/+}Rosa^{TOM}* mice were sorted, pulsed with OVA_{323–339}, and co-cultured with CTV-labeled OT-II cells under Th0 or polarizing conditions for 3.5 days. **e** Left: CTV dilution of OT-II cells co-cultured with the indicated populations or CD11c-enriched splenocytes without OVA_{323–339} (gray). Right: division and proliferation indexes of OT-II cells after co-culture with the indicated DC2 populations ($n = 5/6$, 2-week-old TOM⁺ and TOM[−] cDC2, $n = 4$, adult TOM⁺ cDC2). **f** T cells were analyzed for expression of Foxp3 and IL-17A. For Th17 conditions (right) numbers in each quadrant represent the mean \pm SD ($n \geq 7$). **g** The percentage of cytokine or Foxp3-positive cells within proliferated OT-II cells is shown. APC : T-cell ratio 1 : 2 for Th0, Th1, Th17 and 1 : 10 for Treg ($n = 6$, Th0/Th1; $n = 3$, Treg; $n = 8$, Th17; for 2-week-old TOM⁺ cDC2; $n = 5$, Th0; $n = 4$, Treg/Th1; $n = 8$, Th17 for TOM[−] DC2; $n = 4$, Th0/Th1/Treg; $n = 7$, Th17 for adult TOM⁺ cDC2). **h** TOM⁺ cDC2 from 2-week-old ($n = 5$) and adult mice ($n = 6$, Treg; $n = 7$, Th17) were sorted as ESAM^{high} and ESAM^{low} cells, pulsed with OVA_{323–339} and cultured with CTV-labeled OT-II cells under Treg and Th17 polarizing conditions as above. The percentage of cytokine or Foxp3-positive cells within proliferated OT-II cells is shown. **i** TOM[−] DC2 and TOM⁺ cDC2 from 2-week-old and TOM⁺ cDC2 from adult *Clec9a^{cre/+}Rosa^{TOM}* mice were co-cultured with OT-II cells in the presence of OVA under Th17 conditions for 4 days. The division index (left) and percentage of IL-17A producing OT-II cells (right, APC : T-cell ratio 1 : 2) are shown ($n = 4$). Each dot represents one biological replicate from four independent experiments, horizontal bars represent mean, error bars represent SD. *** $p < 0.001$, **** $p < 0.0001$. Statistical analysis was performed using two-tailed paired *t*-test (comparing TOM[−]DC2 and TOM⁺ cDC2 groups), one-way ANOVA (comparing 2-week-old and adult groups) or two-tailed *t*-test in (**c, d, h**). Only statistically significant comparisons are indicated. Source data are provided as a Source Data file.

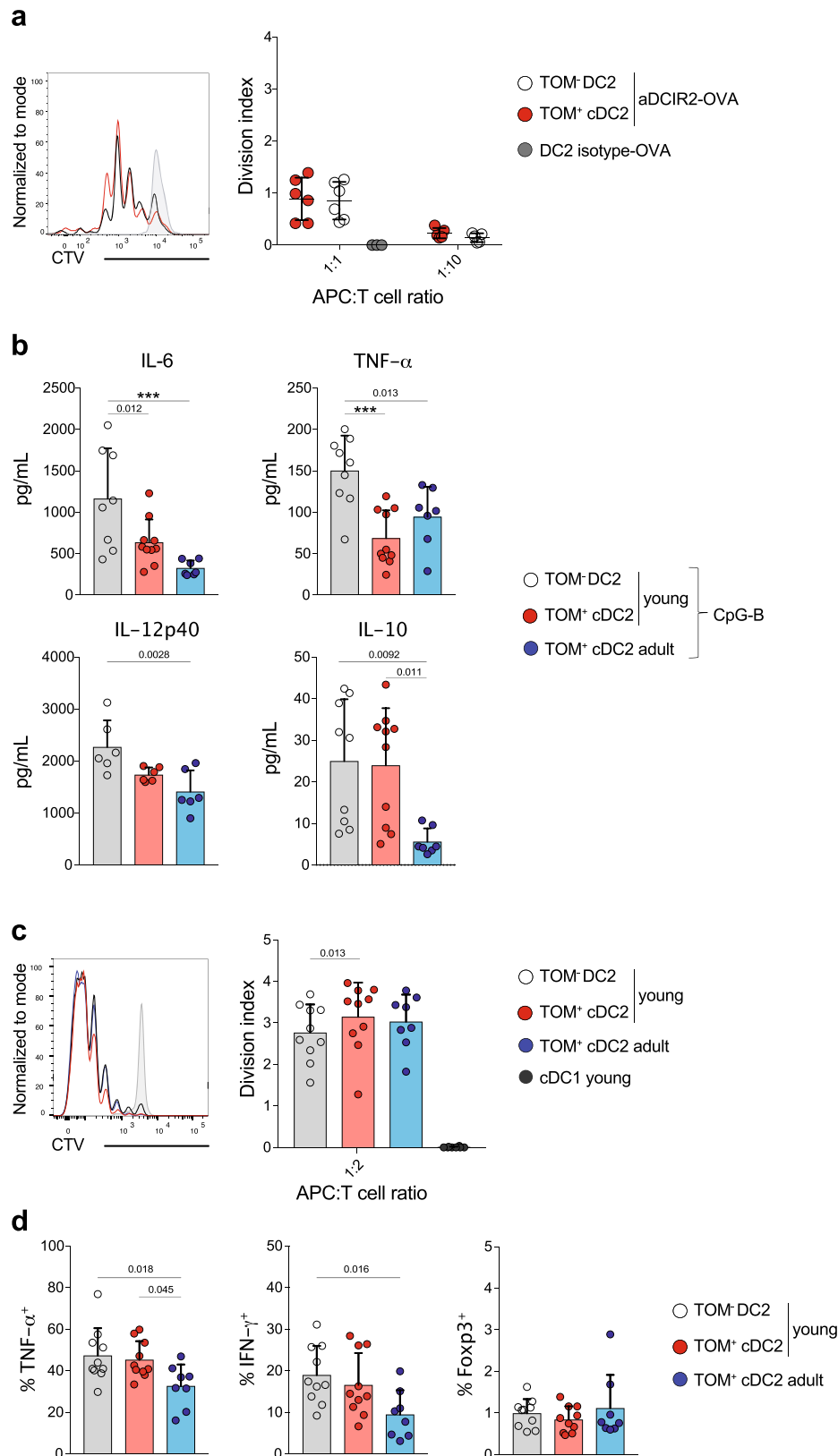
populations took up fluorescently labeled beads with similar efficiency (Supplementary Fig. 6H). Bead uptake was mediated by phagocytosis, as it was inhibited by cytochalasin D (Supplementary Fig. 6H). Thus, TOM⁺ cDC2 and TOM[−] DC2 do not differ in their phagocytic ability. We next cultured TOM⁺ cDC2 and TOM[−] DC2 from young mice and adult TOM⁺ cDC2 with CellTrace Violet (CTV)-labeled OT-II T cells in the presence of OVA under Th17 conditions (Fig. 5i). As observed before, TOM⁺ cDC2 and TOM[−] DC2 from young mice induced a higher frequency of IL-17A-producing T cells than adult cDC2 (Fig. 5i). Thus, TOM⁺ cDC2 and TOM[−] DC2 from young mice are comparable to their adult counterparts in their ability to process antigen and induce naive T-cell proliferation in an antigen-specific manner. TOM⁺ cDC2 and TOM[−] DC2 from young mice promoted similar Th17 and Treg differentiation; however, compared to adult cDC2, Th17 and Treg differentiation was increased, supporting the notion that distinct environmental cues in young and adult mice shape the ability of DCs to induce T-cell differentiation. Although such cytokines could be regulated in response to the microbiota, cDC2 from adult mice housed in germ-free (GF) and specific pathogen-free (SPF) conditions induced similar OT-II cell differentiation under Th0, Th17, and Treg conditions, and did not recapitulate the phenotype of young cDC2 in terms of PDL-1 and CD38 expression (Supplementary Fig. 6I, J). These data suggest that functional differences of cDC2 in early life are not simply due to a lower microbial load at this age.

Early-life cDC2 induce distinct T-cell responses upon targeted antigen delivery compared to adult-life cDC2. Having established that cDC2 from young mice can activate T cells in vitro, we next asked whether cDC2 from young mice have this capacity upon direct delivery of antigens in vivo. We relied on an established method to target the model antigen OVA to cDC2 by coupling it to an antibody directed against the C-type lectin receptor CLEC4A4/DCIR2^{25,107}. As TOM⁺ cDC2 and TOM[−] DC2 were phenotypically identical, we were unable to target either cell population individually but CLEC4A4 was expressed by both TOM⁺ cDC2 and TOM[−] DC2 (Fig. 3a). We injected 2-week-old *Clec9a^{cre/+}Rosa^{TOM}* mice with anti-DCIR2-OVA or isotype-matched control antibody of irrelevant specificity. Twelve hours later, we sort-purified splenic TOM⁺ cDC2 and TOM[−]

DC2, and co-cultured them with CTV-labeled OT-II T cells from adult mice (Fig. 6a) to overcome any T-cell intrinsic differentiation bias in early life². In this experimental set up, TOM⁺ cDC2 and TOM[−] DC2 induced OT-II proliferation upon targeting with anti-DCIR2-OVA but not isotype-matched control antibody (Fig. 6a). Thus, TOM⁺ cDC2 and TOM[−] DC2 from 2-week-old mice could be targeted with anti-DCIR2 and process antibody–antigen complexes for presentation to CD4⁺ T cells, although OT-II proliferation in the absence of adjuvant was low, as expected¹⁰⁷.

Immune responses in early life are Th2 biased but such predisposition can be overcome through the use of Th1 adjuvants, such as CpG-B^{108,109}. CpG-B signals through TLR9, which was similarly expressed between the profiled cDC2 populations in bulk mRNA sequencing (Supplementary Fig. 6A). Nonetheless, TOM⁺ cDC2 and TOM[−] DC2 from 2-week-old and TOM⁺ cDC2 from adult mice showed a distinct cytokine profile after CpG-B stimulation. In response to CpG-B TOM[−] DC2 from young mice were the most efficient cytokine producers and secreted higher amounts of IL-6, IL-12p40, and TNF- α than cDC2 from adults (Fig. 6b). Interestingly, IL-6 and TNF- α production were significantly higher in TOM[−] DC2 compared to TOM⁺ cDC2 from young mice, raising the possibility that these cells have distinct inflammatory potential. Independent of origin cDC2 from young mice produced higher IL-10 and IL-27 than their adult counterparts (Fig. 6b and Supplementary Fig. 7A). Although IL-27 production was low and not detectable in all samples, it is noteworthy, because DCs from peripheral blood of children show increased IL-27 production compared to DCs from adults¹¹⁰. Thus, despite exhibiting similar *Tlr9* expression cDC2 from young mice have different cytokine response to CpG-B than cDC2 from adults, indicating distinct signaling downstream of TLR9 and supporting the hypothesis that age imprints cDC2 with distinct immune reactivity.

We next tested whether the distinct response to CpG-B stimulation would influence the ability of cDC2 to activate T cells and induce their differentiation. We injected 2.5-week-old or adult mice with anti-DCIR2-OVA in the presence of CpG-B as adjuvant. Twelve hours later, we sorted TOM⁺ cDC2 and TOM[−] DC2 from young mice, as well as TOM⁺ cDC2 from adult mice and co-cultured them with CTV-labeled OT-II T cells isolated from adult mice (Fig. 6c, d). After 3.5 days, T-cell proliferation, cytokine production, and Foxp3 expression were analyzed. In this



assay, TOM⁺ cDC2 and TOM⁻ DC2 from young mice and cDC2 from adult mice induced similar OT-II T-cell proliferation (Fig. 6c). Targeting was cell-type specific as cDC1 did not promote T-cell proliferation (Fig. 6c). Importantly, T cells stimulated with TOM⁺ cDC2 and TOM⁻ DC2 from young mice produced more TNF- α than T cells stimulated with cDC2 from adult mice (Fig. 6d). Notably, this is in contrast to splenic

human cDC2 from fetal tissue, which suppress T-cell-derived TNF- α through ARGINASE 2⁴³. T cells stimulated with TOM⁻ DC2 from young mice also produced more IFN- γ than T cells stimulated with cDC2 from adult mice (Fig. 6d and Supplementary Fig. 7B). Increased IFN- γ production was also observed for T cells stimulated with TOM⁺ cDC2 from young mice compared to cDC2 from adults (Fig. 6d and Supplementary Fig. 7B),

Fig. 6 Early-life cDC2 induce distinct T-cell responses upon targeted antigen delivery compared to adult-life cDC2. **a** 2-Week-old *Clec9a^{cre}/Rosa^{TOM}* mice were injected i.p. with aDCIR2-OVA or isotype-OVA control antibody. After 12 h, TOM⁺ cDC2 and TOM⁻ DC2 were sorted and co-cultured with OT-II cells for 3.5 days. CTV dilution (left) and division index of OT-II cells after co-culture with the indicated DC2 populations (right) are shown ($n = 6$, 1:1 ratio; $n = 5$, 1:10 ratio; $n = 3$, isotype-OVA). **b** TOM⁺ cDC2 and TOM⁻ DC2 from 2-week-old and TOM⁺ cDC2 from adult *Clec9a^{cre}/Rosa^{TOM}* mice were sorted and stimulated with CpG-B. Cytokine production was analyzed 18–20 h later. Each dot represents a biological replicate from 4 (IL-6, TNF- α , and IL-10) or two (IL-12p40) independent experiments. **c, d** 2-Week-old and adult *Clec9a^{cre}/Rosa^{TOM}* mice were injected i.p. with anti-DCIR2-OVA antibody plus CpG-B. After 12 h DC populations were sorted and co-cultured with OT-II T cells as in **a**. **c** CTV dilution (left) and division index (right) of OT-II cells after co-culture with the indicated DC populations ($n = 10$, 2-week-old; $n = 8$, adult and cDC1 from 2-week-old mice). **d** Percentage of TNF- α , IFN- γ , and Foxp3-positive cells within proliferated OT-II cells ($n = 10$, 2-week-old; $n = 8$, adult). Each dot represents one biological replicate from at least three independent experiments, horizontal bars represent mean, error bars represent SD. *** $p < 0.001$. Statistical analysis was performed using two-tailed paired *t*-test (comparing TOM⁻DC2 and TOM⁺cDC2 groups) or one-way ANOVA (comparing 2-week-old and adult groups). Only statistically significant comparisons are indicated. Source data are provided as a Source Data file.

although differences did not reach statistical significance. Thus, TOM⁺ cDC2 and TOM⁻ DC2 from young mice induced more TNF- α production from T cells and greater Th1 differentiation than adult cDC2. Increased Th1 differentiation could be related to the slight increase in IL-12p40 production in cDC2 from young compared to adult mice upon CpG-B stimulation (Fig. 6b); however, it is likely that other factors, such as costimulatory molecules (Fig. 5a), also contribute. Notably, production of Th2 cytokines and Foxp3 expression was similar between T cells stimulated with cDC2 from young and adult mice (Fig. 6d and Supplementary Fig. 7B) and Th17 cytokine production was not observed. Taken together, early-life TOM⁺ cDC2 and TOM⁻ DC2 are fully capable of inducing T-cell proliferation upon targeted antigen delivery in vivo but in the context of CpG-B stimulation early-life cDC2 induce an increased Th1 response compared to adult-life cDC2.

Discussion

The cDC compartment in early, compared to adult life, exhibits quantitative and qualitative differences in its ability to induce immunity, leading some to suggest that cDCs in early life may be functionally immature. Here we set out to define the reasons underlying age-dependent functional differences of cDCs. We demonstrate that early-life cDC2 exhibit a distinct hematopoietic origin and, similar to other myeloid and lymphoid cells, develop sequentially at specified times during development. In contrast to other cell types that develop in waves^{42,80–82}, cell origin appeared negligible for cell function, as ontogenetically distinct cDC2 in early life were transcriptionally and functionally similar and within 2 weeks after birth could prime naive T cells at levels comparable to cDC2 from adult mice. Instead our data suggest that cytokine environments in early and adult life imprint cDC2 with a distinct gene expression profile that alters their ability to respond to pathogenic stimuli, secrete cytokines, and induce T-cell differentiation. Thus, cDC2 in early life are functionally capable but transcriptionally pre-disposed to respond differently to pathogens and induce distinct T-cell responses than their adult counterparts.

In early life, the majority of cDC2 originated from *Clec9a*-negative progenitors denoted here as TOM⁻ DC2. These cells were replaced within the first few weeks after birth by cells arising from bona fide *Clec9a*-expressing myeloid cDC progenitors, denoted as TOM⁺ cDC2. Coinciding with the increase in *Clec9a-cre* expression history, we found evidence of a lymphoid contribution to the early-life cDC2 compartment using *Rag1^{cre}* and *Il7^{cre}* mice that declined with age. *Rag1^{cre}* also labels the progeny of yolk sac-derived lymphomyeloid primed progenitors⁶⁶ and *Il7^{cre}* expression history is found in macrophages of yolk sac origin¹¹¹. As we exclude a yolk sac origin but demonstrate cDCs to be *Myb*-dependent, our data indicate an HSC-

derived lymphoid contribution to early-life cDCs. Such lymphoid progenitors likely arise from fetal liver-resident progenitors, as we find splenic cDC2 as early as E16.5 (Fig. 2c and Supplementary Fig. 1D), at which stage hematopoiesis has yet to colonize bone marrow^{112,113}. This notion is further supported by in utero *Cxcr4^{creER}* fate mapping⁷⁷. A lymphoid path to generating cDCs has been suggested^{69,71–74} but does not contribute to the steady-state cDC pool in adult mice^{48,74,76}. Our data suggest that lymphopoiesis contributes to the cDC compartment of mice in early life. Such layered ontogeny is reminiscent of other immune cells that develop in waves during development, including macrophages, mast cells, ILCs, B, and T cells^{42,80,81,114,115}. Although layered immune development can generate progressively adapted immune populations^{80–82}, TOM⁺ cDC2 and TOM⁻ DC2 exhibit apparently identical phenotype, transcriptional profile, and similar cell function, which is consistent with other studies comparing human and murine cDCs generated from lymphoid or myeloid progenitors^{74,116}. It is possible that functional differences exist between TOM⁺ cDC2 and TOM⁻ DC2 in situations that we have not yet explored; however, lymphopoiesis may compensate DC poiesis when bona fide cDC progenitors are not present in sufficient quantities to generate a full repertoire of cDCs⁷⁴. This hypothesis is consistent with the low frequency of CDPs and pre-cDCs in bone marrow from neonatal compared to adult mice. Whether cDC-like cells in early life arise from lymphoid-committed progenitors, such as CLPs, or from conversion of already differentiated lymphoid cells, such as pDCs or ILCs^{117–119} needs to be investigated. We and others have proposed that cDCs and other mononuclear phagocytes should predominantly be defined on the basis of their ontogeny^{5,114,120}; however, our data imply that an ontogenetic view to cell definition may not be plausible if populations with different origins turn out to be identical by all measures examined^{74,79,121–123}.

In continuation of earlier studies^{9,10,17}, we profiled the cDC compartment by flow cytometry with age using large marker panels. We demonstrate that the major subsets of splenic cDCs, including cDC1, non-canonical CD8⁺ cDCs, as well as ESAM^{high} and ESAM^{low} cDC2, are present in murine spleen as early as 1 week after birth. These findings were further substantiated using unbiased dissection of the cDC compartment of 1-week-old mice using scRNA-seq. In this analysis, cDC1 segregated across several clusters, possibly reflecting functional heterogeneity within this compartment^{17,124}. Non-canonical CD8⁺ cDCs were positioned more closely to cDC2 than pDCs or cDC1, which is consistent with bulk transcriptome profiling in adult mice^{59,60}. Although non-canonical CD8⁺ cDCs were recently suggested to constitute a transitional cell type with pDC and cDC2 characteristics in adult mice¹²⁵, our data indicate non-canonical CD8⁺ cDCs as a unique DC subset with close resemblance to cDC2 in early life. In scRNA-seq, early-life cDC2 spread across two main clusters resembling ESAM^{high} and ESAM^{low} subsets found in adult

spleen⁶², which, despite being profiled at a different age, also resembled the T-bet-positive and T-bet-negative cDC2, respectively⁹². We also identified a cluster of cells resembling migratory cDCs, which has recently been observed in adult spleen⁹². Importantly, scRNA-seq revealed TOM⁺ DC2 and TOM⁺ cDC2 as transcriptionally identical. Although bulk RNA-seq identified differences in gene expression between TOM⁺ DC2 from TOM⁺ cDC2, we could correlate these genes to a unique cluster of *Rorc*-expressing cells that transcriptionally resembles cDC2 but lacks *Clec9a*^{cre} expression history. Accordingly, RORγt⁺ cells could be identified by flow cytometry within TOM⁺ DC2 in early life but RORγt⁺ cDC2 were not found in adult spleen. *Rorc*^{cre}-mediated fate mapping and trajectory analyses indicate that these cells are unlikely to serve as progenitors for cDC2 or other cDC subsets. The fact that *Rorc*-expressing cluster 11 segregated away from the putative RORγt-regulated cDC2B⁹² (cluster 3) further supports that RORγt⁺ TOM⁺ DC2 constitute a unique cDC subtype present transiently during early life.

Although in adult spleen ESAM^{high} cells constituted the dominant cDC2 population, this subset was a minority of cDC2 in mice under 1 week of age. ESAM^{high} and ESAM^{low} cDC2 can activate CD4⁺ T cells but they may differ in their ability to promote effector differentiation^{62,92,126}. We mostly characterized bulk cDC2 in 2- to 2.5-week-old mice when ESAM^{high} and ESAM^{low} subset distribution had reached adult levels, because sufficient TOM⁺ cDC2 and TOM⁺ DC2 could be isolated to probe cell function. At this time, splenic TOM⁺ cDC2 and TOM⁺ DC2 were fully capable of initiating T-cell activation but they induced greater Th17 and Treg differentiation under in vitro polarizing conditions than adult cDC2. These observations could be correlated to the unique gene expression profile of cDC2 in early and adult life. Early-life cDC2 expressed higher levels of factors known to promote Tregs, such as *Lgals1*, *Aldh2*, and *Sema4a*^{100–103,106}, suggesting increased tolerogenic potential of cDC2 in early life, which is also consistent with their greater IL-10 production in response to CpG-B stimulation. Higher levels of *Il6ra* on cDC2 from young mice could increase IL-6 transpresentation¹⁰⁴ and promote Th17 differentiation in conjunction with reduced expression of *Tnfrsf4* (OX40L) and *Cd274* (PD-L1) in early life, which can suppress Th17 differentiation^{97,98,127,128}. Some of these age-dependent transcriptional changes could be related to small differences in the composition of cDC2 in 1-week-old and adult mice. We nonetheless consider age to be the most prominent contributor to variation, because we demonstrated that both ESAM^{high} and ESAM^{low} cDC2 function differently in early and adult life.

The notion that cDC2 are equipped with an age-dependent gene expression profile that alters their ability to induce T-cell differentiation was further supported using targeted antigen delivery to cDC2 in early and adult life followed by ex vivo antigen presentation^{25,107}. This approach allowed us to (a) compare cell function in vivo across age, while excluding age-dependent functional regulation of other immune components as confounding factor and (b) to demonstrate the potential to target cDC2 to induce T-cell responses. CpG-B was chosen as adjuvant, because despite similar *Thl9* expression across age, TOM⁺ cDC2, and TOM⁺ DC2 from 2-week-old mice showed distinct cytokine production after CpG-B stimulation in vitro, including higher levels of IL-12p40, IL-6, IL-10, and IL-27, supporting a distinct immune reactivity of cDC2 with age. IL-27 is a pleiotropic cytokine with pro- and anti-inflammatory properties in multiple cell types¹²⁹, but after vaccination in mice its expression correlates with protective CD8⁺ T-cell responses¹³⁰. DCs from peripheral blood of children show higher IL-27 production than DCs from adults¹¹⁰ but whether cDC2-derived IL-27 plays a role in early-life immunity needs to be investigated. Despite producing

increased amounts of IL-10, which dampens CD4⁺ T-cell responses¹³¹, early-life TOM⁺ cDC2 and TOM⁺ DC2 induced similar OT-II T-cell proliferation compared to cDC2 from adults upon DCIR2-mediated antigen targeting in the context of CpG stimulation. However, early-life cDC2 induced greater Th1 differentiation and TNF-α production from T cells. Human fetal DC2 suppress TNF-α production from T cells⁴³, suggesting that cDC2 function changes dynamically after birth. Transcriptional profiling of fetal and neonatal cDC2, possibly at the single-cell level, may provide further insights into the processes involved in shaping early-life cDC2 function. Differences in cytokine production and T-cell stimulatory capacity between cDC2 from young and adult mice were not simply regulated at the level of PRR expression but most probably involve downstream signaling events, costimulatory molecules, or epigenetic modification. Therefore, it is likely that age-dependent differences in cDC2 function will be magnified when cells are stimulated through PRRs with differential gene expression across age and additional adjuvants must be tested for their ability to promote cDC2-mediated T-cell priming and differentiation with age.

Our studies indicate that splenic cDC2 do not exhibit a Th2 bias, which is in contrast to cDC2 in the developing lung. In this organ, IL-33 induces OX40L expression on cDC2, which promotes Th2 skewing³⁰. Therefore, site-specific cytokine environments appear to play a major role in imprinting cDC function in different organs and with age. This is consistent with previous studies^{38,92} and our observation that cDC2 from adult compared to young mice showed an enrichment of genes involved in signaling downstream of IL-2, IFN-γ, TNF-α, and IFN-α. In our hands, cDC2 from GF mice did not recapitulate the phenotypic and functional features of neonatal cDC2. Although GF mice have a complete absence of commensals, in an SPF environment cDC2 are expected to encounter a variety of microbial signals within the first days of birth. We therefore believe that these observations do not exclude the possibility that microbially derived signals or signals induced in response to commensals play a role in imprinting cDC2 function with age. During weaning, the intestinal microbiota induces a cytokine response termed the “weaning reaction,” which is required for normal immune development¹³². As cDC2 function in our hands has been assessed before this period, it is intriguing to speculate that cytokines or other factors that change in response to alterations in commensals or diet during weaning are involved in shaping cDC function with age. Such effects could even be mediated by lasting alterations on progenitor populations similar to the concept of trained immunity.

Neonates are highly susceptible to infections with *Candida albicans*, *Bordetella pertussis*, and *Streptococcus pneumoniae*, which can cause life-threatening complications in early life^{1,133,134}. Defense against these pathogens requires Th17 responses^{135,136}. Our demonstration that early-life cDC2 are fully capable of activating naive CD4⁺ T cells, and supporting Th1 and Th17 differentiation highlights the potential of harnessing these cells for boosting protective immunity in early life. This could for instance be achieved by delivering antigens specifically to cDC2 in the context of adjuvants that target age-specific parameters of cDC2 function.

Methods

Mice. *Clec9a*^{tm2.1(cre)Crs (*Clec9a*^{cre})⁴⁸ (Jackson Laboratory Stock No: 025523), Gt (ROSA)26Sor^{tm1(EYFP)Cos} (*Rosa26*^{lox-STOP-lox-EYFP})¹³⁷ (Jackson Laboratory Stock No: 006148), Gt(ROSA)26Sor^{tm9(CAG-tdTomato)Hze} (*Rosa26*^{lox-STOP-lox-tdtomato})⁹¹ (Jackson Laboratory Stock No: 007909), Tg(Csf1r-cre/Esr1*)1Jwp (*Csf1r*^{Mer-iCre-Mer})¹³⁸ (Jackson Laboratory Stock No: 019098), Flt3^{tm1Imx} (*Flt3*^{l-/-})⁶⁵ (MMRRC Stock No: 37395-JAX), Myb^{tm1Ssp} (*Myb*^{+/-})⁶⁸ (Jackson Laboratory Stock No: 004757), Rag1^{tm1(cre)Thr} (*Rag1*^{cre})¹³⁹, Tg(TcrαTcrβ)425Cbn (OT-II)¹⁴⁰ (Jackson Laboratory Stock No: 004194) crossed to a Thy1.1 (CD90.1) background, Tg(Rorc-EGFP)1Ebe}

(*Rorc^{creGFP}*)¹⁴¹, *Cxcr4^{creER77}*, Gt(ROSA)26Sor^{tm4}(ACTB-tdTomato, EGFP)^{Luo}/J (*Rosa^{mtmG}*)¹⁴² (Jackson Laboratory Stock No: 007576), Ly5.1 (CD45.1) B6.SJL (Jackson Laboratory Stock No: 002014), and C57BL/6J mice were bred at the Bio-medical Center or Walter-Brendel-Centre for Experimental Medicine. Tg(*Rorc-cre*)1Litt (*Rorc-cre*)⁹⁴ (Jackson Laboratory Stock No: 022791), Il7r^{tm1.1(cre)Hrr} (*Il7r-cre*)⁷⁶, and Gt(ROSA)26Sor^{tm1Hfr} (*Rosa26lox-STOP-lox-RFP*)¹⁴³ (EMMA strain ID EM:021112) mice were bred at the University of Birmingham, UK. Ifnar1^{tm1Agt} (*Ifnar^{-/-}*)¹⁴⁴ (MMRRC Stock No: 32045-JAX) mice were bred at the University Hospital Erlangen, Germany. Mice were maintained in SPF conditions with a 12 h dark/light cycle, in individually vented cages (type II long, measuring 18 × 30 × 13 cm with stocking density according to EU guideline 2010/63) supplied with autoclaved bedding, play tunnels, nestles, and mouse houses. Irradiated food and sterile filtered and ultraviolet-light exposed water were provided ad libitum. Cage manipulations took place in laminar flow hoods. Air temperature was 22 ± 2 °C and humidity 55 ± 10% with daily control and record. GF mice were provided by Dirk Haller. For timed matings, mice of desired genotypes were mated overnight. Embryonic development was estimated considering the day of vaginal plug formation as E0.5. Mice over the age of 8 weeks were considered adults. The neonatal period was defined as the first 10 days of life. Mice younger than 3 weeks of age were killed by decapitation. Adult mice were killed by cervical dislocation. Mice were sex-matched but male and female mice were used for all experiments. In most experiments, littermates were used. When littermates could not be used, e.g., in experiments involving mice of different age, mice were kept under the same barrier conditions and in the same racks. All animal procedures were performed in accordance with national and institutional guidelines for animal welfare and approved by the Regierung of Oberbayern.

Cell isolation for flow cytometry. Spleens were minced into small pieces and digested in 1 mL of RPMI (Thermo Fisher Scientific) with 200 U/mL collagenase IV (Worthington) and 0.2 mg/mL DNase I (Roche) for 30 min at 37 °C while shaking. After digestion, cells were passed through a 70 µm strainer and washed once with FACS buffer (phosphate-buffered saline (PBS), 1% fetal calf serum (FCS), 2.5 mM EDTA, 0.02% sodium azide). Erythrocytes were lysed with Red Blood Cell Lysing Buffer Hybri-Max (Sigma-Aldrich) for 2 min at room temperature (RT), washed once, and resuspended in FACS buffer for further analysis. Bone marrow from adult mice was isolated from femurs and tibiae by flushing, and bone marrow from mice under 2 weeks of age was isolated by crushing the bones through a 70 µm cell strainer. Erythrocytes were lysed as above and cells were resuspended in FACS buffer for further analysis. Liver was minced into small pieces and digested in 2 mL PBS containing Mg²⁺ and Ca²⁺ (Sigma-Aldrich) with 1 mg/mL collagenase IV (Worthington), 60 U/mL DNase I (Roche), 2.4 mg/mL Dispase II (Roche), and 3% FCS (Sigma-Aldrich) for 30 min at 37 °C while shaking. After digestion, cells were passed through a 100 µm strainer and centrifuged for 3 min at 50 g at 4 °C, to pellet hepatocytes. The supernatant was collected and recentrifuged for 7 min at 320 × g at 4 °C. Pelleted cells were resuspended in FACS buffer for further analysis.

Cell isolation for cell sorting and functional analyses. Cell isolation from spleen was performed as above but FACS buffer without sodium azide was used for all functional and RNA profiling experiments. For sorting of cDC2 CD11c⁺ cells were enriched from splenic single-cell suspensions by positive selection using anti-CD11c magnetic beads and LS columns (Miltenyi) according to the manufacturer's instructions. For OT-II cell isolation, the spleen was mechanically disrupted through a 70 µm strainer and washed once with FACS buffer without sodium azide. OT-II cells were then enriched from total splenocytes using the EasySep[™] Mouse Naive CD4⁺ T Cell Isolation Kit (Stemcell Technologies) according to the manufacturer's instructions. Erythrocytes were not lysed prior to OT-II cell enrichment, following the manufacturer's recommendations.

Flow cytometry. For staining of surface epitopes, cells were incubated first in 50 µL with purified anti-mouse CD16/32 (FcBlock) for 10 min at 4 °C, before additional antibodies were added to a final staining volume of 100 µL in a 2× Mastermix. Cells were stained at 4 °C for 20 min then washed twice and resuspended in FACS buffer for analysis. CCR6 staining was performed at 37 °C for 45 min before staining with additional antibodies. For intracellular staining, cells were first stained with antibodies against surface epitopes in the presence of fixable viability dye eFluor[™] 780 (Thermo Fisher Scientific) and then washed with FACS buffer. Intracellular staining for cytokines was performed using intracellular Fixation & Permeabilization Buffer Set and intranuclear staining was performed with the Foxp3 transcription factor staining set (both Thermo Fisher Scientific) according to the manufacturer's instructions. A pre-fixation step with 2% paraformaldehyde at RT for 15 min was performed after surface epitope staining to preserve TOMATO signal during intranuclear staining. Dead cells were excluded from analysis by 4',6-diamidino-2-phenylindole staining (Sigma-Aldrich) for live samples or fixable viability dye eFluor[™] 780 (Thermo Fisher Scientific). Data were collected on an LSR Fortessa (BD Biosciences) using BD FACSDiva Software (BD BioSciences, Version 8) and data analysis was performed using FlowJo software (Tree Star, Inc.). Cell sorting was performed on an Aria III Fusion (BD Biosciences). Cells counts were quantified using CountBright[™] Absolute Counting Beads (Thermo Fisher Scientific). Mean fluorescence intensity was calculated as the geometric mean of the

indicated fluorescent parameter using FlowJo software (Tree Star, Inc.). Antibodies used for flow cytometry are provided in Supplementary Data 4.

Immunofluorescence microscopy. Spleens were fixed overnight at 4 °C in paraformaldehyde, then dehydrated in P-buffer (0.2 M Na₂HPO₄ and 0.2 M NaH₂PO₄ at an 81 : 19 analogy), containing 30% sucrose overnight at 4 °C as described¹⁴⁵, transferred to Tissue-Tek O.C.T. (Sakura), and frozen on dry ice. Twelve-micrometer-thick frozen sections were cut on a cryostat at −20 °C (Leica CM3050S), rehydrated in PBS, and permeabilized with Acetone (Sigma-Aldrich). Afterwards, the sections were circled with a PAP Pen (Kisker Biotech GmbH) and blocked for 1 h at RT in the dark with blocking buffer containing 10% goat serum in PBS. Antibodies were diluted in blocking buffer and sections were incubated for 2 h at RT in the dark with the antibody mixture. Finally, stained sections were washed with PBS, mounted with ProLong[™] Diamond Antifade Mountant (Thermo Fisher Scientific), cured at RT for 24 h in the dark, and stored at 4 °C until imaging. Confocal microscopy was performed at the Core Facility Bioimaging of the Bio-medical Center with an upright Leica SP8X WLL microscope, equipped with 405 nm laser, WLL2 laser (470 - 670 nm), and acousto-optical beam splitter. Three-dimensional tile scans were acquired with a 20 × 0.75 objective, image voxel size was 180 nm in x/y direction and 0.5 in z direction. The following channel settings were used: BV421 (excitation 405 nm; emission 415–470 nm), AF488 (500; 510–542), TOMATO (553; 563–591), AF594 (592; 605–640), and AF647 (650; 656–718). Recording was done sequentially to avoid bleed-through. BV421, AF488, AF594, AF647, and TOMATO were recorded with hybrid photo detectors. Tile scans were merged in LAS X (Leica, Version 3.4.1.17670). Images were imported in Fiji¹⁴⁶ to create maximum projections, adjust brightness/contrast, and to add scale bars. Antibodies used for microscopy are provided in Supplementary Data 4.

Pulse labeling of yolk sac progenitors. For labeling of yolk sac-derived macrophages, heterozygous *Csf1r^{Mer-1Cre-Mer}* mice were crossed with homozygous *Rosa^{YFP}* reporter mice. Pregnant females were injected at E8.5 with a single dose of 75 µg per gram body weight 4-hydroxytamoxifen (4'OHT, Sigma-Aldrich) supplemented with 37.5 µg per gram body weight progesterone (Sigma-Aldrich)⁴¹. The spleen and liver of F1 mice were analyzed at embryonic day 18.5, as well as at 2 and 4 weeks after birth by flow cytometry.

RNA isolation, library construction, and RNA-seq analysis. CD11c⁺ cells were enriched from splenocytes of adult and 1-week-old *Clec9a^{cre/cre}Rosa^{TOM}* mice. cDC2 were identified as live, single, autofluorescence-negative, CD11c⁺MHCII⁺CD11b⁺ cells, and divided based on TOMATO expression into TOM⁺ cDC2 and TOM[−] cDC2. Spleens from 1-week-old mice were pooled to increase the yield of sorted cells. Total RNA was isolated using column-based PicoPure[™] RNA Isolation Kit (Thermo Fisher Scientific). RNA quality was assessed using a 2100 Bioanalyzer (Agilent) and samples with RNA Integrity Number > 8 were used for cDNA synthesis by using ultra-low input RNA SMART-seq v4 kit (Clontech) according to the manufacturer's instructions. cDNA was transferred to AFA Fiber Pre-Slit Snap-Cap 6 × 16 mm microTUBEs (Covaris) and sheared by sonication. Sheared cDNA was cleaned using ethanol precipitation and sonication efficiency was determined using the 2100 Bioanalyzer. A maximum of 10 ng sheared cDNA was used to generate libraries for RNA-seq with the MicroPlex Library Preparation kit v2 (Diagenode). The libraries were amplified until a DNA concentration above 5 ng/µL was reached as determined by Qubit 2 DNA quantification (Thermo Fisher Scientific). Amplified libraries were cleaned using AMPure XP beads (Beckman Coulter) as described in the SMART-seq v4 kit (Clontech) protocol and the final concentration, as well as the purity of the libraries were assessed by using the 2100 Bioanalyzer. Sequencing was performed on an Illumina HiSeq1500 sequencer with 50 base pair single-end reads and a sequencing depth of 20 million reads per sample. For analysis, RNA-seq reads were mapped to the mouse genome (mm10) using STAR¹⁴⁷. Expression of genes in transcripts per million was calculated with RSEM¹⁴⁸. RNA-seq analysis was performed in R (Version 3.5.3) with R-Studio (R-Studio, Inc., Version 1.1.383). Differential gene expression analysis and PCA was performed using DESeq2 (Version 1.22.2). Genes with average gene counts < 1 were discarded and log₂ FC shrinkage was performed using the Apeglm package¹⁴⁹. Heatmaps were generated using pheatmap (Version 1.0.12) and graphs were plotted with ggplot2 (Version 3.0.2). Tables containing differentially expressed genes were created using Microsoft Excel version 16.34.

scRNA-seq and data processing. MHCII⁺ cells from splenocytes of 9-day-old female *Clec9a^{cre/cre}Rosa^{TOM}* mice were sorted after gating out CD19⁺ B cells and autofluorescence⁺F4/80^{hi} macrophages. To increase cell yield, spleens from three mice were pooled. Sorted cells were pelleted, resuspended at 1 × 10³ cells/µL in PBS containing 0.04% bovine serum albumin, and loaded onto the Chromium Controller (10X Genomics). Samples were processed for single-cell encapsulation and cDNA library generation using the Chromium Single Cell 3' v3 Reagent Kits (10X Genomics). The constructed library was sequenced on an Illumina HiSeq2500 (Rapid Run) sequencer with 28 (read 1) + 91 (read 2) base pair paired-end reads and a sequencing depth of 320 million reads in total. Sequencing data were processed using 10X Genomics Cell Ranger v3.0.2 pipeline. Sequencing reads were mapped to the mouse genome (mm10) using STAR¹⁴⁷ after spiking in the

sequences of iCRE (GenBank ID: [AY056050.1](#)), the predicted transcript of the unrecombined *Rosa* locus and *Tomato* sequence (GenBank ID: [AY678269.1](#)). Cell Ranger's count pipeline was run under default parameters. The output of Cell Ranger's count pipeline was a gene-barcode matrix consisting of ~1788 cellular barcodes with 179,245 mean reads per barcode. This matrix was inserted to the R (Version 3.5.3) software package Seurat (v3.0.2)^{86,87} for all downstream analyses. Cells expressing <200 genes, having >7.5% of mitochondrial associated genes and genes detected in <3 cells were removed from further analysis according to the software suggestions. In addition, cells were scored based on their cell cycle score and the differences between G2M and S phase cells were regressed. The SCTransform package was used to normalize, scale, and find the variable features of the dataset before PCA. Genes associated with the top 40 PCs were used for graph-based cluster identification (resolution 1.3) and subsequent dimensionality reduction using UMAP. Identification of cluster defining markers and differential expression analysis were performed using the FindAllMarkers and FindMarkers commands of the Seurat package. To score single cells based on their *Tomato* expression, we calculated the ratio of normalized *Tomato* reads per cell to normalized reads per cell of the predicted transcript of the unrecombined *Rosa* locus (Ratio Tom/unrec. Rosa). Cells with a ratio above 0.5 or below -0.5 were denoted *Tom*⁺ or *Tom*⁻, respectively. The selected thresholds included more than 90% of the total cells in each cluster. Tables containing differentially expressed genes were created using Microsoft Excel version 16.34.

For trajectory analysis using Palantir, we selected clusters 0, 3, 6, 7, 11, and 14, and generated diffusion maps as described⁹³. We provided a defined starting point in cluster 11 and used Palantir to characterize potential pseudo-time trajectories from this point. The terminal states found in the analysis were automatically calculated by the Palantir algorithm.

Cytospins and Hemacolor staining. *TOM*⁺ cDC2 and *TOM*⁻ DC2 were sorted from CD11c⁺ enriched splenocytes from 11-day-old *Clec9a^{cre/+}Rosa^{TOM}* mice as live, single, autofluorescence-negative, CD11c⁺MHCII⁺CD11b⁺ *TOM*⁺ or *TOM*⁻ cells. Cells (2×10^4) were spun onto a microscope slide in a Shandon Cytospin 2 for 5 min at 8000 r.p.m. and stained with Hemacolor[®] rapid staining kit (Merck). Microscopy was performed at the Core Facility Bioimaging of the Biomedical Center using a Leica DM 2500 LED microscope with a $\times 100$ magnification.

Bone marrow FLT3L cultures. Bone marrow cells from adult *Clec9a^{cre/+}Rosa^{TOM}* (CD45.2) were isolated as described above.

After lineage depletion using negative selection (lineage: CD3, TER119, Ly6G, CD19), CLPs were sorted as live, single, lin⁻CD115⁻CD117^{int}CD135⁺CD127⁺B220⁻*TOMATO*⁻ cells. CLPs (10^4) were seeded in 300 μ L complete medium (RPMI supplemented with 10% FCS, penicillin/streptomycin, 1% non-essential amino acids, 1% sodium pyruvate, 1% L-glutamine, 0.05 mM β -mercaptoethanol) in a 48-well plate together with 1.5×10^5 total bone marrow cells isolated from congenic B6.SJL (CD45.1) mice. As controls, total bone marrow cells from *Clec9a^{cre/+}Rosa^{TOM}* and B6.SJL congenic mice were seeded at a 1:1 ratio. FLT3L (purified from supernatant of CHO-*flk2* cell line, a kind gift from Dr. Anne Krug, Institute for Immunology, Biomedical Center, Munich) was added to all wells at a concentration of 50 ng/mL. Culture wells were left unperturbed for 7 days and then the culture output was analyzed by flow cytometry.

In vitro T-cell proliferation. DCs were sorted from CD11c⁺ enriched cells from spleen of 2-week-old and adult *Clec9a^{cre/+}Rosa^{TOM}* mice, as live, single, autofluorescence-negative, CD11c⁺MHCII⁺CD11b⁺ *TOMATO*⁺, or *TOMATO*⁻ cells. In some experiments, DCs were further subset based on ESAM and ROR γ expression, as indicated. In experiments comparing cDC2 from SPF and GF mice, cDC2 were sorted from CD11c-enriched splenocytes as live, single, autofluorescence-negative, CD11c⁺MHCII⁺CD11b⁺ cells. Sorted cells were incubated in the wells of a V-bottom 96-well plate with 10 μ g/mL chicken OVA peptide (OVA_{323–339}, InvivoGen) for 3 h in complete medium (prepared as indicated above). After washing two times to remove any residual OVA_{323–339} DCs were resuspended in complete medium, serially diluted, and co-cultured at the indicated ratios with naive CTV-labeled OT-II cells from adult mice. Naive OT-II cells were isolated as described above and labeled with CTV (Thermo Fisher Scientific). First, OT-II cells were resuspended in PBS at 20×10^6 cells/mL and an equal volume of CTV working solution was added to a final concentration of 5 mM. Cells were incubated for 20 min at 37 °C in the dark and were mixed at the midpoint of the incubation. An excess of pre-warmed complete medium was added and after a 5 min incubation, cells were washed with PBS. Cultures were supplemented with 20 ng/mL IL-12 (PeproTech) and 10 μ g/mL anti-IL-4 (Biolegend) for Th1; 5 ng/mL TGF- β , 10 μ g/mL anti-IL-4, and 10 μ g/mL anti-IFN- γ for Treg; 5 ng/mL TGF- β , 20 ng/mL IL-6, 10 μ g/mL anti-IL-4, and 10 μ g/mL anti-IFN- γ (all Biolegend) for Th17 conditions. After 3.5 days of culture, supernatant was collected from each well and cells were restimulated with 10 ng/mL phorbol 12-myristate 13-acetate (PMA) (Calbiochem) and 1 μ g/mL ionomycin (Sigma-Aldrich) for 5 h. After 2 h, brefeldin A (5 μ g/mL, Biolegend) was added for the remaining 3 h. Cytokines and Foxp3 expression were detected by intracellular staining. Cytokine secretion

in culture supernatants was quantified using LEGENDplex[™] Mouse Th Cytokine Panel (Biolegend) according to the manufacturer's instructions. For co-culture experiments with OVA, DCs were sorted as above resuspended in complete medium in the wells of a V-bottom 96-well plate, serially diluted and co-cultured at the indicated ratios with CTV-labeled naive OT-II cells in the presence of 20 μ g/mL OVA (Hyglos). After 4 days of culture, cytokine production was assessed as above.

Antigen targeting. Antigen targeting was performed as described^{25,107}. To establish targeting specificity 2-week-old *Clec9a^{cre/+}Rosa^{TOM}* mice were injected intraperitoneally (i.p.) with 10 μ g α DCIR2-OVA or 10 μ g OVA coupled isotype control antibody. Mice were killed 12 h later and splenocytes were isolated by mechanically disrupting the spleens through a 70 μ m strainer and washing once with PBS containing 1% FCS. Splenic single-cell suspensions were then enriched for CD11c⁺ cells by positive selection using anti-CD11c magnetic beads and LS columns (Miltenyi). PBS containing 1% FCS was used throughout the procedures of isolation, enrichment and preparation of cells for sorting. *TOM*⁺ cDC2 and *TOM*⁻ DC2 were sorted as CD11c⁺B220⁻Ly6G⁻Ly6C⁻CD90.2⁺CD11b⁺ *TOMATO*⁺ or *TOMATO*⁻ cells and cDC1 were sorted as CD11c^{high}B220⁻Ly6G⁻Ly6C⁻CD90.2⁺CD24⁺XCR-1⁺ cells. Sorted DCs were co-cultured with CTV-labeled naive CD90.1 OT-II cells in complete medium. After 3.5 days, supernatant was collected from each well and OT-II proliferation analyzed by flow cytometry. For targeting experiments with adjuvant, 2-week-old and adult, *Clec9a^{cre/+}Rosa^{TOM}* mice were injected i.p. with 10 μ g of α DCIR2-OVA plus 0.2 μ g/g body weight of CpG-B ODN 1826 (Sigma-Aldrich). DC populations were sorted and co-cultured with CTV-labeled naive CD90.1 OT-II cells as above. After 3.5 days, OT-II cells were restimulated with PMA/ionomycin for 5 h in the presence of Brefeldin A and cytokine production and Foxp3 expression assessed by flow cytometry as described above. T-cell proliferation, cytokine production after restimulation, and quantification of secreted cytokines in culture supernatants were assessed as above.

TOMATO stability in vitro. *TOM*⁺ cDC2 and *TOM*⁻ DC2 from 1-week-old *Clec9a^{cre/+}Rosa^{TOM}* mice were sorted as above. Cells (2.5×10^3) were seeded in 200 μ L complete medium together with 10^5 total splenocytes from CD45.1 congenic mice. Cultures were supplemented with 50 ng/mL murine recombinant GM-CSF (PeproTech) and 200 ng/mL murine recombinant FLT3L (R&D Systems). After 24 h, cells were collected and analyzed by flow cytometry.

In vitro phagocytosis. CD11c-enriched splenocytes (5×10^4) from 2-week-old and adult *Clec9a^{cre/+}Rosa^{TOM}* mice cells were cultured with beads (FluoSpheres[®], Polystyrene Microspheres, 1.0 μ m, yellow-green fluorescent (505/515)), Invitrogen) at a 50:1 bead to cell ratio for 2 h at 37 °C in humidified atmosphere containing 5% CO₂ in complete medium. To inhibit phagocytosis, cells were pre-treated with 10 μ g/mL cytochalasin D (Sigma-Aldrich) for 1 h at 37 °C. After incubation, antibody staining for surface epitopes was performed as described above and phagocytosis of beads by cDC2 was quantified by flow cytometry.

In vitro stimulation and cytokine production. *TOM*⁺ cDC2 and *TOM*⁻ DC2 from 2-week-old *Clec9a^{cre/+}Rosa^{TOM}* mice and *TOM*⁺ cDC2 from adult *Clec9a^{cre/+}Rosa^{TOM}* mice were sorted as above. Then, 0.7×10^6 cells/mL were stimulated in a total volume of 50 μ L complete medium in 96-well V-bottom plates with 0.5 μ g/mL CpG-B ODN 1826 (Sigma). After 18–20 h, cytokine secretion was quantified using LEGENDplex[™] Mouse Inflammation Panel and LEGENDplex[™] Mouse Cytokine Panel 2 for IL-12p40 (both from Biolegend) according to the manufacturer's instructions.

Statistical analysis. Statistical significance was calculated in Prism 7 software (GraphPad) using two-tailed *t*-test with Welch's correction (unless otherwise stated) or two-tailed paired *t*-test. For multiple comparisons, one-way analysis of variance with Tukey's test (unless otherwise stated) was performed. A *p*-value < 0.05 was considered significant.

Reporting summary. Further information on research design is available in the Nature Research Reporting Summary linked to this article.

Data availability

The authors declare that the data supporting the findings of this study are available within the paper and its Supplementary Files. Raw data are available from the authors upon reasonable request. Datasets related to bulk and single-cell sequencing experiments that were generated and analyzed for the current study have been deposited and made publicly available in the Gene Expression Omnibus under the accession number [GSE151595](#). The sequences of iCRE and Tomato used for the single-cell RNA sequencing analysis are publicly available and can be found under the GenBank IDs [AY056050.1](#) and [AY678269.1](#), respectively. Source data are provided with this paper.

Received: 16 April 2020; Accepted: 13 December 2020;

Published online: 19 January 2021

References

- Whittaker, E., Goldblatt, D., McIntyre, P. & Levy, O. Neonatal immunization: rationale, current future prospects. *Front. Immunol.* **9**, 1069–10 (2018).
- Zaghoulani, H., Hoeman, C. M. & Adkins, B. Neonatal immunity: faulty T-helpers and the shortcomings of dendritic cells. *Trends Immunol.* **30**, 585–591 (2009).
- Zhang, X., Zhivaki, D. & Lo-Man, R. Unique aspects of the perinatal immune system. *Nat. Rev. Immunol.* **17**, 495–507 (2017).
- Coffman, R. L., Sher, A. & Seder, R. A. Vaccine adjuvants: putting innate immunity to work. *Immunity* **33**, 492–503 (2010).
- Guilliams, M. et al. Dendritic cells, monocytes and macrophages: a unified nomenclature based on ontogeny. *Nat. Rev. Immunol.* **14**, 571–578 (2014).
- Merad, M., Sathe, P., Helft, J., Miller, J. & Mortha, A. The dendritic cell lineage: ontogeny and function of dendritic cells and their subsets in the steady state and the inflamed setting. *Annu. Rev. Immunol.* **31**, 563–604 (2013).
- Lehmann, C. et al. Direct delivery of antigens to dendritic cells via antibodies specific for endocytic receptors as a promising strategy for future therapies. *Vaccines* **4**, 8–32 (2016).
- Kastenmüller, W., Kastenmüller, K., Kurts, C. & Seder, R. A. Dendritic cell-targeted vaccines—hope or hype? *Nat. Rev. Immunol.* **14**, 705–711 (2014).
- Dakic, A. et al. Development of the dendritic cell system during mouse ontogeny. *J. Immunol.* **172**, 1018–1027 (2004).
- Sun, C.-M., Fiette, L., Tanguy, M., Leclerc, C. & Lo-Man, R. Ontogeny and innate properties of neonatal dendritic cells. *Blood* **102**, 585–591 (2003).
- Prabhu, S. B. et al. Comparison of human neonatal and adult blood leukocyte subset composition phenotypes. *PLoS ONE* **11**, e0162242–17 (2016).
- Muthukumar, S., Goldstein, J. & Stein, K. E. The ability of B cells and dendritic cells to present antigen increases during ontogeny. *J. Immunol.* **165**, 4803–4813 (2000).
- Langrish, C. L., Buddle, J. C., Thrasher, A. J. & Goldblatt, D. Neonatal dendritic cells are intrinsically biased against Th-1 immune responses. *Clin. Exp. Immunol.* **128**, 118–123 (2002).
- Goriely, S. et al. Deficient IL-12(p35) gene expression by dendritic cells derived from neonatal monocytes. *J. Immunol.* **166**, 2141–2146 (2001).
- Granot, T. et al. Dendritic cells display subset and tissue-specific maturation dynamics over human life. *Immunity* **46**, 504–515 (2017).
- Lee, H.-H. et al. Delayed maturation of an IL-12-producing dendritic cell subset explains the early Th2 bias in neonatal immunity. *J. Exp. Med.* **205**, 2269–2280 (2008).
- Torres, D. et al. IL-12p40/IL-10 producing preCD8α/Clec9A+ dendritic cells are induced in neonates upon *Listeria monocytogenes* infection. *PLoS Pathog.* **12**, e1005561 (2016).
- Upham, J. W. et al. Development of interleukin-12-producing capacity throughout childhood. *Infect. Immun.* **70**, 6583–6588 (2002).
- Vollstedt, S. et al. Flt3 ligand-treated neonatal mice have increased innate immunity against intracellular pathogens and efficiently control virus infections. *J. Exp. Med.* **197**, 575–584 (2003).
- Vollstedt, S. et al. Treatment of neonatal mice with Flt3 ligand leads to changes in dendritic cell subpopulations associated with enhanced IL-12 and IFN-α production. *Eur. J. Immunol.* **34**, 1849–1860 (2004).
- Durai, V. & Murphy, K. M. Functions of murine dendritic cells. *Immunity* **45**, 719–736 (2016).
- Hildner, K. et al. Batf3 deficiency reveals a critical role for CD8α+ dendritic cells in cytotoxic T cell immunity. *Science* **322**, 1097–1100 (2008).
- Reis e Sousa, C. et al. In vivo microbial stimulation induces rapid CD40 ligand-independent production of interleukin 12 by dendritic cells and their redistribution to T cell areas. *J. Exp. Med.* **186**, 1819–1829 (1997).
- Mashayekhi, M. et al. CD8α+ dendritic cells are the critical source of interleukin-12 that controls acute infection by *Toxoplasma gondii* Tachyzoites. *Immunity* **35**, 249–259 (2011).
- Dudziak, D. et al. Differential antigen processing by dendritic cell subsets in vivo. *Science* **315**, 107–111 (2007).
- Shin, C. et al. Intrinsic features of the CD8α– dendritic cell subset in inducing functional T follicular helper cells. *Immunol. Lett.* **172**, 21–28 (2016).
- Persson, E. K. et al. IRF4 transcription-factor-dependent CD103+CD11b+ dendritic cells drive mucosal T helper 17 cell differentiation. *Immunity* **38**, 958–969 (2013).
- Schlitz, A. et al. IRF4 transcription factor-dependent CD11b+ dendritic cells in human and mouse control mucosal IL-17 cytokine responses. *Immunity* **38**, 970–983 (2013).
- Tussiwand, R. et al. Klf4 expression in conventional dendritic cells is required for T helper 2 cell responses. *Immunity* **42**, 916–928 (2015).
- de Kleer, I. M. et al. Perinatal activation of the interleukin-33 pathway promotes type 2 immunity in the developing lung. *Immunity* **45**, 1285–1298 (2016).
- Pakalniškytė, D. & Schraml, B. U. Tissue-specific diversity and functions of conventional dendritic cells. *Adv. Immunol.* **134**, 89–135 (2017).
- Ruckwardt, T. J., Morabito, K. M., Bar-Haim, E., Nair, D. & Graham, B. S. Neonatal mice possess two phenotypically and functionally distinct lung-migratory CD103+ dendritic cell populations following respiratory infection. *Mucosal Immunol.* **11**, 186–198 (2018).
- Lau-Kilby, A. W. et al. Type I IFN ineffectively activates neonatal dendritic cells limiting respiratory antiviral T-cell responses. *Mucosal Immunol.* **13**, 371–380 (2019).
- Papaioannou, N. E., Pasztoi, M. & Schraml, B. U. Understanding the functional properties of neonatal dendritic cells: a doorway to enhance vaccine effectiveness? *Front. Immunol.* **9**, 553–558 (2019).
- Ruckwardt, T. J., Malloy, A. M. W., Morabito, K. M. & Graham, B. S. Quantitative and qualitative deficits in neonatal lung-migratory dendritic cells impact the generation of the CD8+ T cell response. *PLoS Pathog.* **10**, e1003934 EP (2014).
- Sharma, P., Levy, O. & Dowling, D. J. The TLR5 agonist Flagellin shapes phenotypic and functional activation of lung mucosal antigen presenting cells in neonatal mice. *Front. Immunol.* **11**, 430–13 (2020).
- Gollwitzer, E. S. et al. Lung microbiota promotes tolerance to allergens in neonates via PD-L1. *Nat. Med.* **20**, 642–647 (2014).
- Bachus, H. et al. Impaired tumor-necrosis-factor-α-driven dendritic cell activation limits lipopolysaccharide-induced protection from allergic inflammation in infants. *Immunity* **50**, 225–240.e4 (2019).
- Lewis, S. M., Williams, A. & Eisenbarth, S. C. Structure and function of the immune system in the spleen. *Sci. Immunol.* **4**, eaau6085 (2019).
- Popescu, D.-M. et al. Decoding human fetal liver haematopoiesis. *Nature* **574**, 365–371 (2019).
- Schulz, C. et al. A lineage of myeloid cells independent of Myb and hematopoietic stem cells. *Science* **336**, 86–90 (2012).
- Gentek, R. et al. Hemogenic endothelial fate mapping reveals dual developmental origin of mast cells. *Immunity* **48**, 1160–1171.e5 (2018).
- McGovern, N. et al. Human fetal dendritic cells promote prenatal T-cell immune suppression through arginase-2. *Nature* **546**, 662–666 (2017).
- Naik, S. H. et al. Development of plasmacytoid and conventional dendritic cell subtypes from single precursor cells derived in vitro and in vivo. *Nat. Immunol.* **8**, 1217–1226 (2007).
- Onai, N. et al. Identification of clonogenic common Flt3+M-CSFR+ plasmacytoid and conventional dendritic cell progenitors in mouse bone marrow. *Nat. Immunol.* **8**, 1207–1216 (2007).
- Breton, G. et al. Circulating precursors of human CD11c+ and CD141+ dendritic cells. *J. Exp. Med.* **212**, 401–413 (2015).
- Lee, J. et al. Restricted dendritic cell and monocyte progenitors in human cord blood and bone marrow. *J. Exp. Med.* **212**, 385–399 (2015).
- Schraml, B. U. et al. Genetic tracing via DNGR-1 expression history defines dendritic cells as a hematopoietic lineage. *Cell* **154**, 843–858 (2013).
- Liu, K. et al. In vivo analysis of dendritic cell development and homeostasis. *Science* **324**, 392–397 (2009).
- Caminschi, I. et al. The dendritic cell subtype-restricted C-type lectin Clec9A is a target for vaccine enhancement. *Blood* **112**, 3264–3273 (2008).
- Joffre, O. P., Sancho, D., Zelenay, S., Keller, A. M. & Reis e Sousa, C. Efficient and versatile manipulation of the peripheral CD4+ T-cell compartment by antigen targeting to DNGR-1/CLEC9A. *Eur. J. Immunol.* **40**, 1255–1265 (2010).
- Sancho, D. et al. Tumor therapy in mice via antigen targeting to a novel, DC-restricted C-type lectin. *J. Clin. Invest.* **118**, 2098–2110 (2008).
- Cabeza-Cabrerizo, M. et al. Tissue clonality of dendritic cell subsets and emergency DCpoiesis revealed by multicolor fate mapping of DC progenitors. *Sci. Immunol.* **4**, eaaw1941 (2019).
- Salei, N. et al. The kidney contains ontogenetically distinct dendritic cell and macrophage subtypes throughout development that differ in their inflammatory properties. *J. Am. Soc. Nephrol.* **31**, 257–278 (2020).
- Meredith, M. M. et al. Expression of the zinc finger transcription factor zDC (Zbtb46, Btbd4) defines the classical dendritic cell lineage. *J. Exp. Med.* **209**, 1153–1165 (2012).
- Satpathy, A. T. et al. Zbtb46 expression distinguishes classical dendritic cells and their committed progenitors from other immune lineages. *J. Exp. Med.* **209**, 1135–1152 (2012).
- Adkins, B., Leclerc, C. & Marshall-Clarke, S. Neonatal adaptive immunity comes of age. *Nat. Rev. Immunol.* **4**, 553–564 (2004).
- Bachem, A. et al. Expression of XCR1 characterizes the Batf3-dependent lineage of dendritic cells capable of antigen cross-presentation. *Front. Immunol.* **3**, 214 (2012).
- Lau, C. M. et al. Leukemia-associated activating mutation of Flt3 expands dendritic cells and alters T cell responses. *J. Exp. Med.* **213**, 415–431 (2016).

60. Bar-On, L. et al. CX3CR1+ CD8 + dendritic cells are a steady-state population related to plasmacytoid dendritic cells. *Proc. Natl Acad. Sci. USA* **107**, 14745–14750 (2010).
61. Dicken, J. et al. Transcriptional reprogramming of CD11b+Esamhi dendritic cell identity and function by loss of Runx3. *PLoS ONE* **8**, e77490–12 (2013).
62. Lewis, K. L. et al. Notch2 receptor signaling controls functional differentiation of dendritic cells in the spleen and intestine. *Immunity* **35**, 780–791 (2011).
63. Satpathy, A. T. et al. Notch2-dependent classical dendritic cells orchestrate intestinal immunity to attaching-and-effacing bacterial pathogens. *Nat. Immunol.* **14**, 937–948 (2013).
64. Liu, J. et al. Non-parallel recombination limits cre-loxP-based reporters as precise indicators of conditional genetic manipulation. *Genesis* **51**, 436–442 (2013).
65. McKenna, H. J. et al. Mice lacking flt3 ligand have deficient hematopoiesis affecting hematopoietic progenitor cells, dendritic cells, and natural killer cells. *Blood* **95**, 3489–3497 (2000).
66. Böiers, C. et al. Lymphomyeloid contribution of an immune-restricted progenitor emerging prior to definitive hematopoietic stem cells. *Stem Cell* **13**, 535–548 (2013).
67. Gomez-Perdiguer, E. et al. Tissue-resident macrophages originate from yolk-sac-derived erythro-myeloid progenitors. *Nature* **518**, 547–551 (2015).
68. Mucenski, M. L. et al. A functional c-myc gene is required for normal murine fetal hepatic hematopoiesis. *Cell* **65**, 677–689 (1991).
69. Ardavin, C., Wu, L., Li, C.-L. & Shortman, K. Thymic dendritic cells and T cells develop simultaneously in the thymus from a common precursor population. *Nature* **362**, 761–763 (1993).
70. Becker, A. M. et al. Irf-8 extinguishes neutrophil production and promotes dendritic cell lineage commitment in both myeloid and lymphoid mouse progenitors. *Blood* **119**, 2003–2012 (2012).
71. Manz, M. G., Traver, D., Miyamoto, T., Weissman, I. L. & Akashi, K. Dendritic cell potentials of early lymphoid and myeloid progenitors. *Blood* **97**, 3333–3341 (2001).
72. Wu, L. et al. Development of thymic and splenic dendritic cell populations from different hemopoietic precursors. *Blood* **98**, 3376–3382 (2001).
73. Izon, D. et al. A common pathway for dendritic cell and early B cell development. *J. Immunol.* **167**, 1387–1392 (2001).
74. Salvermoser, J. et al. Clec9a-mediated ablation of conventional dendritic cells suggests a lymphoid path to generating dendritic cells in vivo. *Front. Immunol.* **9**, 563–15 (2018).
75. Igarashi, H., Gregory, S. C., Yokota, T., Sakaguchi, N. & Kincade, P. W. Transcription from the RAG1 locus marks the earliest lymphocyte progenitors in bone marrow. *Immunity* **17**, 117–130 (2002).
76. Schlenger, S. M. et al. Fate mapping reveals separate origins of T cells and myeloid lineages in the thymus. *Immunity* **32**, 426–436 (2010).
77. Werner, Y. et al. Cxcr4 distinguishes HSC-derived monocytes from microglia and reveals monocyte immune responses to experimental stroke. *Nat. Neurosci.* **23**, 351–362 (2020).
78. Gibbings, S. L. et al. Transcriptome analysis highlights the conserved difference between embryonic and postnatal-derived alveolar macrophages. *Blood* **126**, 1357–1366 (2015).
79. Lavin, Y. et al. Tissue-resident macrophage enhancer landscapes are shaped by the local microenvironment. *Cell* **159**, 1312–1326 (2014).
80. Smith, N. L. et al. Developmental origin governs CD8+ T cell fate decisions during infection. *Cell* **174**, 117–130.e14 (2018).
81. Mold, J. E. et al. Fetal and adult hematopoietic stem cells give rise to distinct T cell lineages in humans. *Science* **330**, 1695–1699 (2010).
82. Beaudin, A. E. et al. A transient developmental hematopoietic stem cell gives rise to innate-like B and T cells. *Stem Cell* **19**, 768–783 (2016).
83. Gury-BenAri, M. et al. The spectrum and regulatory landscape of intestinal innate lymphoid cells are shaped by the microbiome. *Cell* **166**, 1231–1239.e13 (2016).
84. Robinette, M. L. et al. Transcriptional programs define molecular characteristics of innate lymphoid cell classes and subsets. *Nat. Immunol.* **16**, 306–317 (2015).
85. Spits, H. & Cupedo, T. Innate lymphoid cells: emerging insights in development, lineage relationships, and function. *Annu. Rev. Immunol.* **30**, 647–675 (2012).
86. Satija, R., Farrell, J. A., Gennert, D., Schier, A. F. & Regev, A. Spatial reconstruction of single-cell gene expression data. *Nat. Biotechnol.* **33**, 495–502 (2015).
87. Stuart, T. et al. Comprehensive integration of single-cell data. *Cell* **177**, 1888–1902.e21 (2019).
88. Liu, Y., Beyer, A. & Aebersold, R. On the dependency of cellular protein levels on mRNA abundance. *Cell* **165**, 535–550 (2016).
89. Shimshek, D. R. et al. Codon-improved Cre recombinase (iCre) expression in the mouse. *Genesis* **32**, 19–26 (2002).
90. Miller, J. C. et al. Deciphering the transcriptional network of the dendritic cell lineage. *Nat. Immunol.* **13**, 888–899 (2012).
91. Madisen, L. et al. A robust and high-throughput Cre reporting and characterization system for the whole mouse brain. *Nat. Neurosci.* **13**, 133–140 (2010).
92. Brown, C. C. et al. Transcriptional basis of mouse and human dendritic cell heterogeneity. *Cell* **179**, 846–863.e24 (2019).
93. Setty, M. et al. Characterization of cell fate probabilities in single-cell data with Palantir. *Nat. Biotechnol.* **37**, 451–460 (2019).
94. Eberl, G. & Littman, D. R. Thymic origin of intestinal $\alpha\beta$ T cells revealed by fate mapping of ROR γ t+ cells. *Science* **305**, 248 (2004).
95. Bazhin, A. V. et al. Interferon- α up-regulates the expression of PD-L1 molecules on immune cells through STAT3 and p38 signaling. *Front. Immunol.* **9**, 119–13 (2018).
96. Nguyen-Pham, T.-N. et al. Type I and II interferons enhance dendritic cell maturation and migration capacity by regulating CD38 and CD74 that have synergistic effects with TLR agonists. *Cell. Mol. Immunol.* **8**, 341–347 (2011).
97. Xiao, X. et al. The costimulatory receptor OX40 inhibits interleukin-17 expression through activation of repressive chromatin remodeling pathways. *Immunity* **44**, 1271–1283 (2016).
98. D’Addio, F. et al. The link between the PDL1 costimulatory pathway and Th17 in fetomaternal tolerance. *J. Immunol.* **187**, 4530–4541 (2011).
99. Browning, L. M. et al. TGF- β -mediated enhancement of TH17 cell generation is inhibited by bone morphogenetic protein receptor 1 α signaling. *Sci. Signal.* **11**, eaar2125 (2018).
100. Blois, S. M. et al. A pivotal role for galectin-1 in fetomaternal tolerance. *Nat. Med.* **13**, 1450–1457 (2007).
101. Cedeno-Laurent, F. & Dimitroff, C. J. Galectin-1 research in T cell immunity: past, present and future. *Clin. Immunol.* **142**, 107–116 (2012).
102. Delgoffe, G. M. et al. Stability and function of regulatory T cells is maintained by a neuropilin-1-semaphorin-4a axis. *Nature* **501**, 252–256 (2013).
103. Garin, M. I. et al. Galectin-1: a key effector of regulation mediated by CD4+CD25+ T cells. *Blood* **109**, 2058–2065 (2006).
104. Heink, S. et al. Trans-presentation of IL-6 by dendritic cells is required for the priming of pathogenic TH17 cells. *Nat. Immunol.* **18**, 74–85 (2016).
105. Jiang, H.-R. et al. Galectin-3 deficiency reduces the severity of experimental autoimmune encephalomyelitis. *J. Immunol.* **182**, 1167–1173 (2009).
106. Lynch, J. P. et al. Plasmacytoid dendritic cells protect from viral bronchiolitis and asthma through semaphorin 4a-mediated T reg expansion. *J. Exp. Med.* **215**, 537–557 (2017).
107. Lehmann, C. H. K. et al. DC subset-specific induction of T cell responses upon antigen uptake via Fc γ receptors in vivo. *J. Exp. Med.* **214**, 1509–1528 (2017).
108. Kovarik, J. et al. Adjuvant effects of CpG oligodeoxynucleotides on responses against T-independent type 2 antigens. *Immunology* **102**, 67–76 (2001).
109. Kovarik, J. et al. CpG oligodeoxynucleotides can circumvent the Th2 polarization of neonatal responses to vaccines but may fail to fully redirect Th2 responses established by neonatal priming. *J. Immunol.* **162**, 1611–1617 (1999).
110. Meyer, C. U. et al. Dendritic cells change IL-27 production pattern during childhood. *BMC Res. Notes* **8**, 232–233 (2015).
111. Leung, G. A. et al. The lymphoid-associated interleukin 7 receptor (IL7R) regulates tissue-resident macrophage development. *Development* **146**, dev176180–25 (2019).
112. Christensen, J. L., Wright, D. E., Wagers, A. J. & Weissman, I. L. Circulation and chemotaxis of fetal hematopoietic stem cells. *PLoS Biol.* **2**, e75–10 (2004).
113. Perdiguer, E. G. & Geissmann, F. The development and maintenance of resident macrophages. *Nat. Immunol.* **17**, 2–8 (2016).
114. Ginhoux, F. & Guillemin, M. Tissue-resident macrophage ontogeny and homeostasis. *Immunity* **44**, 439–449 (2016).
115. Schneider, C. et al. Tissue-resident group 2 innate lymphoid cells differentiate by layered ontogeny and in situ perinatal priming. *Immunity* **50**, 1425–1438.e5 (2019).
116. Helft, J. et al. Dendritic cell lineage potential in human early hematopoietic progenitors. *Cell Rep.* **20**, 529–537 (2017).
117. Villani, A.-C. et al. Single-cell RNA-seq reveals new types of human blood dendritic cells, monocytes, and progenitors. *Science* **356**, eaah4573–14 (2017).
118. Dress, R. J. et al. Plasmacytoid dendritic cells develop from Ly6D+ lymphoid progenitors distinct from the myeloid lineage. *Nat. Immunol.* **20**, 852–864 (2019).
119. Rodrigues, P. F. et al. Distinct progenitor lineages contribute to the heterogeneity of plasmacytoid dendritic cells. *Nat. Immunol.* **19**, 711–722 (2018).
120. Schraml, B. U., Reis, E. & Sousa, C. ScienceDirect defining dendritic cells. *Curr. Opin. Immunol.* **32**, 13–20 (2015).
121. Gosselin, D. et al. An environment-dependent transcriptional network specifies human microglia identity. *Science* **356**, eaal3222–13 (2017).
122. Gosselin, D. et al. Environment drives selection and function of enhancers controlling tissue-specific macrophage identities. *Cell* **159**, 1327–1340 (2014).

123. van de Laar, L. et al. Yolk sac macrophages, fetal liver, and adult monocytes can colonize an empty niche and develop into functional tissue-resident macrophages. *Immunity* **44**, 755–768 (2016).
124. Janela, B. et al. A subset of type I conventional dendritic cells controls cutaneous bacterial infections through VEGF α -mediated recruitment of neutrophils. *Immunity* **50**, 1069–1083.e8 (2019).
125. Leyle, R. et al. Integrated cross-species analysis identifies a conserved transitional dendritic cell population. *Cell Rep.* **29**, 3736–3750.e8 (2019).
126. Briseño, C. G. et al. Notch2-dependent DC2s mediate splenic germinal center responses. *Proc. Natl Acad. Sci. USA* **115**, 10726–10731 (2018).
127. Hirahara, K. et al. Interleukin-27 priming of T cells controls IL-17 production in trans via induction of the ligand PD-L1. *Immunity* **36**, 1017–1030 (2012).
128. Francisco, L. M., Sage, P. T. & Sharpe, A. H. The PD-1 pathway in tolerance and autoimmunity. *Immunol. Rev.* **236**, 219–242 (2010).
129. Hunter, C. A. New IL-12-family members: IL-23 and IL-27, cytokines with divergent functions. *Nat. Rev. Immunol.* **5**, 521–531 (2005).
130. Kilgore, A. M. et al. IL-27p28 production by XCR1+ dendritic cells and monocytes effectively predicts adjuvant-elicited CD8+ T cell responses. *Immunohorizons* **2**, 1–11 (2018).
131. Ng, T. H. S. et al. Regulation of adaptive immunity; the role of interleukin-10. *Front. Immunol.* **4**, 129 (2013).
132. Nabhani, Al.Z. et al. A weaning reaction to microbiota is required for resistance to immunopathologies in the adult. *Immunity* **50**, 1276–1288.e5 (2019).
133. Bogaert, D., Weinberger, D., Thompson, C., Lipsitch, M. & Malley, R. Impaired innate and adaptive immunity to *Streptococcus pneumoniae* and its effect on colonization in an infant mouse model. *Infect. Immun.* **77**, 1613–1622 (2009).
134. Tsai, M.-H. et al. Clinical and microbiological characteristics, and impact of therapeutic strategies on the outcomes of children with candidemia. *Sci. Rep.* **7**, 1083–1089 (2017).
135. Fedele, G., Cassone, A. & Ausiello, C. M. T-cell immune responses to *Bordetella pertussis* infection and vaccination. *Pathog. Dis.* **73**, fiv051 (2015).
136. Vogel, K. et al. Developmental induction of human T-cell responses against *Candida albicans* and *Aspergillus fumigatus*. *Sci. Rep.* **8**, 16904 (2018).
137. Srinivas, S. et al. Cre reporter strains produced by targeted insertion of EYFP and ECFP into the ROSA26 locus. *BMC Dev. Biol.* **1**, 4–8 (2001).
138. Qian, B.-Z. et al. CCL2 recruits inflammatory monocytes to facilitate breast-tumour metastasis. *Nature* **475**, 222–225 (2011).
139. McCormack, M. P., Forster, A., Drynan, L., Pannell, R. & Rabbitts, T. H. The LMO2 T-cell oncogene is activated via chromosomal translocations or retroviral insertion during gene therapy but has no mandatory role in normal T-cell Development. *Mol. Cell Biol.* **23**, 9003–9013 (2003).
140. Barnard, M. J., Allison, J., Heath, W. R. & Carbone, F. R. Defective TCR expression in transgenic mice constructed using cDNA-based α - and β -chain genes under the control of heterologous regulatory elements. *Immunol. Cell Biol.* **76**, 34–40 (1998).
141. Lochner, M. et al. In vivo equilibrium of proinflammatory IL-17+ and regulatory IL-10+Foxp3+ROR γ T+ T cells. *J. Exp. Med.* **205**, 1381–1393 (2008).
142. Muzumdar, M. D., Tasic, B., Miyamichi, K., Li, L. & Luo, L. A global double-fluorescent Cre reporter mouse. *Genesis* **45**, 593–605 (2007).
143. Luche, H., Weber, O., Rao, T. N., Blum, C. & Fehling, H. J. Faithful activation of an extra-bright red fluorescent protein in 'knock-in' Cre-reporter mice ideally suited for lineage tracing studies. *Eur. J. Immunol.* **37**, 43–53 (2007).
144. Muller, U. et al. Functional role of type I and type II interferons in antiviral defense. *Science* **264**, 1918–1921 (1994).
145. Bajénoff, M., Glaichenhaus, N. & Germain, R. N. Fibroblastic reticular cells guide T lymphocyte entry into and migration within the splenic T cell zone. *J. Immunol.* **181**, 3947–3954 (2008).
146. Schindelin, J. et al. Fiji: an open-source platform for biological-image analysis. *Nat. Methods* **9**, 676–682 (2012).
147. Dobin, A. et al. STAR: ultrafast universal RNA-seq aligner. *Bioinformatics* **29**, 15–21 (2012).
148. Li, B. & Dewey, C. N. RSEM: accurate transcript quantification from RNA-Seq data with or without a reference genome. *BMC Bioinformatics* **12**, 323 (2011).
149. Zhu, A., Ibrahim, J. G. & Love, M. I. Heavy-tailed prior distributions for sequence count data: removing the noise and preserving large differences. *Bioinformatics* **35**, 2084–2092 (2018).

Acknowledgements

We thank members of the Schraml lab, Anne Krug, Caetano Reis e Sousa, and Markus Sperandio for helpful discussions and critical reading of the manuscript. We acknowledge the Core Facility Flow Cytometry and the Core Facility Bioimaging at the Bio-medical Center, Ludwig-Maximilians-Universität München, for providing equipment and expertise. High-throughput sequencing was performed by the laboratory for Functional Genome Analysis (LAFUGA) of the LMU Munich. Some flow cytometry experiments were performed at the Core Unit Cell Sorting and Immunomonitoring of the University Hospital Erlangen. We thank Hans-Reimer Rodewald for providing *Il7^{cre}* mice. This work was supported by ERC Starting Grant awarded to B.S. (ERC-2016-STG-715182). Work in the Schraml lab is also funded by the Deutsche Forschungsgemeinschaft (DFG, German Research Foundation) Emmy Noether Grant: Schr 1444/1-1 (to B.S.) and Projektnummer 360372040 – SFB 1335/P08 (to B.S.). C.O. is supported by an ERC Starting Grant (ERC-2016-STG-716718) and by DFG within CRC1371 (project P07) and FOR2599 (project P07). C.S. was supported by the SFB914 (project A10), as well as the DZHK (German Centre for Cardiovascular Research) and the BMBF (German Ministry of Education and Research) (grant 81Z0600204). D.D. received funding from the DFG (DU548/5-1, CRC1181-A7) and Agency national research (ANR)/German Research Foundation program (DU548/6-1).

Author contributions

N.E.P., N.S., S.R., K.R., J.P., V.K., C.H.K.L., R.F., J.S., D.W.G., R.M., D.M., and B.S. performed experiments. N.E.P., G.S., and T.S. performed sequencing analysis. C.H.K.L. and D.D. helped with targeting experiments. C.O. provided *Rorc^{GFP}* mice, D.H. germ-free mice, S.E.J. *Rag1^{cre}* mice, and R.S. *CXCR4^{CreER}* mice, and helped in planning the corresponding experiments. S.E.J. and J.C. provided critical input for fate mapping lymphoid progenitors. C.S., G.S., D.D., and D.W. provided reagents and critical intellectual input. B.S. designed and supervised the study.

Funding

Open Access funding enabled and organized by Projekt DEAL.

Competing interests

The authors declare no competing interests.

Additional information

Supplementary information is available for this paper at <https://doi.org/10.1038/s41467-020-20659-2>.

Correspondence and requests for materials should be addressed to B.U.S.

Peer review information *Nature Communications* thanks Roxane Tussiwand and the other, anonymous, reviewer(s) for their contribution to the peer review of this work. Peer reviewer reports are available.

Reprints and permission information is available at <http://www.nature.com/reprints>

Publisher's note Springer Nature remains neutral with regard to jurisdictional claims in published maps and institutional affiliations.



Open Access This article is licensed under a Creative Commons Attribution 4.0 International License, which permits use, sharing, adaptation, distribution and reproduction in any medium or format, as long as you give appropriate credit to the original author(s) and the source, provide a link to the Creative Commons license, and indicate if changes were made. The images or other third party material in this article are included in the article's Creative Commons license, unless indicated otherwise in a credit line to the material. If material is not included in the article's Creative Commons license and your intended use is not permitted by statutory regulation or exceeds the permitted use, you will need to obtain permission directly from the copyright holder. To view a copy of this license, visit <http://creativecommons.org/licenses/by/4.0/>.

© The Author(s) 2021

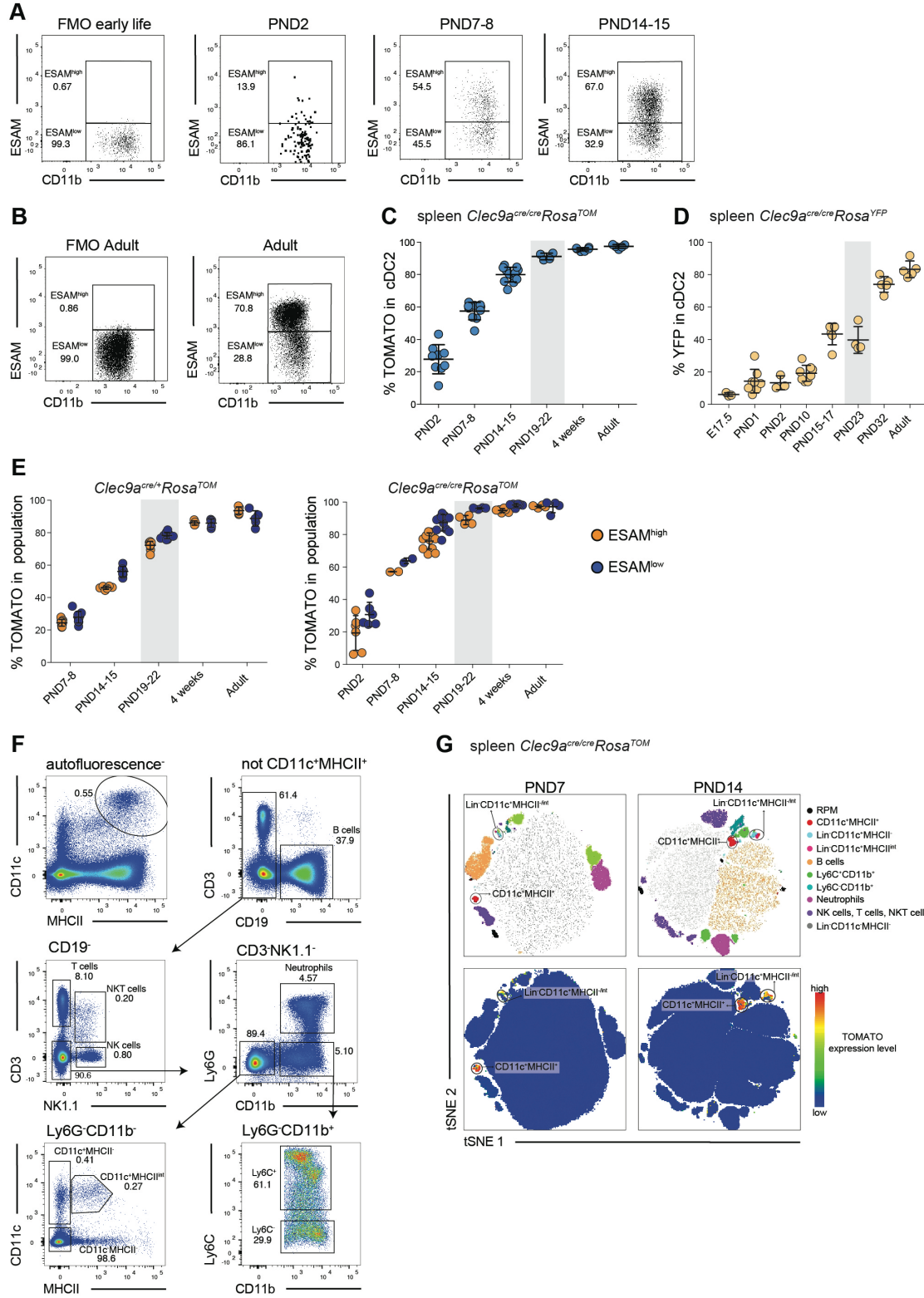
Supplementary information

Environmental signals rather than layered ontogeny imprint the function of type 2 conventional dendritic cells in young and adult mice

First author: Nikos E. Papaioannou

Corresponding author: Barbara U. Schraml

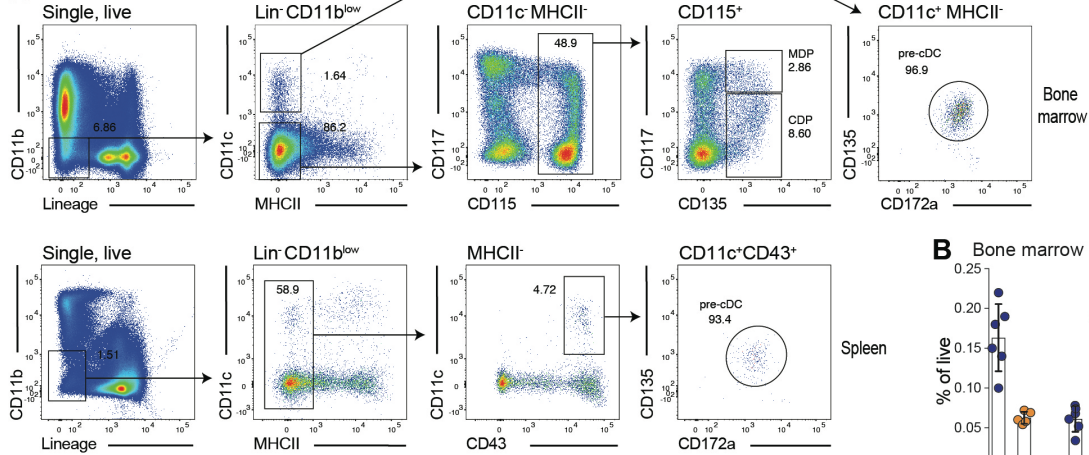
Supplementary Figure 1



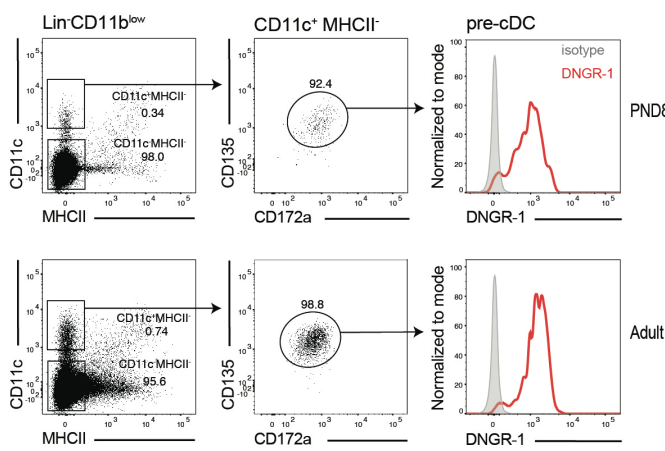
Supplementary Figure 1. *Clec9^{cre}* mice faithfully trace cDCs in early life. (A, B) Splenic cDC2 (CD11c⁺MHCII⁺CD11b⁺) from *Clec9a^{cre/+}Rosa^{TOM}* or *Clec9a^{cre/cre}Rosa^{TOM}* mice of the indicated ages were analyzed for ESAM expression. Fluorescence minus one (FMO) controls used to set the gates are shown. (C-E) Splenic cDC2 from *Clec9a^{cre/cre}Rosa^{TOM}* (C) and *Clec9a^{cre/cre}Rosa^{YFP}* mice (D) were analyzed for TOMATO and YFP expression at the indicated ages (n=9, PND2; n=10, PND7-8; n=12, PND14-15; n=4, PND19-22; n=6, 4 weeks; n=5, adult (C) and n=3, E17.5; n=8, PND1; n=3, PND2; n=8, PND10; n=6, PND15-17; n=4, PND23; n=5, PND32; n=5, adult (D)). (E) Splenic ESAM^{high} and ESAM^{low} cDC2 from *Clec9a^{cre/+}Rosa^{TOM}* (left) and *Clec9a^{cre/cre}Rosa^{TOM}* (right) mice were analyzed for TOMATO expression at the indicated ages (n=9, PND7-8; n=6, PND14-15; n=10, PND19-22; n=5, 4 weeks; n=5, adult for left plot and n=6, PND2; n=2, PND7-8; n=12, PND14-15; n=4, PND19-22; n=6, 4 weeks; n=4, adult for right plot). Each dot represents one mouse, horizontal bars represent mean, error bars represent SD, grey rectangles indicate weaning. (F, G) Spleens from one- and two-week-old *Clec9a^{cre/cre}Rosa^{TOM}* mice were analyzed by flow cytometry as indicated, to profile TOMATO expression in lymphoid and myeloid populations. (F) Representative gating strategy. (G) t-Distributed Stochastic Neighbor Embedding (tSNE) of splenocytes from PND7 and PND14 *Clec9a^{cre/cre}Rosa^{TOM}* mice. Cells were clustered independent of TOMATO. Manually gated populations were overlaid on the tSNE plot and indicated by color. Blue-to-red gradient indicates increasing intensity of TOMATO expression. Source data are provided as a Source Data file.

Supplementary Figure 2

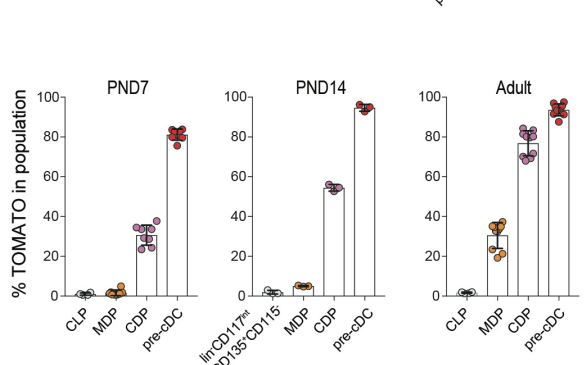
A Gating strategy for cDC progenitors



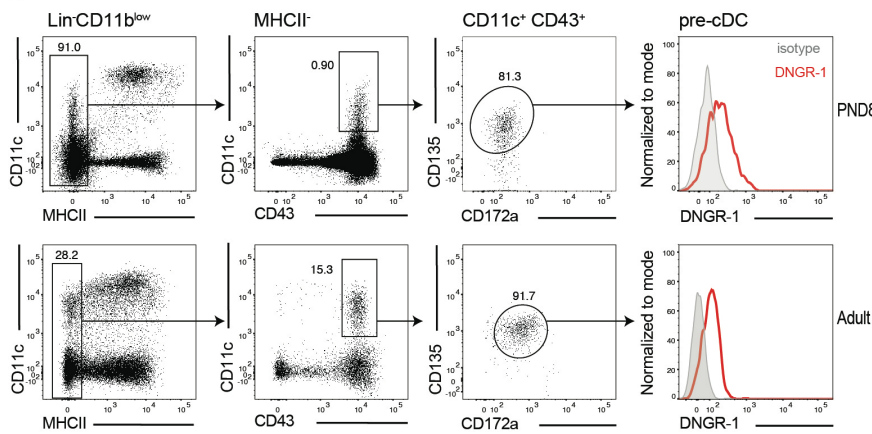
C Bone marrow



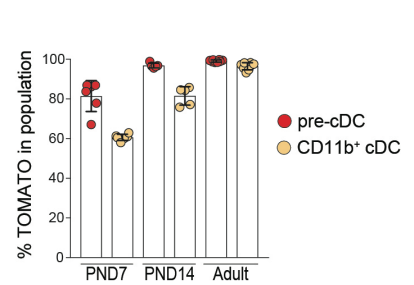
E Bone marrow



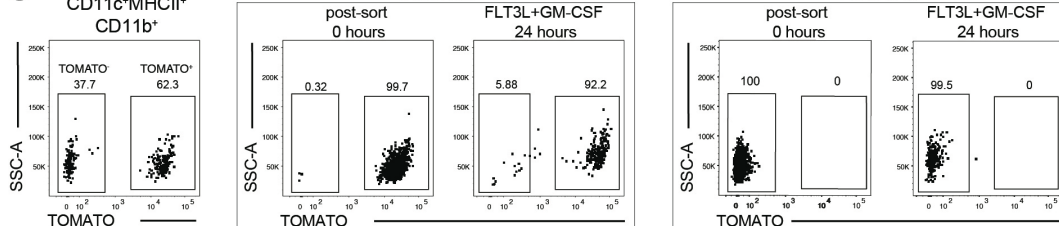
D Spleen



F Spleen

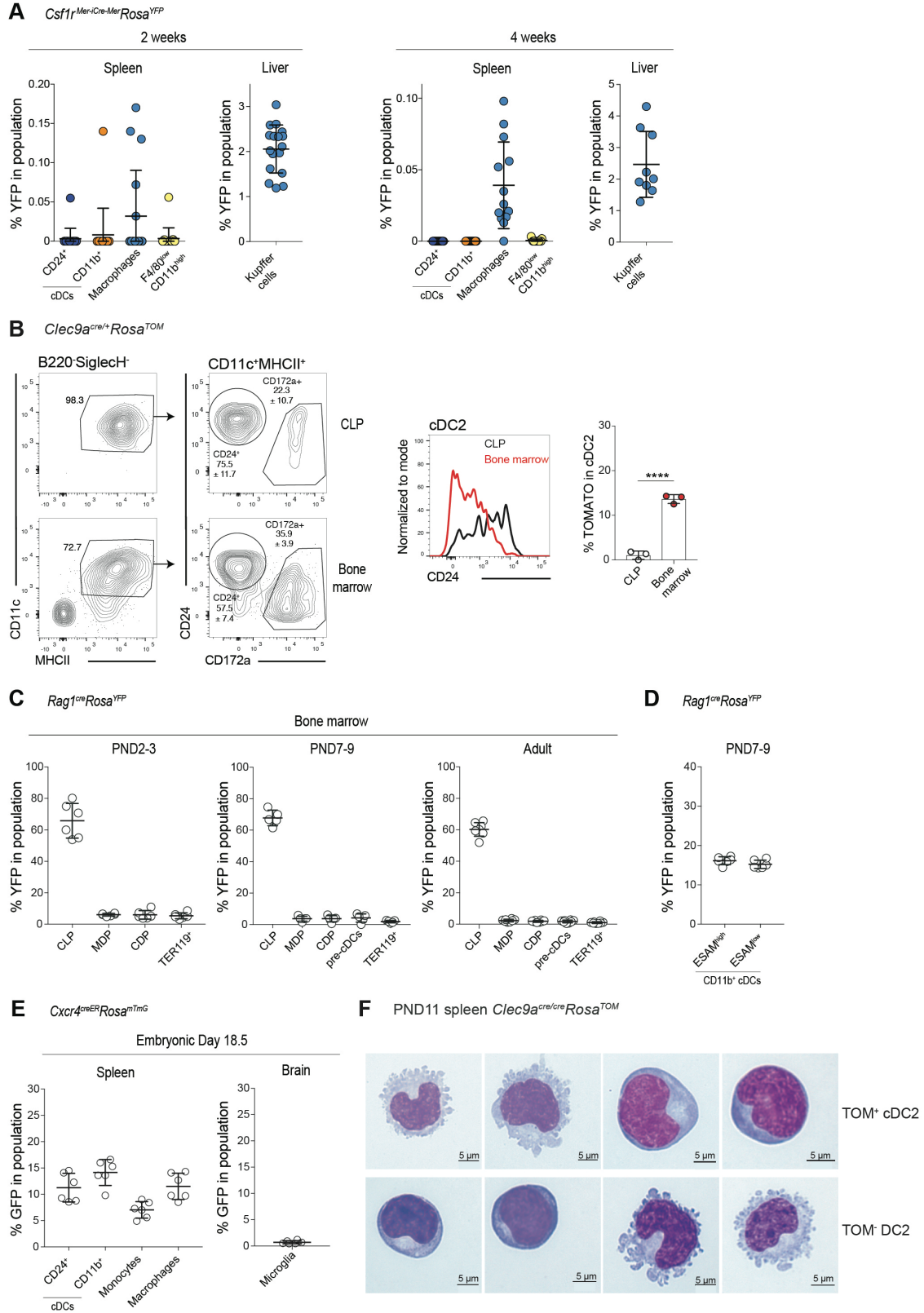


G



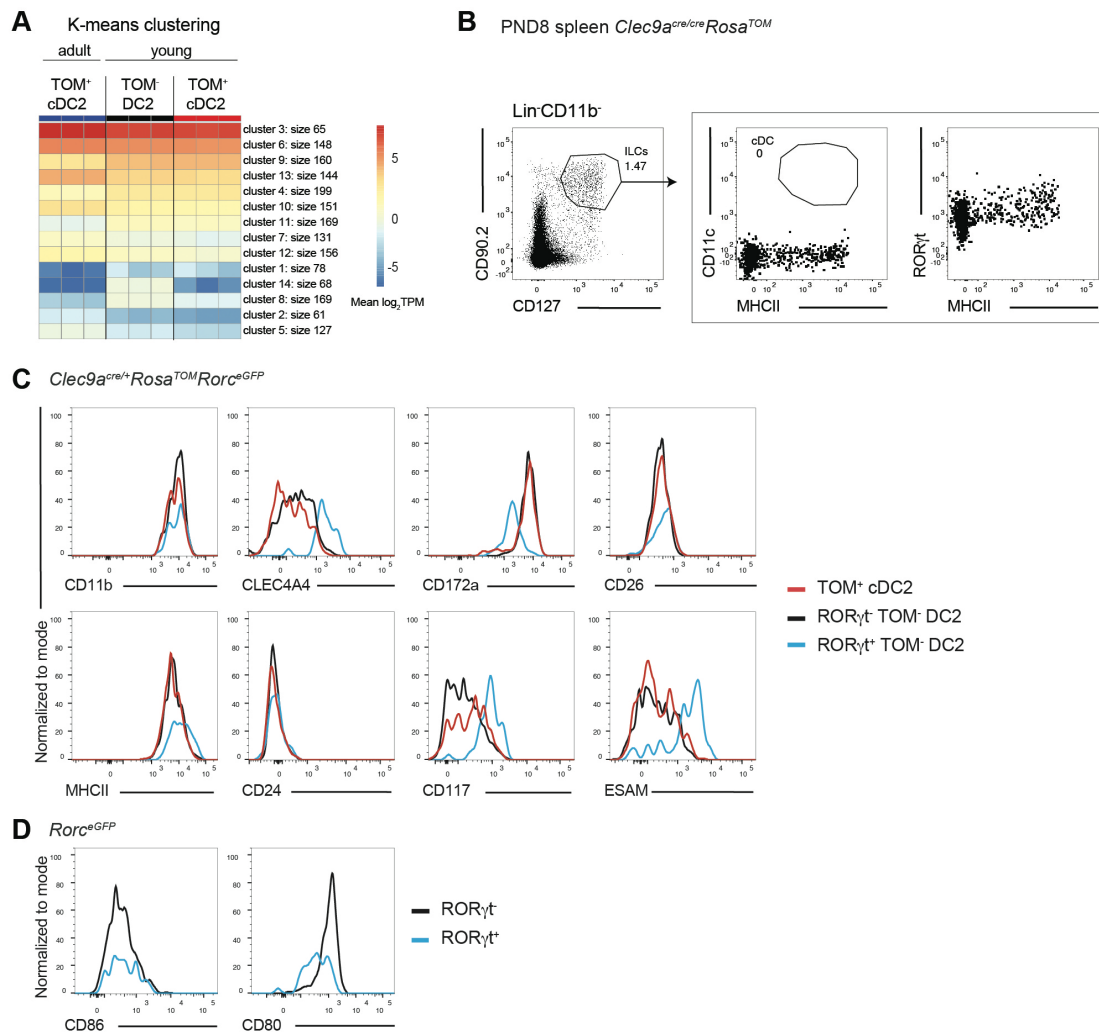
Supplementary Figure 2. Identification of cDC progenitors in early life. (A) Representative gating strategy for the identification of cDC progenitors in bone marrow (upper row) and spleen (lower row) of adult mice. (B) Frequency of cDC progenitors as identified in (A) in the bone marrow of wild type mice at the indicated ages (n=6, MDP and CDP PND2; n=3, pre-cDC PND2; n=5, adult). Each dot represents one biological replicate, horizontal bars represent mean, error bars represent SD. (C, D) Bone marrow (C) and spleen (D) from wild type mice of the indicated ages were analyzed by flow cytometry. Lin⁻ cells were gated, pre-cDCs were identified as indicated and stained with anti-DNGR-1 (red) or isotype-matched control antibody (grey). Lineage: CD3, B220, NK1.1, CD4, CD8 α , TER119. (E, F) Bone marrow (E) and spleen (F) of *Clec9a^{cre/cre}Rosa^{TOM}* mice was analyzed by flow cytometry at the indicated ages. (E) CLPs (lin⁻CD11b⁻CD115⁻CD117^{int}Sca-1^{int}CD135⁺CD127⁺), MDPs (lin⁻CD11c⁻MHCII⁻CD11b^{low}CD115⁺CD135⁺CD117^{high}), CDPs (lin⁻CD11c⁻MHCII⁻CD11b^{low}CD115⁺CD135⁺CD117^{low}) and pre-cDCs (lin⁻MHCII⁻CD11b^{low}CD11c⁺CD135⁺CD172a^{int}) were analyzed for TOMATO expression. The lin⁻CD11b⁻CD117^{int}CD115⁻CD135⁺ fraction of bone marrows that contains CLPs was used to assess TOMATO expression in PND14 and adult mice (n=8, PND7; n=3, PND14; n=10, adult; n=4, CLP PND7 and adult). (F) TOMATO expression was analyzed in splenic pre-cDCs (lin⁻MHCII⁻CD11b^{low}CD11c⁺CD43⁺CD135⁺CD172a^{int}) and CD11b⁺ cDCs (n=6, PND7; n=5, PND14; n=8, adult). Each dot represents one mouse, horizontal bars represent mean, error bars represent SD. Lineage: CD3, B220, NK1.1, CD4, CD8 α , TER119. (G) TOM⁻ and TOM⁺ CD11b⁺ cDC2 cells were sorted from spleens of one-week-old *Clec9a^{cre/cre}Rosa^{TOM}* mice and cultured *in vitro* with congenic CD45.1 filler splenocytes in the presence of FLT3L and GM-CSF. After 24 hours, TOM⁻ and TOM⁺ cells were analyzed for TOMATO labeling. FACS plots show TOMATO labeling in CD11b⁺ cDC2 before sorting (left), sort purity of TOMATO⁻ and TOMATO⁺ fractions (right upper plots) and TOMATO labeling after 24 hours in culture (right bottom plots). Data are representative of two independent experiments with at least 2 biological replicates each. Source data are provided as a Source Data file.

Supplementary Figure 3



Supplementary Figure 3. Fate mapping reveals a lymphoid contribution to cDC2 in early life and TOM⁻ DC2 morphologically resemble TOM⁺ cDC2. (A) *Csf1r*^{Mer-iCre-Mer} dams were mated with male *Rosa*^{YFP} mice and injected with 4OH-tamoxifen on E8.5. Spleen and liver from offspring mice were analyzed by flow cytometry two (n=17) or four weeks (n=13, n=9 for liver) after birth. The percentage of YFP⁺ cells in the indicated populations is plotted. (B) Unfractionated bone marrow and 10⁴ CLPs (lin⁻CD11b⁻CD115⁻CD117^{int}CD135⁺CD127⁺B220⁻TOMATO⁻) from adult CD45.2⁺ *Clec9a*^{cre/+}*Rosa*^{TOM} mice were cultured with FLT3L for 7 days in the presence of CD45.1⁺ congenic bone marrow filler cells. Left: CD11c⁺MHCII⁺ cells were identified by FACS and divided into CD24⁺ cDC1 and CD172a⁺ cDC2 equivalents. Numbers indicate mean frequency±SD. Middle: Expression of CD24 on cDC2 equivalents. Right: The frequency of TOMATO positive cells in cDC2 equivalents derived from bone marrow and CLP is shown. Data are representative of two independent experiments (n=3). Statistical analysis was performed using two-tailed t test. (C, D) Bone marrow (C) and spleen (D) from *Rag1*^{cre}*Rosa*^{YFP} mice at the indicated ages was analyzed by flow cytometry. (C) CLPs (lin⁻CD11b⁻CD115⁻CD117^{int}Sca-1^{int}CD135⁺CD127⁺), MDPs (lin⁻CD11c⁻MHCII⁻CD11b^{low}CD115⁺CD135⁺CD117^{high}), CDPs (lin⁻CD11c⁻MHCII⁻CD11b^{low}CD115⁺CD135⁺CD117^{low}), pre-cDCs (lin⁻MHCII⁻CD11b^{low}CD11c⁺CD135⁺CD172a^{int}), as well as TER119⁺ erythroid cells were analyzed for YFP expression (n=6, PND2-3; n=5, PND7-9; n=8, adult; lineage: Ly6G, CD3, B220, NK1.1, CD8α). (D) cDC2 from spleen of *Rag1*^{cre}*Rosa*^{YFP} mice on PND7-9 were divided into ESAM^{high} and ESAM^{low} populations and analyzed for YFP expression (n=6). (E) Male *Cxcr4*^{creER} mice were mated with female *Rosa*^{mTmG} mice. Pregnant dams were injected with tamoxifen on E12.5. On E18.5 spleen and brain from offspring mice were analyzed by flow cytometry for GFP expression (n=6). Each dot in (A-E) represents one mouse, horizontal bars represent mean, error bars represent SD. **** p<0.0001. (F) Cytopsin analysis of splenic TOM⁺ cDC2 and TOM⁻ DC2 of 11-day-old *Clec9a*^{cre/cre}*Rosa*^{TOM} mice. Scale bar 5μm. Data are representative of two independent experiments. Source data are provided as a Source Data file.

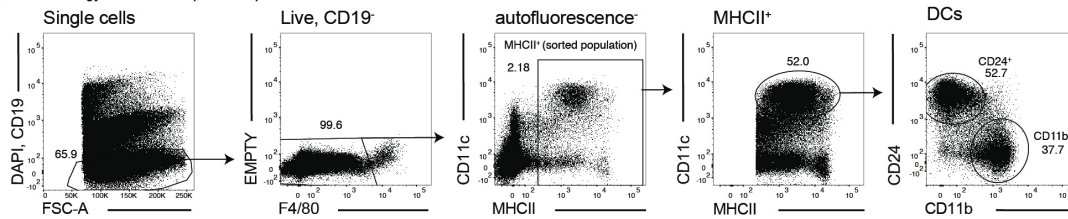
Supplementary Figure 4



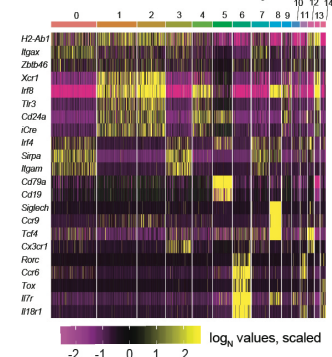
Supplementary Figure 4. ROR γ ⁺TOM⁻ DC2 in early life are distinct from ILCs and exhibit phenotypic profile that resembles ESAM^{hi} cDC2. (A) TOM⁻ DC2 and TOM⁺ cDC2 from 8-day-old and TOM⁺ cDC2 from adult *Clec9a^{cre/cre}Rosa^{TOM}* mice were sorted and analyzed by mRNA sequencing. k-means clustering of differentially expressed genes (log₂ FC >1 and padj <0.05) between TOM⁺ cDC2 from young mice, TOM⁻ DC2 from young mice and TOM⁺ cDC2 from adult mice. Significance of differentially expressed genes was tested using default commands of DESeq2. (B) Splenic ILCs, identified as lin⁻ (CD3, B220, NK1.1) CD11b⁻CD90.2⁺CD127⁺, from one-week-old *Clec9a^{cre/cre}Rosa^{TOM}* mice were analyzed for expression of CD11c, MHCII and ROR γ t. Plots are representative of three biological replicates. (C) TOM⁺ cDC2 (red), ROR γ t⁻TOM⁻ DC2 (black) and ROR γ t⁺TOM⁻ DC2 (blue) from one-week-old *Clec9a^{cre/+}Rosa^{TOM}Rorc^{eGFP}* mice were identified and analyzed for surface expression of the indicated markers. (D) ROR γ t⁻CD11b⁺ DCs (black) and ROR γ t⁺CD11b⁺ DCs (blue) from one-week-old *Rorc^{eGFP}* mice were identified and compared for expression of indicated surface markers. (C, D) Data are representative of n=2.

Supplementary Figure 5

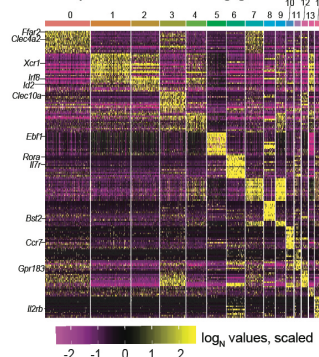
A Sort strategy for scRNAseq, PND9 spleen *Clec9a^{cre/cre} Rosa^{Tom}*



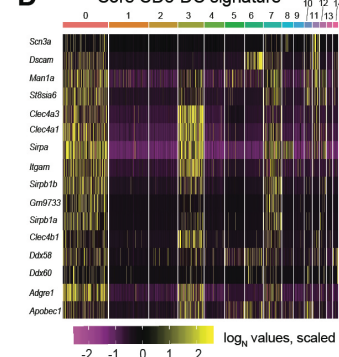
B Genes for cluster identity



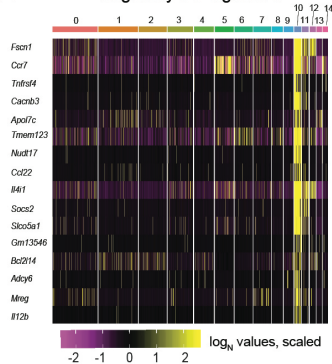
C Top 15 cluster defining genes



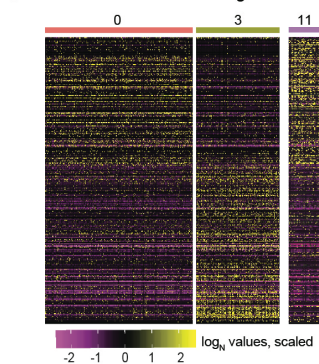
D Core CD8+ DC signature



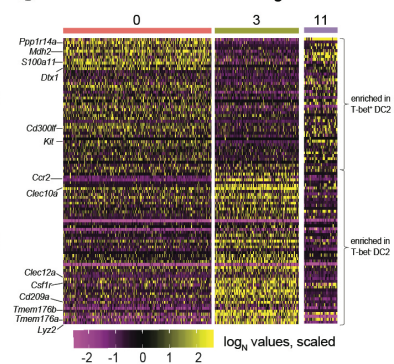
E Migratory DC signature



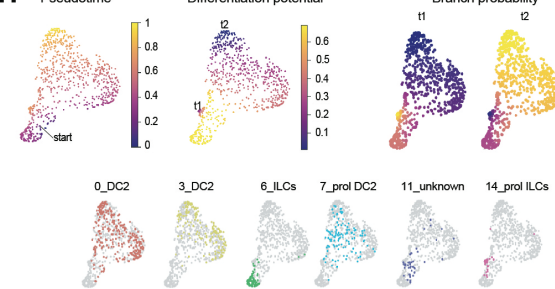
F ESAM^{high} vs ESAM^{low} genes



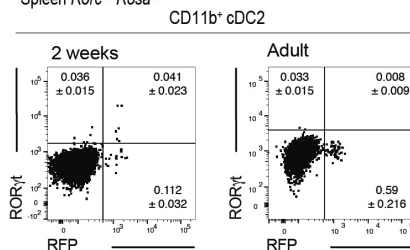
G T-bet^{hi} DC2 vs T-bet^{lo} DC2 genes



H Pseudotime

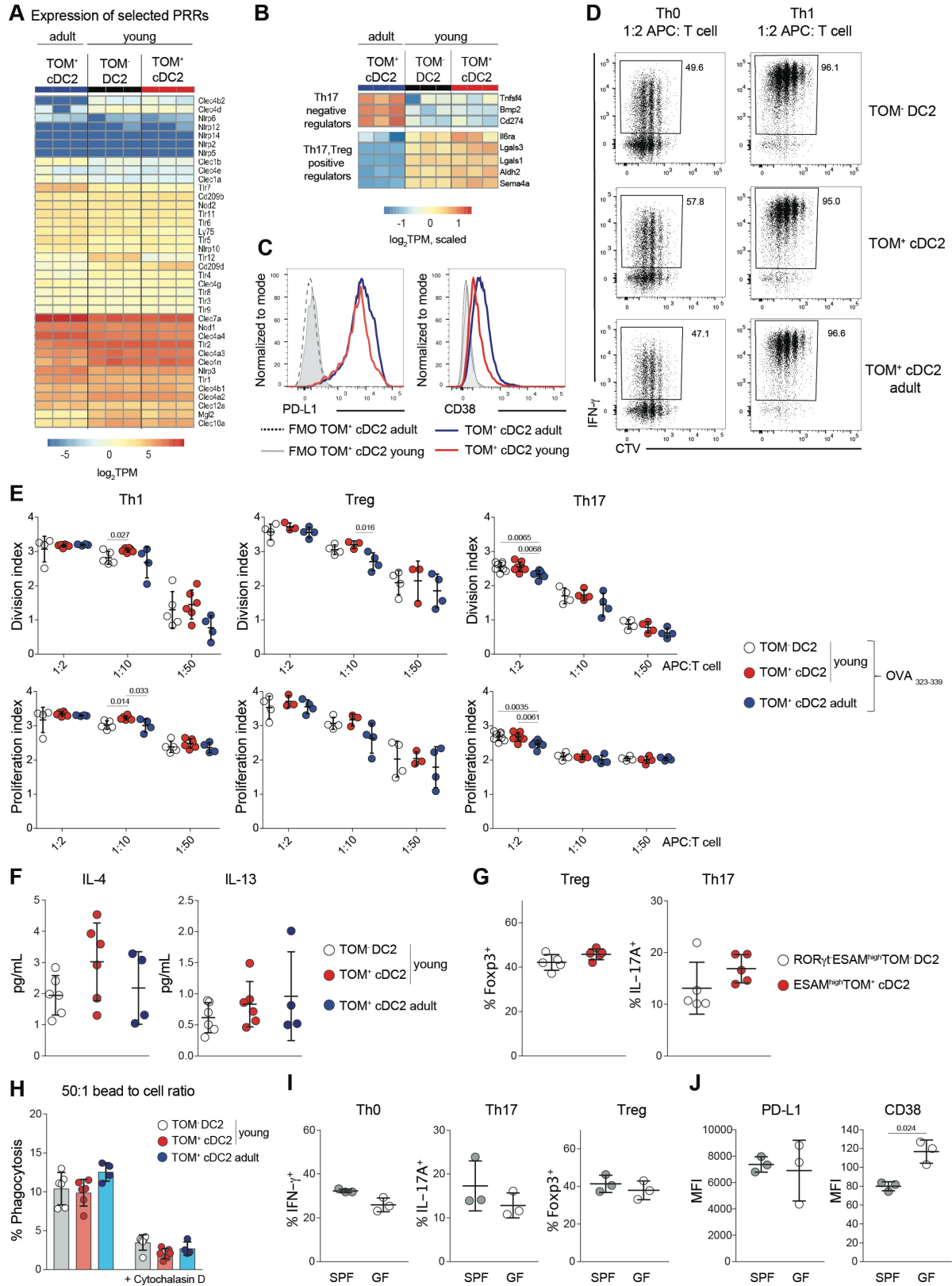


I Spleen *Rorc^{cre} Rosa^{RFP}*



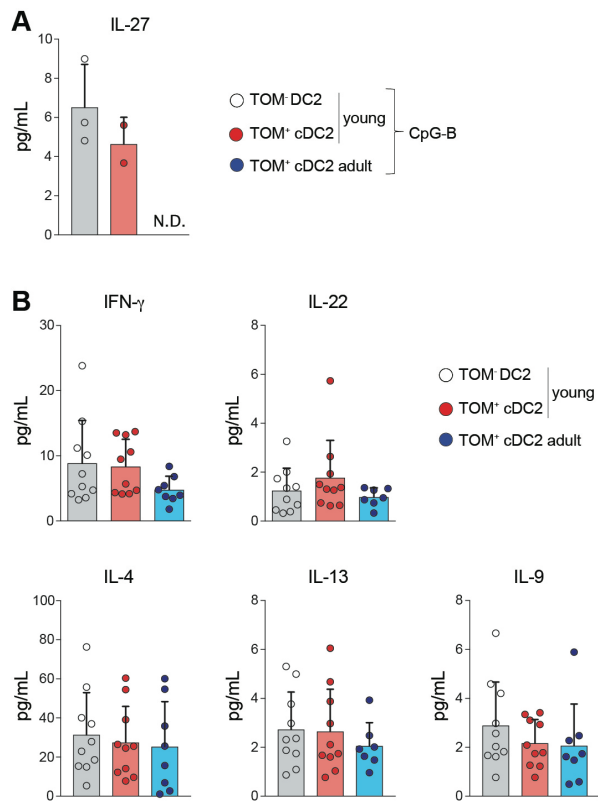
Supplementary Figure 5. TOM⁺ cDC2 and TOM⁻ DC2 in early life are transcriptionally identical. (A) Sort strategy for MHCII⁺ cells from spleens of 9-day-old *Clec9a^{cre/cre}Rosa^{TOM}* mice for single cell RNA-seq. (B) Heatmap showing expression of genes used for cluster identification. (C) Heatmap displaying expression of the top 15 cluster defining genes. (D-G) Heatmaps displaying the expression of (D) core CD8⁻ DC genes, (E) core migratory DC genes, (F) genes characteristic for ESAM^{high} and ESAM^{low} cDC2, as well as genes characteristic for T-bet⁺ and T-bet⁻ cDC2 (G) among cells of indicated clusters. (B-G) Expression is shown in logN values scaled by row. (H) Palantir pseudo-time analysis of differentiation potential and branch probabilities from cluster 11 (upper row). Start point and terminal states are indicated. The positioning of clusters 0, 3, 6, 7, 11 and 14 used for Palantir analysis is shown in tSNE embedding of the diffusion map (lower row). (I) Spleen from two-week-old and adult *Rorc^{cre}Rosa^{RFP}* mice were analyzed by flow cytometry. CD11c⁺MHCII⁺CD11b⁺ cDC2 were identified and analyzed for the expression of RORγt and RFP. Numbers represent mean ± SD (n=7, two-week-old; n=4, adult). Source data are provided as a Source Data file.

Supplementary Figure 6



Supplementary Figure 6. TOM⁺ cDC2 and TOM⁻ DC2 can prime naïve T cell proliferation comparable to cDC2 from adults. (A, B) Sort-purified TOM⁻ DC2 and TOM⁺ cDC2 from 8-day-old and TOM⁺ cDC2 from adult *Clec9a^{cre/cre}Rosa^{TOM}* mice were analyzed by mRNA sequencing. Heatmaps showing expression of selected pattern recognition receptors (log₂TPM values) **(A)** and genes involved in Th17 and Treg differentiation (log₂TPM values, scaled by row) **(B)**. **(C)** TOM⁺ cDC2 from two-week-old and adult *Clec9a^{cre/+}Rosa^{TOM}* mice were analyzed by flow cytometry for PD-L1 and CD38 expression (n=4-7). **(D-F)** TOM⁻ DC2 and TOM⁺ cDC2 from two-week-old and TOM⁺ cDC2 from adult *Clec9a^{cre/+}Rosa^{TOM}* mice were sorted, pulsed with OVA₃₂₃₋₃₃₉ and co-cultured with CTV-labelled OT-II cells as indicated. 3.5 days later OT-II cells were analyzed for cytokine expression **(D)** and cell division **(E)**. **(F)** Cytokine levels in supernatants of OT-II cells co-cultured with the indicated DC2 populations under Th0 conditions. Data in **(D-F)** are pooled from four independent experiments. **(G)** Sort-purified RORγt⁺ESAM^{high}TOM⁻ DC2 and ESAM^{high}TOM⁺ cDC2 from two-week-old *Clec9a^{cre/+}Rosa^{TOM}Rorc-eGFP* mice were co-cultured with CTV-labelled OT-II cells in Treg or Th17 conditions for 3.5 days. The percentage of cytokine or Foxp3 positive proliferated OT-II cells is shown (n=5). **(H)** CD11c-enriched splenocytes from two-week-old (n=6) and adult (n=4) *Clec9a^{cre/+}Rosa^{TOM}* mice were cultured with yellow fluorescent beads at the indicated bead to cell ratio *in vitro* for 2 hours +/- cytochalasin D. Bead uptake was quantified by flow cytometry in TOM⁺ cDC2 (Autofluorescence⁻CD11c⁺MHCII⁺CD11b⁺TOMATO⁺) and TOM⁻ DC2 (Autofluorescence⁻CD11c⁺MHCII⁺CD11b⁺TOMATO⁻). **(I)** Sort-purified splenic CD11c⁺MHCII⁺CD11b⁺ cDC2 from SPF or GF mice were co-cultured with CTV-labelled OT-II cells as indicated. 3.5 days later proliferated OTII cells were analyzed for cytokines and Foxp3 expression (n=3). **(J)** PD-L1 and CD38 expression on splenic cDC2 from SPF and GF mice (n=3). Each dot represents individual biological replicates **(E-H)** or mice **(I-J)**, horizontal bars represent mean, error bars represent SD. Comparison of TOM⁻ DC2 and TOM⁺ cDC2 was performed using two-tailed paired t test. Comparison of two-week-old and adult groups was performed using one-way ANOVA. Statistical analysis in **(I-J)** was performed using two-tailed t test. Only statistically significant comparisons are indicated. Source data are provided as a Source Data file.

Supplementary Figure 7



Supplementary Figure 7. Early life cDC2 show distinct responsiveness to CpG and induce distinct T cell responses upon targeted antigen delivery compared to adult life cDC2. (A) TOM⁺ cDC2 and TOM⁻ DC2 from two-week-old and TOM⁺ cDC2 from adult *Clec9a^{cre/+}Rosa^{TOM}* mice were sorted and stimulated with CpG-B. Cytokine production was analyzed 18-20h later (n=4, with IL-27 detected in 3 out of 4 replicates from two-week-old TOM⁻ DC2, 2 out of 4 replicates from two-week-old TOM⁺ cDC2, while it was not detected in supernatants from adult TOM⁺ cDC2). Each dot represents one biological replicate. **(B)** Two-week-old and adult *Clec9a^{cre/+}Rosa^{TOM}* mice were injected i.p. with anti-DCIR2-OVA antibody plus CpG-B. After 12 hours DC populations were sorted and co-cultured with OT-II T cells for 3.5 days. The indicated cytokines were quantified in supernatants from co-cultures (n=10, two-week-old; n=8, adult; IL-22 and IL-13 were detected in 7 out 8 adult replicates). Each dot represents one biological replicate from two independent experiments, horizontal bars represent mean, error bars represent SD. Statistical analysis was performed using two-tailed paired t test (comparing TOM⁻ DC2 and TOM⁺ cDC2 groups) or one-way ANOVA (comparing two-week-old and adult groups). No statistically significant differences were found. Source data are provided as a Source Data file.

References

1. Steinman RM, Cohn ZA. Identification of a novel cell type in peripheral lymphoid organs of mice. I. Morphology, quantitation, tissue distribution. *J Exp Med*. 1973;137(5):1142–62.
2. Durai V, Murphy KM. Functions of Murine Dendritic Cells. *Immunity*. 2016;45(4):719–36..
3. Eberl G, Pradeu T. Towards a General Theory of Immunity? *Trends Immunol*. 2018;39(4):261–3.
4. Hilligan KL, Ronchese F. Antigen presentation by dendritic cells and their instruction of CD4+ T helper cell responses. *Cell Mol Immunol*. 2020;17(6):587–99.
5. Iberg CA, Jones A, Hawiger D. Dendritic Cells As Inducers of Peripheral Tolerance. *Trends in Immunol*. 2017;38(11):793–804.
6. Leventhal DS, Gilmore DC, Berger JM, Nishi S, Lee V, Malchow S, et al. Dendritic Cells Coordinate the Development and Homeostasis of Organ-Specific Regulatory T Cells. *Immunity*. 2016;44(4):847–59.
7. Guilliams M, Ginhoux F, Jakubzick C, Naik SH, Onai N, Schraml BU, et al. Dendritic cells, monocytes and macrophages: a unified nomenclature based on ontogeny. *Nat Rev Immunol*. 2014;14(8):571–8.
8. Schulz C, Perdiguero EG, Chorro L, Szabo-Rogers H, Cagnard N, Kierdorf K, et al. A Lineage of Myeloid Cells Independent of Myb and Hematopoietic Stem Cells. *Science*. 2012;336(6077):86–90.
9. Ginhoux F, Guilliams M. Tissue-Resident Macrophage Ontogeny and Homeostasis. *Immunity*. 2016;44(3):439–49.
10. Gomez-Perdiguero E, Klapproth K, Schulz C, Busch K, Azzoni E, Crozet L, et al. Tissue-resident macrophages originate from yolk-sac-derived erythro-myeloid progenitors. *Nature*. 2015;518(7540):547–51.
11. Perdiguero EG, Geissmann F. The development and maintenance of resident macrophages. *Nat Immunol*. 2016;17(1):2–8.
12. Hoeffel G, Chen J, Lavin Y, Low D, Almeida FF, See P, et al. C-Myb+ Erythro-Myeloid Progenitor-Derived Fetal Monocytes Give Rise to Adult Tissue-Resident Macrophages. *Immunity*. 2015;42(4):665–78.
13. Gentek R, Ghigo C, Hoeffel G, Bulle MJ, Msallam R, Gautier G, et al. Hemogenic Endothelial Fate Mapping Reveals Dual Developmental Origin of Mast Cells. *Immunity*. 2018;48(6):1160–5.
14. Sawai CM, Babovic S, Upadhaya S, Knapp DJHF, Lavin Y, Lau CM, et al. Hematopoietic Stem Cells Are the Major Source of Multilineage Hematopoiesis in Adult Animals. *Immunity*. 2016;45(3):597–609.

-
15. Dakic A, Shao QX, D'Amico A, O'Keeffe M, Chen WF, Shortman K, et al. Development of the Dendritic Cell System during Mouse Ontogeny. *J Immunol.* 2004;172(2):1018–27.
 16. Fogg DK, Sibon C, Miled C, Jung S, Aucouturier P, Littman DR, et al. A Clonogenic Bone Marrow Progenitor Specific for Macrophages and Dendritic Cells. *Science.* 2006;311(5757):83.
 17. Hettinger J, Richards DM, Hansson J, Barra MM, Joschko A-C, Krijgsveld J, et al. Origin of monocytes and macrophages in a committed progenitor. *Nat Immunol.* 2013;14(8):821–30.
 18. Naik SH, Sathe P, Park H-Y, Metcalf D, Proietto AI, Dakic A, et al. Development of plasmacytoid and conventional dendritic cell subtypes from single precursor cells derived in vitro and in vivo. *Nat Immunol.* 2007;8(11):1217–26.
 19. Onai N, Kurabayashi K, Hosoi-Amaike M, Toyama-Sorimachi N, Matsushima K, Inaba K, et al. A Clonogenic Progenitor with Prominent Plasmacytoid Dendritic Cell Developmental Potential. *Immunity.* 2013;38(5):943–57.
 20. Breton G, Lee J, Zhou YJ, Schreiber JJ, Keler T, Pühr S, et al. Circulating precursors of human CD1c+ and CD141+ dendritic cells. *J Exp Med.* 2015;212(3):401–13.
 21. Schraml BU, van Blijswijk J, Zelenay S, Whitney PG, Filby A, Acton SE, et al. Genetic Tracing via DNGR-1 Expression History Defines Dendritic Cells as a Hematopoietic Lineage. *Cell.* 2013;154(4):843–58.
 22. Liu K, Vitorica GD, Schwickert TA, Guermonprez P, Meredith MM, Yao K, et al. In vivo analysis of dendritic cell development and homeostasis. *Science.* 2009;324(5925):392–7.
 23. Bain CC, Bravo-Blas A, Scott CL, Perdiguero EG, Geissmann F, Henri S, et al. Constant replenishment from circulating monocytes maintains the macrophage pool in the intestine of adult mice. *Nat Immunol* 2014;15(10):929–37.
 24. Serbina NV, Salazar-Mather TP, Biron CA, Kuziel WA, Pamer EG. TNF/iNOS-Producing Dendritic Cells Mediate Innate Immune Defense against Bacterial Infection. *Immunity.* 2003;19(1):59–70.
 25. Shortman K, Sathe P, Vremec D, Naik S, O'Keeffe M. Plasmacytoid dendritic cell development. *Adv Immunol.* 2013;120:105–26.
 26. Reizis B. Regulation of plasmacytoid dendritic cell development. *Curr Opin in Immunol.* 2010;22(2):206–11.
 27. Dress RJ, Dutertre C-A, Giladi A, Schlitzer A, Low I, Shadan NB, et al. Plasmacytoid dendritic cells develop from Ly6D+ lymphoid progenitors distinct from the myeloid lineage. *Nat Immunol.* 2019;20(7):852–64.
 28. Rodrigues PF, Alberti-Servera L, Eremin A, Grajales-Reyes GE, Ivanek R, Tussiwand R. Distinct progenitor lineages contribute to the heterogeneity of plasmacytoid dendritic cells. *Nat Immunol.* 2018;19(7):711–22.

-
29. Liu K, Waskow C, Liu X, Yao K, Hoh J, Nussenzweig M. Origin of dendritic cells in peripheral lymphoid organs of mice. *Nat Immunol.* 2007;8(6):578–83.
 30. Schlitzer A, Sivakamasundari V, Chen J, Sumatoh HRB, Schreuder J, Lum J, et al. Identification of cDC1- and cDC2-committed DC progenitors reveals early lineage priming at the common DC progenitor stage in the bone marrow. *Nat Immunol.* 2015;16(7):718–28.
 31. Grajales-Reyes GE, Iwata A, Albring J, Wu X, Tussiwand R, KC W, et al. *Batf3* maintains autoactivation of *Irf8* for commitment of a CD8 α ⁺ conventional DC clonogenic progenitor. *Nat Immunol.* 2015;16(7):708–17.
 32. McKenna HJ, Stocking KL, Miller RE, Brasel K, De Smedt T, Maraskovsky E, et al. Mice lacking *flt3* ligand have deficient hematopoiesis affecting hematopoietic progenitor cells, dendritic cells, and natural killer cells. *Blood.* 2000;95(11):3489–97.
 33. Durai V, Bagadia P, Briseño CG, Theisen DJ, Iwata A, Davidson JT IV, et al. Altered compensatory cytokine signaling underlies the discrepancy between *Flt3* $-/-$ and *Flt3l* $-/-$ mice. *J Exp Med.* 2018;96:jem.20171784–25.
 34. Naik SH, Proietto AI, Wilson NS, Dakic A, Schnorrer P, Fuchsberger M, et al. Cutting Edge: Generation of Splenic CD8⁺ and CD8⁻ Dendritic Cell Equivalents in *Fms*-Like Tyrosine Kinase 3 Ligand Bone Marrow Cultures. *J Immunol.* 2005;174(11):6592–7.
 35. Karsunky H, Merad M, Cozzio A, Weissman IL, Manz MG. *Flt3* Ligand Regulates Dendritic Cell Development from *Flt3* ⁺Lymphoid and Myeloid-committed Progenitors to *Flt3* ⁺Dendritic Cells In Vivo. *J Exp Med.* 2003;198(2):305–13.
 36. Vollstedt S, O’Keeffe M, Odermatt B, Beat R, Glanzmann B, Riesen M, et al. Treatment of neonatal mice with *Flt3* ligand leads to changes in dendritic cell subpopulations associated with enhanced IL-12 and IFN- α production. *Eur J Immunol.* 2004;34(7):1849–60.
 37. Vollstedt S, Franchini M, Hefti HP, Odermatt B, O’Keeffe M, Alber G, et al. *Flt3* Ligand-treated Neonatal Mice Have Increased Innate Immunity Against Intracellular Pathogens and Efficiently Control Virus Infections. *J Exp Med.* 2003;197(5):575–84.
 38. Merad M, Sathe P, Helft J, Miller J, Mortha A. The Dendritic Cell Lineage: Ontogeny and Function of Dendritic Cells and Their Subsets in the Steady State and the Inflamed Setting. *Annu Rev Immunol.* 2013;31(1):563–604.
 39. Miller JC, Brown BD, Shay T, Jojic V, Cohain A, Pandey G, et al. Deciphering the transcriptional network of the dendritic cell lineage. *Nat Immunol.* 2012;13(9):888–99.
 40. Bosteels C, Scott CL. Transcriptional regulation of DC fate specification. *Mol Immunol.* 2020;121:38–46.

-
41. Granot T, Senda T, Carpenter DJ, Matsuoka N, Weiner J, Gordon CL, et al. Dendritic Cells Display Subset and Tissue-Specific Maturation Dynamics over Human Life. *Immunity*. 2017;46(3):504–15.
 42. Pakalniškytė D, Schraml BU. Tissue-Specific Diversity and Functions of Conventional Dendritic Cells. *Adv Immunol*. 2017;134:89–135.
 43. Sichien D, Scott CL, Martens L, Vanderkerken M, Van Gassen S, Plantinga M, et al. IRF8 Transcription Factor Controls Survival and Function of Terminally Differentiated Conventional and Plasmacytoid Dendritic Cells, Respectively. *Immunity*. 2016;45(3):626–40.
 44. Hildner K, Edelson BT, Purtha WE, Diamond M, Matsushita H, Kohyama M, et al. Batf3 Deficiency Reveals a Critical Role for CD8 α ⁺ Dendritic Cells in Cytotoxic T Cell Immunity. *Science*. 2008;322(5904):1097–100.
 45. Reis e Sousa C, Hieny S, Schariton-Kersten T, Jankovic D, Charest H, Germain RN, et al. In vivo microbial stimulation induces rapid CD40 ligand-independent production of interleukin 12 by dendritic cells and their redistribution to T cell areas. *J Exp Med*. 1997;186(11):1819–29.
 46. Mashayekhi M, Sandau MM, Dunay IR, Frickel EM, Khan A, Goldszmid RS, et al. CD8 α ⁺ Dendritic Cells Are the Critical Source of Interleukin-12 that Controls Acute Infection by *Toxoplasma gondii* Tachyzoites. *Immunity*. 2011;35(2):249–59.
 47. Bachem A, Hartung E, Güttler S, Mora A, Zhou X, Hegemann A, et al. Expression of XCR1 Characterizes the Batf3-Dependent Lineage of Dendritic Cells Capable of Antigen Cross-Presentation. *Front Immunol*. 2012;3:214.
 48. Lau CM, Nish SA, Yogev N, Waisman A, Reiner SL, Reizis B. Leukemia-associated activating mutation of Flt3 expands dendritic cells and alters T cell responses. *J Exp Med*. 2016;213(3):415–31.
 49. Bar-On L, Birnberg T, Lewis KL, Edelson BT, Bruder D, Hildner K, et al. CX3CR1⁺ CD8⁺ dendritic cells are a steady-state population related to plasmacytoid dendritic cells. *Proc Natl Acad Sci USA*. 2010;107(33):14745–50.
 50. Leylek R, Alcántara-Hernández M, Lanzas Z, Lüdtke A, Perez OA, Reizis B, et al. Integrated Cross-Species Analysis Identifies a Conserved Transitional Dendritic Cell Population. *CellReports*. 2019;29(11):3736–8.
 51. Wylie B, Read J, Buzzai AC, Wagner T, Troy N, Syn G, et al. CD8⁺XCR1^{neg} Dendritic Cells Express High Levels of Toll-Like Receptor 5 and a Unique Complement of Endocytic Receptors. *Front Immunol*. 2019;9:245–16.
 52. Dudziak D, Kamphorst AO, Heidkamp GF, Buchholz VR, Trumpfheller C, Yamazaki S, et al. Differential Antigen Processing by Dendritic Cell Subsets in Vivo. *Science*. 2007;315(5808):107–11.

-
53. Shin C, Han J-A, Choi B, Cho Y-K, Do Y, Ryu S. Intrinsic features of the CD8 α -dendritic cell subset in inducing functional T follicular helper cells. *Immunol Letters*. 2016;172:21–8.
 54. Persson EK, Uronen-Hansson H, Semmrich M, Rivollier A, Hägerbrand K, Marsal J, et al. IRF4 Transcription-Factor-Dependent CD103+CD11b+ Dendritic Cells Drive Mucosal T Helper 17 Cell Differentiation. *Immunity*. 2013;38(5):958–69.
 55. Schlitzer A, McGovern N, Teo P, Zelante T, Atarashi K, Low D, et al. IRF4 Transcription Factor-Dependent CD11b+ Dendritic Cells in Human and Mouse Control Mucosal IL-17 Cytokine Responses. *Immunity*. 2013;38(5):970–83.
 56. Tussiwand R, Everts B, Grajales-Reyes GE, Kretzer NM, Iwata A, Bagaitkar J, et al. Klf4 Expression in Conventional Dendritic Cells Is Required for T Helper 2 Cell Responses. *Immunity*. 2015;42(5):916–28.
 57. Fujita K, Chakarov S, Kobayashi T, Sakamoto K, Voisin B, Duan K, et al. Cell-autonomous FLT3L shedding via ADAM10 mediates conventional dendritic cell development in mouse spleen. *Proc Natl Acad Sci USA*. 2019;116(29):14714–23.
 58. Bajaan S, Roach K, Turner S, Paul J, Kovats S. IRF4 Promotes Cutaneous Dendritic Cell Migration to Lymph Nodes during Homeostasis and Inflammation. *J Immunol*. 2012;189(7):3368–77.
 59. Lewis KL, Caton ML, Bogunovic M, Greter M, Grajkowska LT, Ng D, et al. Notch2 Receptor Signaling Controls Functional Differentiation of Dendritic Cells in the Spleen and Intestine. *Immunity*. 2011;35(5):780–91.
 60. Briseño CG, Satpathy AT, Davidson JT, Ferris ST, Durai V, Bagadia P, et al. Notch2-dependent DC2s mediate splenic germinal center responses. *Proc Natl Acad Sci USA*. 2018;115(42):10726–31.
 61. Dicken J, Mildner A, Leshkowitz D, Touw IP, Hantisteanu S, Jung S, et al. Transcriptional Reprogramming of CD11b+Esamhi Dendritic Cell Identity and Function by Loss of Runx3. *PLoS ONE*. 2013;8(10):e77490–12.
 62. Satpathy AT, Briseño CG, Lee JS, Ng D, Manieri NA, KC W, et al. Notch2-dependent classical dendritic cells orchestrate intestinal immunity to attaching-and-effacing bacterial pathogens. *Nat Immunol*. 2013;14(9):937–48.
 63. Brown CC, Gudjonson H, Pritykin Y, Deep D, Lavallée V-P, Mendoza A, et al. Transcriptional Basis of Mouse and Human Dendritic Cell Heterogeneity. *Cell*. 2019;179(4):846–863.e24.
 64. Bosteels C, Neyt K, Vanheerswynghe M, Van Helden MJ, Sichien D, Debeuf N, et al. Inflammatory Type 2 cDCs Acquire Features of cDC1s and Macrophages to Orchestrate Immunity to Respiratory Virus Infection. *Immunity*. 2020;52(6):1039–9.

-
65. Jung S, Unutmaz D, Wong P, Sano G-I, De los Santos K, Sparwasser T, et al. In vivo depletion of CD11c⁺ dendritic cells abrogates priming of CD8⁺ T cells by exogenous cell-associated antigens. *Immunity*. 2002;17(2):211–20.
 66. Meredith MM, Liu K, Darrasse-Jèze G, Kamphorst AO, Schreiber HA, Guermónprez P, et al. Expression of the zinc finger transcription factor zDC (Zbtb46, Btbd4) defines the classical dendritic cell lineage. *J Exp Med*. 2012;209(6):1153–65.
 67. Satpathy AT, KC W, Albring JC, Edelson BT, Kretzer NM, Bhattacharya D, et al. Zbtb46 expression distinguishes classical dendritic cells and their committed progenitors from other immune lineages. *J Exp Med*. 2012;209(6):1135–52.
 68. Yamazaki C, Sugiyama M, Ohta T, Hemmi H, Hamada E, Sasaki I, et al. Critical Roles of a Dendritic Cell Subset Expressing a Chemokine Receptor, XCR1. *J Immunol*. 2013;190(12):6071–82.
 69. Muzaki ARBM, Tetlak P, Sheng J, Loh SC, Setiagani YA, Poidinger M, et al. Intestinal CD103(+)CD11b(-) dendritic cells restrain colitis via IFN- γ -induced anti-inflammatory response in epithelial cells. *Mucosal Immunol*. 2016;9(2):336–51.
 70. Tussiwand R, Lee W-L, Murphy TL, Mashayekhi M, KC W, Albring JC, et al. Compensatory dendritic cell development mediated by BATF-IRF interactions. *Nature*. 2012;490(7421):502–7.
 71. Baerenwaldt A, Burg von N, Kreuzaler M, Sitte S, Horvath E, Peter A, et al. Flt3 Ligand Regulates the Development of Innate Lymphoid Cells in Fetal and Adult Mice. *J Immunol*. 2016;196(6):2561–71.
 72. Sharma S, Zhu J. Immunologic Applications of Conditional Gene Modification Technology in the Mouse. *Current Protocols in Immunology*. 2014;105(1):165–13.
 73. Caton ML, Smith-Raska MR, Reizis B. Notch–RBP-J signaling controls the homeostasis of CD8[–] dendritic cells in the spleen. *J Exp Med*. 2007;204(7):1653–64.
 74. Zaft T, Sapoznikov A, Krauthgamer R, Littman DR, Jung S. CD11c^{high} dendritic cell ablation impairs lymphopenia-driven proliferation of naive and memory CD8⁺ T cells. *J Immunol*. 2005;175(10):6428–35.
 75. Cabeza-Cabrerizo M, van Blijswijk J, Wienert S, Heim D, Jenkins RP, Chakravarty P, et al. Tissue clonality of dendritic cell subsets and emergency DCpoiesis revealed by multicolor fate mapping of DC progenitors. *Sci Immunol*. 2019;4(33):eaaw1941.
 76. Salei N, Rambichler S, Salvermoser J, Papaioannou NE, Schuchert R, Pakalniškytė D, et al. The Kidney Contains Ontogenetically Distinct Dendritic Cell and Macrophage Subtypes throughout Development That Differ in Their Inflammatory Properties. *J Am Soc Nephrol*. 2020;31(2):257–78.

-
77. Harbeson D, Ben-Othman R, Amenyogbe N, Kollmann TR. Outgrowing the Immaturity Myth: The Cost of Defending From Neonatal Infectious Disease. *Front Immunol.* 2018;9:307–9.
 78. Dowling DJ, Levy O. Ontogeny of early life immunity. *Trends Immunol.* 2014;35(7):299–310.
 79. Kollmann TR, Kampmann B, Mazmanian SK, Marchant A, Levy O. Protecting the Newborn and Young Infant from Infectious Diseases: Lessons from Immune Ontogeny. *Immunity.* 2017;46(3):350–63.
 80. Nabhani AI Z, Dulauroy S, Marques R, Cousu C, Bounny AI S, Déjardin F, et al. A Weaning Reaction to Microbiota Is Required for Resistance to Immunopathologies in the Adult. *Immunity.* 2019;50(5):1276–1288.e5.
 81. Dowling DJ, Levy O. Ontogeny of early life immunity. *Trends Immunol.* 2014;35(7):299–310.
 82. Zhang X, Lepelley A, Azria E, Lebon P, Roguet G, Schwartz O, et al. Neonatal Plasmacytoid Dendritic Cells (pDCs) Display Subset Variation but Can Elicit Potent Anti-Viral Innate Responses. *PLoS ONE.* 2013;8(1):e52003.
 83. Papaioannou NE, Pasztoi M, Schraml BU. Understanding the Functional Properties of Neonatal Dendritic Cells: A Doorway to Enhance Vaccine Effectiveness? *Front Immunol.* 2019;9:553–8.
 84. Adkins B, Leclerc C, Marshall-Clarke S. Neonatal adaptive immunity comes of age. *Nat Rev Immunol.* 2004;4(7):553–64.
 85. PrabhuDas M, Adkins B, Gans H, King C, Levy O, Ramilo O, et al. Challenges in infant immunity: implications for responses to infection and vaccines. *Nat Immunol.* 2011;12(3):189–94.
 86. Elahi S. Neonatal and Children's Immune System and COVID-19: Biased Immune Tolerance versus Resistance Strategy. *J Immunol.* 2020;205(8):1990–7.
 87. Smith NL, Patel RK, Reynaldi A, Grenier JK, Wang J, Watson NB, et al. Developmental Origin Governs CD8+ T Cell Fate Decisions during Infection. *Cell.* 2018;174(1):117–130.e14.
 88. Galindo-Albarrán AO, López-Portales OH, Gutiérrez-Reyna DY, Rodríguez-Jorge O, Sánchez-Villanueva JA, Ramírez-Pliego O, et al. CD8+ T Cells from Human Neonates Are Biased toward an Innate Immune Response. *Cell Reports.* 2016;17(8):2151–60.
 89. Chen SF, Tu W-W, Sharp MA, Tongson EC, He X-S, Greenberg HB, et al. Antiviral CD8 T cells in the control of primary human cytomegalovirus infection in early childhood. *J Infect Dis.* 2004;189(9):1619–27.
 90. Zaghouani H, Hoeman CM, Adkins B. Neonatal immunity: faulty T-helpers and the shortcomings of dendritic cells. *Trends Immunol.* 2009;30(12):585–91.

-
91. Lee H-H, Hoeman CM, Hardaway JC, Guloglu FB, Ellis JS, Jain R, et al. Delayed maturation of an IL-12-producing dendritic cell subset explains the early Th2 bias in neonatal immunity. *J Exp Med*. 2008;205(10):2269–80.
 92. Mold JE, Venkatasubrahmanyam S, Burt TD, Michaelsson J, Rivera JM, Galkina SA, et al. Fetal and Adult Hematopoietic Stem Cells Give Rise to Distinct T Cell Lineages in Humans. *Science*. 2010;330(6011):1695–9.
 93. Mold JE, Michaelsson J, Burt TD, Muench MO, Beckerman KP, Busch MP, et al. Maternal alloantigens promote the development of tolerogenic fetal regulatory T cells in utero. *Science*. 2008;322(5907):1562–5.
 94. Mastelic-Gavillet B, Vono M, Gonzalez-Dias P, Ferreira FM, Cardozo L, Lambert P-H, et al. Neonatal T Follicular Helper Cells Are Lodged in a Pre-T Follicular Helper Stage Favoring Innate Over Adaptive Germinal Center Responses. *Front Immunol*. 2019;10:185–12.
 95. Sun C-M, Deriaud E, Leclerc C, Lo-Man R. Upon TLR9 Signaling, CD5+ B Cells Control the IL-12-Dependent Th1-Priming Capacity of Neonatal DCs. *Immunity*. 2005;22(4):467–77.
 96. Nussbaum C, Gloning A, Pruenster M, Frommhold D, Bierschenk S, Genzel-Boroviczeny O, et al. Neutrophil and endothelial adhesive function during human fetal ontogeny. *J Leuk Biol*. 2013;93(2):175–84.
 97. Sperandio M, Quackenbush EJ, Sushkova N, Altstätter J, Nussbaum C, Schmid S, et al. Ontogenetic regulation of leukocyte recruitment in mouse yolk sac vessels. *Blood*. 2013;121(21):e118–28.
 98. Yost CC, Cody MJ, Harris ES, Thornton NL, McInturff AM, Martinez ML, et al. Impaired neutrophil extracellular trap (NET) formation: a novel innate immune deficiency of human neonates. *Blood*. 2009;113(25):6419–27.
 99. Ulas T, Pirr S, Fehlhaber B, Bickes MS, Loof TG, Vogl T, et al. S100-alarmin-induced innate immune programming protects newborn infants from sepsis. *Nat Immunol*. 2017;18(6):622–32.
 100. De Kleer I, Willems F, Lambrecht B, Goriely S. Ontogeny of myeloid cells. *Front Immunol*. 2014;5(21):423.
 101. Krow-Lucal ER, Kim CC, Burt TD, McCune JM. Distinct functional programming of human fetal and adult monocytes. *Blood*. 2014;123(12):1897–904.
 102. He Y-M, Li X, Perego M, Nefedova Y, Kossenkova AV, Jensen EA, et al. Transitory presence of myeloid-derived suppressor cells in neonates is critical for control of inflammation. *Nat Med*. 2018;24(2):224–31.
 103. Sun C-M, Fiette L, Tanguy M, Leclerc C, Lo-Man R. Ontogeny and innate properties of neonatal dendritic cells. *Blood*. 2003;102(2):585–91.
 104. Prabhu SB, Rathore DK, Nair D, Chaudhary A, Raza S, Kanodia P, et al. Comparison of Human Neonatal and Adult Blood Leukocyte Subset Composition Phenotypes. *PLoS ONE*. 2016;11(9):e0162242–17.

-
105. Ruckwardt TJ, Morabito KM, Bar-Haim E, Nair D, Graham BS. Neonatal mice possess two phenotypically and functionally distinct lung-migratory CD103+ dendritic cell populations following respiratory infection. *Mucosal Immunol.* 2018;11(1):186–98.
 106. Torres D, Köhler A, Delbauve S, Caminschi I, Lahoud MH, Shortman K, et al. IL-12p40/IL-10 Producing preCD8 α /Clec9A+ Dendritic Cells Are Induced in Neonates upon *Listeria monocytogenes* Infection. *PLOS Pathogens.* 2016;12(4):e1005561.
 107. Ruckwardt TJ, Malloy AMW, Morabito KM, Graham BS. Quantitative and Qualitative Deficits in Neonatal Lung-Migratory Dendritic Cells Impact the Generation of the CD8+ T Cell Response. *PLOS Pathogens.* 2014;10(2):e1003934–12.
 108. Muthukkumar S, Goldstein J, Stein KE. The Ability of B Cells and Dendritic Cells to Present Antigen Increases During Ontogeny. *J Immunol.* 2000;165(9):4803–13.
 109. Langrish CL, Buddle JC, Thrasher AJ, Goldblatt D. Neonatal dendritic cells are intrinsically biased against Th-1 immune responses. *Clin Exp Immunol.* 2002;128(1):118–23.
 110. Goriely S, Vincart B, Stordeur P, Vekemans J, Willems F, Goldman M, et al. Deficient IL-12(p35) Gene Expression by Dendritic Cells Derived from Neonatal Monocytes. *J Immunol.* 200;166(3):2141–6.
 111. de Kleer IM, Kool M, de Bruijn MJW, Willart M, van Moorlegghem J, Schuijs MJ, et al. Perinatal Activation of the Interleukin-33 Pathway Promotes Type 2 Immunity in the Developing Lung. *Immunity.* 2016;45(6):1285–98.
 112. Lau-Kilby AW, Turfkruyer M, Kehl M, Yang L, Buchholz UJ, Hickey K, et al. Type I IFN ineffectively activates neonatal dendritic cells limiting respiratory antiviral T-cell responses. *Mucosal Immunol.* 2019;13(2):371–80.
 113. McGovern N, Shin A, Low G, Low D, Duan K, Yao LJ, et al. Human fetal dendritic cells promote prenatal T-cell immune suppression through arginase-2. *Nature.* 2017;546(7660):662–6.
 114. Ardavin C, Wu L, Li C-L, Shortman K. Thymic dendritic cells and T cells develop simultaneously in the thymus from a common precursor population. *Nature.* 1993;362(6422):761–3.
 115. Wu L, D'Amico A, Hochrein H, O'Keeffe M, Shortman K, Lucas K. Development of thymic and splenic dendritic cell populations from different hemopoietic precursors. *Blood.* 2001;98(12):3376–82.
 116. Izon D, Rudd K, DeMuth W, Pear WS, Clendenin C, Lindsley RC, et al. A common pathway for dendritic cell and early B cell development. *J Immunol.* 2001;167(3):1387–92.

-
117. Helft J, Anjos-Afonso F, van der Veen AG, Chakravarty P, Bonnet D, Reis e Sousa C. Dendritic Cell Lineage Potential in Human Early Hematopoietic Progenitors. *Cell Reports*. 2017;20(3):529–37.
 118. Igarashi H, Gregory SC, Yokota T, Sakaguchi N, Kincade PW. Transcription from the RAG1 locus marks the earliest lymphocyte progenitors in bone marrow. *Immunity*. 2002;17(2):117–30.
 119. Schneider C, Lee J, Koga S, Ricardo-Gonzalez RR, Nussbaum JC, Smith LK, et al. Tissue-Resident Group 2 Innate Lymphoid Cells Differentiate by Layered Ontogeny and In Situ Perinatal Priming. *Immunity*. 2019;50(6):1425–5.

Acknowledgements

First and foremost, I would like to thank my supervisor Dr. Barbara Schraml-Schotta for giving me the chance to work in her team and entrusting me with this challenging and interesting project. Her guidance and faith in the project throughout the course of my PhD contributed essentially to the result presented in this thesis. I am also grateful for the opportunity that she gave me to collaborate with many international scientists and visit their labs to perform experiments.

In continuation, I would like to acknowledge the members of my thesis advisor committee, namely Prof. Dr. Christian Schulz and Prof. Dr. med. Markus Sperandio. I was fortunate to have them as my mentors and thank them for giving me precious advice and feedback within and outside of our thesis committee meetings.

Additionally, the IRTG914 for providing me with the ideal scientific environment for cultivating my skills as a researcher. Special thanks to our coordinator Dr. Verena Kochan for all the support throughout my PhD and excellent cooperation during my time as a student speaker.

Of course, I would like to thank all the past and current members of the Schraml group with who I had the honor of working together and especially Stephan, Natallia, Vanessa and Johanna that honor me with their friendship even after our common time in the lab was over.

I would also like to acknowledge the European and German funding resources without research projects like mine would not be possible.

Finally, I dedicate this thesis to my parents, brother, friends and my wife Zoe whose contribution was and resumes to be beyond measure.

Curriculum vitae

Nikos Papaioannou

PhD Candidate in Immunology

nikolaos.papaioannou@med.uni-muenchen.de

Education and Employment History

- December 2016 – present
PhD student, Biomedical Center, LMU Munich,
Planegg-Martinsried, Germany
Supervisor: Prof. Dr. Barbara Schraml
- June 2016 – July 2016
Internship Researcher, IKYDA 2016 Internship Researcher,
IKYDA 2016
Project Title: 'Exploitation and clinical validation of the novel sepsis
biomarker prothymosin alpha (100-109)'
- December 2014 – June 2016
M.Sc. "Applications of Biology in Medicine", NKUA, Athens, Greece
Thesis Advisor Committee:
Dr. Ourania Tsitsiloni, Dr. Evangelos Terpos, Dr. Andreas Skorilas
Academic Diploma Grade: 9.69/10
- October 2014 – September 2015
Biologist-Researcher, Scientific Project ISPEBREAST
- September 2010 – September 2014
B.Sc. in Biology, NKUA, Athens, Greece
Thesis Supervisor: Dr. Ourania Tsitsiloni
Academic Diploma Grade: 8.81/10

Languages

Greek (native speaker), English (C2, highly proficient), Spanish (B2)

Extra-curricular activities

September 2017 – September 2019
Student speaker of Integrated Research Group (IRTG) 914

Publications

- 1) **Papaioannou NE**, et al. Environmental signals rather than layered ontogeny imprint the function of type 2 conventional dendritic cells in young and adult mice. Nat Commun. 2021;12:464. doi: 10.1038/s41467-020-20659-2
- 2) Salei N, Rambichler S, Salvermoser J, **Papaioannou NE**, et al. The Kidney Contains Ontogenetically Distinct Dendritic Cell and Macrophage Subtypes throughout Development That Differ in Their Inflammatory Properties. J Am Soc Nephrol. 2020 Feb;31(2):257-278. doi: 10.1681/ASN.2019040419
- 3) **Papaioannou NE**, et al. Understanding the Functional Properties of Neonatal Dendritic Cells: A Doorway to Enhance Vaccine Effectiveness? Front Immunol. 2019 Jan 10;9:3123. doi: 10.3389/fimmu.2018.03123
- 4) Salvermoser J, van Blijswijk J, **Papaioannou NE**, et al. Clec9a-Mediated Ablation of Conventional Dendritic Cells Suggests a Lymphoid Path to Generating Dendritic Cells In Vivo. Front Immunol. 2018 Apr 16;9:699. doi: 10.3389/fimmu.2018.00699

5) Samara P, Karachaliou CE, Ioannou K, **Papaioannou NE**, et al. Prothymosin Alpha: An Alarmin and More... Curr Med Chem. 2017;24(17):1747-1760. doi:10.2174/0929867324666170518110033

6) **Papaioannou NE**, et al. Harnessing the immune system to improve cancer therapy. Ann Transl Med. 2016 Jul;4(14):261. doi: 10.21037/atm.2016.04.01

7) **Papaioannou NE**, et al. A flow cytometric approach for studying alterations in the cytoplasmic concentration of calcium ions in immune cells following stimulation with thymic peptides. Cell Immunol. 2016 Apr;302:32-40. doi: 10.1016/j.cellimm.2016.01.004

Pubmed link: <https://www.ncbi.nlm.nih.gov/pubmed/?term=Papaioannou+N+E>

Oral/Poster presentations at international conferences

- 1) 5th European Congress of Immunology
- 2) 2nd International Conference on Leukocyte Trafficking
- 3) 30th Congress of the International Society for Advancement of Cytometry
- 4) INsPiRE Final Evaluation Meeting

Awards

- 1) EFIS-EJI Travel Grant for participation in the 5th European Congress of Immunology, Amsterdam, 2018
- 2) Travel award for participation in the 30th Congress of the International Society for Advancement of Cytometry, Glasgow, 2014
- 3) Award from the Greek State Scholarships Foundations (IKY), for excellence in biology studies during the academic year 2011-2012

Indicative lab expertise

- 1) Multiparameter conventional flow cytometry applied for basic research and clinical purposes, using up to 18 fluorescent parameters.
- 2) Fluorescence-activated cell sorting of murine immune cell isolated from both lymphoid and non-lymphoid tissues for downstream molecular and functional analysis.
- 3) Basic principles of spectral flow cytometry.
- 4) Handling of neonatal and adult mice. Experience both *in vivo* and *in vitro* experiments after tissue isolation. Experience in mouse colony management.
- 5) Generation of bulk and single cell (10x Genomics platform) RNA sequencing libraries and analysis using computational R environments.
- 6) Cellular immunology experiments including cell culture for *in vitro* dendritic cell and T cell differentiation and functional assays.
- 7) PCR for bulk DNA and single cell-derived samples.